UNITED STATES NAVY

PROJECT SQUID

Technical Memorandum No. Pur-11

REGULARITY OF TURBULENT FLOW IN SMOOTH PIPES

by
J. Nikuradse
Translated by
E. W. Bowditch
W. G. Agnew
Transmitted by
H. J. Buttner

PURDUE RESEARCH FOUNDATION
AND
PURDUE UNIVERSITY
Lafayette, Indiana
1 August 1949

UNITED STATES NAVY

PROJECT SQUID

TECHNICAL MEMORANDUM NO. PUR-11

REGULARITY OF TURBULENT FLOW IN SMOOTH PIPES*

by

J. Nikuradse

Translated by

F. W. Bowditch

W. G. Agnew

Transmitted by

H. J. Buttner

Project SQUID is a Program of Fundamental Research on Liquid Rocket and Pulse Jet Propulsion, for the [redacted] Office of Naval Research of the Navy Department, Contract N6 ori-104, Task Order No. 1, Designation No. Nr 220042

PURDUE RESEARCH FOUNDATION

and

PURDUE UNIVERSITY

Lafayette, Indiana

1 August 1949

*Forschungsheft 356 Supplement to Forschung auf dem Gebeite des Ingenieurwesens, Edition B, Vol. 3, Sept.-Oct. 1932.

PREFACE

"Regularity of Turbulent Flow in Smooth Pipes" is probably the earliest thorough experimental and analytical treatment of turbulence in smooth pipes, and is still considered one of the best sources of turbulence data available.

The translation of this technical article was undertaken for the purpose of comparing values of turbulent velocities appearing herein with those determined by means of a constant temperature hot wire anemometer at the Project SQUID Combustion Laboratory, Purdue University. Since Nikuradse has been extensively quoted in treatises on turbulent flow, and since his turbulence data have been previously used in combustion studies, it was felt that this article would provide the best possible comparison for the present hot wire anemometer studies.

The decision to publish this work was made when the translation was partially completed and it became evident that the material contained in the study was of such value as to merit a wider distribution. The report is thus published in full in order that other investigators in the fields of fluid flow and combustion may have the benefit of this translation.

H.J.B.

TABLE OF CONTENTS

Introduction

The existing experimental knowledge of turbulent flow, which has been the object of numerous investigations, has still not been sufficient to produce a satisfactory foundation for the theory of turbulence. The older investigations, which were primarily directed toward the laws of flow resistance in tubes, could satisfy neither the theoretical nor the practical worker. The results of these researches were not clearly arranged for a long time, since they were not referred to the physically correct parameter, the Reynolds' Number Re . In many cases it was not considered that the velocity distribution develops its stable form in a tube only after a long distance. H. Blasius [1] succeeded in organizing the experimental data of the flow in smooth tubes from the viewpoint of similarity. He obtained an empirical formula, which in a region of Reynolds' Numbers up to about $Re = \frac{\bar{u} d}{\nu} = 100\ (10^3)$ ($\bar{u}$ = average velocity, d = tube diameter, ν = kinematic viscosity) fairly accurately reproduces the regularity of the flow resistance. For the formulation of his resistance formula Blasius used the investigations of Saph and Schoder [2] who worked with water and measured the pressure loss in 15 drawn brass tubes of diameter d = 2.77 mm. to 53.1 mm. in the region of Reynolds' Numbers between 1.4 (10^3) and 104 (10^3). Blasius found for laminar flow the formula

$$\lambda = \frac{64}{Re}$$

and for turbulent flow

$$\lambda = \frac{0.316}{Re^{1/4}}$$

(λ = the resistance coefficient). The investigations of Saph and Schoder show that the transition of laminar flow into turbulent flow occurs at about the Reynolds' Number (critical Reynolds' Number) $Re = 2000$. The transition region lies between the Reynolds' Numbers 2000 and 3000. Besides the investigations with water by Saph and Schoder, Blasius used for the formulation of his similarity law the investigations of Nusselt [3], who studied the pressure loss for the flow of compressed air in a tube of diameter $d = 2.201$ cm. If the resistance coefficient is calculated from these investigations and plotted in relation to the Reynolds' Number, one obtains the same results as were obtained from the investigations of Saph and Schoder. The Nusselt values, which lie in the region of Reynolds' Numbers of 6 (10^3) to about 150 (10^3) are in good agreement with the resistance formula of Blasius. In this way the similarity for different fluids, water and air, is confirmed. In addition Blasius used the studies of Lang, which were made in a copper tube of $d = 6$ mm and at Reynolds' Numbers up to $Re = 326$ (10^3). The investigations were aimed at formulating a comparison between high velocities in small tubes on the one hand and small velocities in large tubes on the other hand. This comparison has led to a very satisfactory confirmation of the similarity law.

After the formulation of the similarity law, Ombeck[4] set himself the task of determining the similarity of the resistance coefficient in relation to Reynolds' Number from the investigations of air in a large range of Reynolds' Numbers, and thus to check the formula of Blasius. The studies were carried out in circular tubes, which were made of different materials and had different diameters ($d = 2.004$ cm to $d = 10$ cm), and reached to a Reynolds' Number of about 450 (10^3). From these investigations Ombeck obtained a

formula similar to that of Blasius, but with a very small deviation; this small deviation, as Ombeck himself explains, is due to the uncertainty in the determination of the kinematic viscosity. Considering this circumstance he found good agreement with the Blasius formula up to a Reynolds' Number $Re = 100\ (10^3)$.

Stanton and Pannell [5], in order to recheck the similarity law, have performed extensive investigations with water and air at different temperatures in circular tubes with different diameters ($d = 0.361$ cm to $d = 12.62$ cm). The investigations were in the region of Reynolds' Numbers from 2.2 (10^3) to 430 (10^3). The results of these studies have confirmed the similarity law in all respects; up to a Reynolds' Number of 100 (10^3) the experimental points lie on the Blasius curve. From this point on one observes with increasing Reynolds' Numbers an increasing deviation upwards from the Blasius curve. Lees [6] has taken as the basis for the formulation of his empirical formula of the resistance law the results of Stanton and Pannell and found

$$\lambda = 0.00714 + \frac{0.6104}{Re^{0.35}}$$

Jakob and Erk [7] carried out experiments with water on the pressure drop in relation to the quantity of flow in drawn brass tubes of diameters $d = 7$ cm and 10 cm in the range of Reynolds' Numbers between 86 (10^3) and 462 (10^3). Within a scattering of the experimental points of about 1%, these studies confirmed the above mentioned measurements of Stanton and Pannell. Jakob and Erk deduced from their own experiments a resistance formula which agrees almost exactly with that of Lees.

Of the more recent experiments on the resistance law, those by Hermann [8] in a still greater range of Reynolds' Numbers should be

mentioned; Hermann carried out his experiments with water in a copper tube of diameter $d = 5$ cm and a brass tube of $d = 6.8$ cm in a range of Reynolds' Numbers between 20 (10^3) and 1900 (10^3) and "running lengths" (length of undisturbed flow between entrance to the tube and point of measurement) between 44 and 300 tube diameters. He investigated the relation between the resistance coefficient and the Reynolds' Number and found for short running lengths and small Reynolds' Numbers good agreement with the resistance law which Stanton and Pannell, Jakob and Erk, and others had established earlier. Hermann observed a running length effect (a decrease in resistance coefficient with running length) in a tube 300 diameters long; moreover he obtained with increasing Reynolds' Numbers an increase in the running length required to insure fully developed flow. The experimental results show that a length of 100 d is to be regarded approximately as the running length required to insure fully developed flow. From these experiments Hermann deduced a formula for the resistance law which is analogous to that of Lees. In conclusion he gives a table which permits the calculation of the resistance coefficient for any running length between 44 and 300 tube diameters. L. Schiller [9], under whose direction Hermann worked, reported on the above mentioned results in 1929 at the "Kongress für Aerodynamik und verwandte Gebiete" in Aachen during which it turned out that these resistance coefficients, which were above the highest Reynolds' Numbers reached by Stanton and Pannell and Jakob and Erk, lay considerably higher than those found in Göttingen. The higher resistance showed, obviously, that Hermann had had a rotation in his tube which brought with it an increase in resistance. This fact induced L. Prandtl [10] to suggest that a device be constructed at the entrance to smooth out the flow, and that the measurements be thus

repeated. The re-measurements resulted, as Schiller reported in a supplement to the publication of his Aachen presentation, in the conclusion that an effect of running length no longer exists after 125 diameters, and that with a sharp entrance after a length of 50 diameters no effect of length can be observed - which agreed with the findings of the Göttingen group. It should still be mentioned here that unpublished extensive measurements of the running length made in Göttingen result in the conclusion that even with rounded entrances, the effect of running length is no longer present after 50 diameters.

The experiments of Stanton[11] are among the first good studies of the velocity distribution of turbulent flow in circular tubes. The measurements were made with air in tubes of 500 cm. length and diameters d = 4.93 cm. and d = 7.4 cm. and extend over the range of Reynolds' Numbers between 14 (10^3) and 60 (10^3). The data on the pressure gradient, from which the velocity distributions were taken, are missing. A further measurement of this kind has been carried out by the author[12] with water in a circular tube of 2.8 cm. diameter at a Reynolds' Number of about 180 (10^3). In addition, there exist also measurements of the velocity distributions in channels and tubes with cross sections other than circular, which bear no relation to this work.

From the works mentioned above one sees that the experimental findings are insufficient for the clarification of the turbulence problem. On this basis, we at Göttingen set ourselves the task of broadening the existing investigations in two directions; on the one hand to extend the experiments to very high Reynolds' Numbers, and on the other hand in addition to the determination of the resistance law, also to clarify the relation between the velocity distributions and the Reynolds' Number of which a knowledge is of great importance for the

exploration of turbulent flow. We have carried out a great number of experiments on the velocity distributions and pressure loss in smooth tubes with the greatest possible accuracy and in as large a range of Reynolds' Numbers as possible. By appropriate evaluation we have succeeded in showing:

1. What regular relation exists between the resistance and the velocity distribution;
2. By what formulas the resistance law and the law for the velocity distribution may be expressed;
3. What regularities result for the exchange quantity and Prandtl's mixing length.

In these investigations free use has been made of the theoretical conclusions of Karman's similarity considerations[13]. The experiments have confirmed very well these conclusions above the limit at which the influence of viscosity on the turbulent processes disappears.

The experiments[14] were carried out in the years 1928-29 at the Kaiser Wilhelm-Institute für Strömungsforschung directed by Prof. Dr. L. Prandtl. The theoretical processing of the experimental results could not be brought to a conclusion until the summer of 1931. The experimental installation and apparatus are set up in the laboratories of the Kaiser Wilhelm-Institute für Strömungsforschung.

To my most honorable chief, Herr Prof. Dr. L. Prandtl, who continually assisted me with his valuable counsel, may I also at this time express my heartfelt thanks.

I. Experimentation

Part 1. Experimental Apparatus

For the investigation of the turbulent flow processes in circular tubes, three different experimental installations were used.

(a) For small Reynolds' Numbers of about 3 (10^3) to 60 (10^3), the overflow from a tank fed by a water conduit was used.

(b) For larger Reynolds' Numbers, up to about 1400 (10^3), the water was circulated by means of a centrifugal pump.

(c) For reaching still higher Reynolds' Numbers, up to about 2500 (10^3), the water stored in the water tank was ejected with compressed air.

(d) In the last two installations, the Reynolds' Number was raised still further by an increase in the temperature of the water, by which in the third case the highest value of Re = 3300 (10^3) could be reached.

(a): Since it is very difficult to produce a completely constant head at small discharges with a centrifugal pump alone, as is required at small Reynolds' Numbers, the following arrangement was made. The water flows from the water system through the feed pipe zl (see Figure 1) into the open water tank wk. On opening the flow-off cock ah, the water rises in the standpipe str to the same height as in the water tank wk. Since the feed pipe delivers a somewhat greater amount of water than flows out through the test pipe vr, the surplus water was disposed of through the standpipe str to the collector basin ft from which it was further led off through the down-pipe fr, so that a constant head was maintained. In order to get a uniform water flow in the test pipe, a flow straightener gl was constructed in the cylindrical portion of the outlet of the water tank wk. This was meant to do away with the great eddying which was produced by the water flowing into the water tank and which was carried over into the test pipe. Through the conical portion of the outlet the water was accelerated, resulting in a further smoothing of the flow. The water

was then brought to the entrance of the test pipe through a tube zr of 25 cm diameter and 250 cm length. Test pipes of the following dimensions were used (Table 1):

Table 1

Dimensions of the Test Pipe

d mm	l_e mm	l_I mm	l_{II} mm	l_a mm	x mm	x/d	Designation
10	550	500	500	450	2000	200	vr1
20	1330	500	500	170	2500	125	vr2
30	1960	500	500	40	3000	100	vr3
50	3300	1000	1000	70	6000	120	vr4
100	4000	1500	1000	550	7050	70,5	vr5

d = inner diameter of the tube; l_e = "running length"; l_I = length of measuring section I: l_{II} = length of measuring section II: l_a = exit length; x = total length; x/d = relative total length.

In order to obtain a smooth inflow to the test pipe, the feed pipe zr was tapered conically to the diameter of the test pipe for all experiments. In the experiments using overflow as the source of water a sharp-edged constriction was used in this tapered section al (Figure 5), which was meant to assure turbulent flow even at the smallest Reynolds' Numbers studied, about Re = 15 (10^3). Shortly before the tapering section, at the highest point in the feed pipe, an air venting valve eh was fitted. The test pipe with the velocity measuring apparatus was mounted on two trucks which permitted a convenient motion, pending the rebuilding. The trucks ran on rails on the side wall of the reservoir vk. Longitudinally in the truck lay an optical bar, on which stood the rider which carried the test pipe and made adjustment of the pipe in the horizontal direction possible.

At the end of the test pipe was a velocity measuring apparatus, which is further described below. Under this in the reservoir vk stood the measuring tank mb (Figure 5).

(b): For the experiments with circulation (Figure 2) the water was taken from the reservoir vk and forced into the water tank wk by a centrifugal pump kp, which was driven by a driving motor am (capacity 14 kw., R.P.M. - variable between 1120 and 1900 revolutions per minute). From here it came back again to the reservoir vk through the test pipe vr. The starter an of the driving motor and the gate valve sb_1, which was inserted between the centrifugal pump kp and the water tank wk, served as a coarse regulation. The fine regulation took place at the throttle valve dv on the velocity measuring apparatus (Figure 4). The centrifugal pump was capable of holding a pressure of about 2 atm on the air above the water level in the tank wk. Generally, a water head of 500 cm was maintained (Dimensions of the tank wk: Height 6500 mm, Diameter 1500 mm). The experimental arrangement just described made it possible to produce water flow up to about Re = 1000 (10^3) at ordinary temperatures. The test section was the same as for the first arrangement described.

(c): The compressed air setup consisted of a compressor which was capable of producing a gauge pressure of about 10 atm. in the compressed air tank dk (Figure 1). The compressed air tank was connected with the water tank wk through an Arca regulator a; the regulator, which is further described below, kept the pressure constant as water left the water tank wk. Since the time of flow was limited (shortest duration about 45 sec), the tripping valve sh was controlled by compressed air. About 0.1 sec. was required for opening or closing. In order to prevent a vacuum from occurring in the test section on

closing the tripping valve, the check valve sv, which is situated at the highest point in the entrance tube zr between the tripping valve and the test section, assures equalization with the outside air pressure. Since in these experiments measurements were made in a free jet, the velocity measuring apparatus gm was in the open, and a rectangular standpipe sr was fitted on it. The free jet was intercepted by the jet collector st, which was mounted on a third truck, and then led back through guides and the quieting chamber br to the reservoir. The inlet pipe zr in these experiments had a length of only 1500 mm. due to lack of space.

(d): In order to reach still higher Reynolds' Numbers, the kinematic viscosity $\nu = \mu/\rho$ of the water was decreased by increasing the temperature. The same method was also applied to some of the measurements with the circulation setup, since the carrying out of the experiments with this setup required much less time and effort than the last experimental apparatus. The water was heated in a tank with steam. The tank delivered about 1.1 liter/sec. of water at 40°C. By decreasing the amount delivered, the water temperature could be increased to about 95°C, which, because of the cooling in the test apparatus, corresponded to a temperature of about 40°C in the test pipe. The tank was situated on the wall of the hydraulics laboratory and opened into the reservoir vk through a hose zf. As a result of the increase in the temperature of the water, the Reynolds' Number amounted to Re = 1400 (10^3) in the second setup, and Re = 3240 (10^3) in the third setup. The general picture of the setups for (c) and (d) is shown in Figure 3.

Part 2. Measuring Apparatus

(a): Velocity Measuring Apparatus with Throttling and Swivel Outlet.

The velocity measuring apparatus consisted of the housing m, the cover d, the spindles sp and su, the sliding carriage schl, and the movable pitot tube pt. The housing had windows f on both sides for observation purposes. In the center was a wall w, which was meant to prevent the reverse flow of fluid into the measuring chamber. The cover d was screwed tightly to the housing, in order that it could be made easily waterproof. A valve e was fitted on the cover for venting.

For the motion of the pitot tube, the spindles sp and su were provided, which at the same time carried the sliding carriage schl. The spindle sp had a screw of 1 mm lead and moved the carriage in the horizontal direction; it was turned from the outside and was sealed with a stuffing box. The movement of the spindle sp was recorded on a micrometer scale zw. In this way one could conveniently read off the displacement of .1 mm with the forward and backward motion of the carriage; the pitot tube was moved, at the same time, in the same direction.

The perpendicular motion of the pitot tube holder ph was accomplished with the spindle su, which had no screw, only a slot. By rotation of the spindle, the screw wheels were rotated. The screw wheel z had an internal screw with a 1 mm lead and screwed the pitot tube holder up and down; the holder was kept from rotating by the side guides fl. The movement was recorded on the scale zw_2 in the same way as for the spindle sp.

The total pressure to be measured was transmitted through the pitot tube holder ph, on which pitot tubes pt of different diameter could be fitted, and then through the hose s to the outside. Since

the velocity distributions were taken 0.1 to 0.2 mm after the exit end of the test pipe, the static pressure also had to be measured in this exact cross section; therefore, a hole scht of about 0.8 mm. diameter was bored in the flange of the test pipe. This hole was about 2 mm from the edge of the jet. The pressure here was essentially equal to that at the jet edge.

In order that the different quantities of flow could be finely regulated, a throttle valve dv was fitted on the velocity measuring apparatus (Figure 4). The position of the throttling cone dk was adjusted by the screw srsp (Figure 4) with its measuring scale msk.

The swivel outlet sch served to quickly conduct the fluid into the measuring tank for mass flow measurement and then to direct it away again quickly. A ball bearing kl made possible a very quick swiveling.

The velocity measuring apparatus, the throttling apparatus, and the swivel outlet were mounted together and were situated on the truck wg (Figure 5), which moved in the lengthwise direction on the already mentioned tracks on the reservoir.

(b): Measuring Tank

For the discharge measurements a cylindrical measuring tank mb (Figure 5) with a capacity of 700 liters with a diameter of 1000mm and height of 900 mm was used; it could be moved under the swivel outlet sch. In the bottom of the measuring tank was an outlet fitted with the valve ab. Ahead of the valve a water level gauge glass ws with millimeter divisions was arranged for reading off the height of the water level in the tank. The measuring tank stood on four screw feet sf, in order that it could be adjusted to horizontal. On the

surface of the water in the measuring tank floated a perforated wooden board, which damped the oscillations of the water surface, thus decreasing the time required to make a reading. For the measurement of smaller quantities a smiliar measuring tank of 178 mm diameter and 700 mm height was used. For the accurate determination of the measuring tank diameter, the relation between the water level in the gauge glass and water quantities previously determined by weighing (about 10 kg) was established.

(c): Micromanometer

The reading accuracy of ordinary water manometers was not sufficient for the small pressure differences occurring. A setup had to be produced which gave the required reading accuracy, and at the same time was useable at higher pressures. The problem was solved for the measurement of pressures from 0.02 mm to 500 mm as follows. On a horizontal glass tube with three valves h_1, h_2, and h_3 (Figure 6) two glass tubes were fused, one between each two valves. Between the two upper ends of these tubes a T-piece with 120° leg angles was so fused that one leg extended vertically upward. This end of the T-piece was closed with the valve h_5. The valve h_4 in another leg of the T-piece permitted breaking the connection between the two glass tubes. The free ends a_3 and a_4 of the glass tubes were closed with pinch clamps.

When this instrument was to be used as a water manometer, the two pressure leads were connected at a_1 and a_2, and the valves h_1, h_2, and h_4 were opened. When the instrument was to be used as a mercury manometer, the pressure leads were connected at a_3 and a_4, and h_3 was opened. For checking the zero point during operation h_3 was opened for the water manometer and h_4 for the mercury manometer. The region in which readings were made had a length of about 500 mm. The increase in measuring accuracy was obtained with reading

microscopes mi. On a massive brass base plate was mounted a four-edged precision tube, on which the two slides sl were arranged to move. Each slide carried a reading microscope mi with cross hairs. The motion was accomplished with a pinion and rack. The engageable and disengageable worm drive sn (Figure 7) made possible an accurate fine adjustment. The lower sliding carriage carried the measuring scale m with millimeter divisions; the upper carriage carried the vernier n divided in fiftieths. In front of the vernier a swiveled magnifying glass lu was used. Illumination was given by the lamp la (Figure 6), which was mounted to move behind the milk glass plate mg. The zone of the meniscus to be observed was darkened by the adjustable screens bl (Figure 7), so that it contrasted with the illuminated milk glass. The manometer was placed exactly vertical by means of adjusting screws and bubble levels (Figure 6).

(d): Arca Regulator

The Arca regulator (Figure 8), a gift of the "Arca Regler" Co., A.G. Berlin, W9, held the desired pressure constant in the water tank. The operation is as follows: Connection is made to the water distribution system with wl. A branch line leads to the throttle valve dr, which regulates the quantity of flow. The water acts on the piston ko and flows through the line l_2 to the disk valve tv, which closes when the pressure in the water tank is high and opens when it is low. The spring sf permits the adjustment of a definite pressure before starting the experiments. The diaphram bellows mb transmits the pressure to the disk valve tv by means of the lever h. If the pressure in the water tank falls off, the disk valve is opened. In this way the flow in l_2 is released; the water in the line l_2 is no longer dammed up; the piston

ko is forced upward by means of the piston spring kf, and with it the control piston sk. This now frees the water path below the piston hk. The water pressure now lifts this piston hk and thus raises the regulating valve rv, by which the compressed air tank dk is connected to the water tank wk. When the pressure in the water tank wk again reaches the correct pressure then this pressure acts through the pressure line dl on the bellows mb, and the disk valve tv closes. In this way the pressure on the piston ko is increased, and the piston is forced downward. Then the water flow from the supply line wl under the piston hk is again obstructed and the flow off wa is opened. The spring hf forces the regulating valve rv closed. By connecting the bellows mb to the water tank below the water line, rather than to the air space above the water level, the water pressure at the outlet port is held constant during the outflow independent of the water column height in the tank.

(e): Tripping Valve (15)

The tripping valve (Figure 9) was operated by compressed air at about 3 atmospheres and could be opened or closed in a time of about 0.1 to 0.2 seconds. The operation in opening or closing this valve is as follows:

By rotation of the control wheel sr a small valve ha is first opened by a cam, which allows compressed air to pass through the line l to the under side of the piston hk. This piston is raised and with it the cone k up to the stop schr, which was adjustable. Now the seating surfaces of the cone k are free, and the cone is rotated by the rotating piston drk. The compressed air is introduced to the control piston sk from the supply line le and fills the chambers ka (see section A-A). If the control wheel sr, and at the same time the

control piston sk, are turned by an electric or manual drive, the slots at c and d open, the compressed air flows through the slot c into the chambers ku and forces the rotating piston drk downward and with it the cone k of the valve. The air in the chambers ko escapes to the atmosphere through the slot d. When the cone k and the rotating piston drk turn through 90^{o}, the small valve ha closes and thus cuts off the air to the under side of piston hk. This piston together with the cone is then forced downward by the adjustable spring f. The closing operation is accomplished by the backwards rotation of the control wheel sr through the same procedure but in reversed order.

In order to prevent the cone k from oscillating, oil damping was provided (Section B-B). The damping piston dmk was joined solidly to the rotating piston drk. The chambers kd were filled with oil, and the inlets e were connected with the pipelines r and the gate valves sch. Upon rotation of the damping piston the oil was forced back through the tubes r and more or less throttled by the adjustment of the gate valves sch. At the instant when the damping piston dmk closed off the ports e, the oil was completely cut off except for leakage. By means of this oil cushion a sudden stop was prevented.

Part 3. Experiments

(a): Mass Flow Measurements.

Mass flow measurements up to a Reynolds' Number $Re = 300\ (10^3)$ were made with the measuring tank. Since there was no certainty that the measuring tank was accurately cylindrical, it had to be calibrated. Previously weighed quantities of water were put in the tank, and the water height in the gauge glass was read off. The calibration showed that the diameter was constant over the whole tank. The cross section of the large measuring tank amounted to $A = 7850\ cm^2$, and that of the

small tank A = 248 cm^2. For every measurement the lowest height in the gauge glass was read before the run and the higher level after the run. The readings were taken with perfectly quiet water and with a mirror, in order to prevent parallax. This method of reading made possible an accuracy of 0.1 to 0.2 mm. The water could be conducted into the measuring bottle in about 0.1 to 0.2 second by the swivel outlet. The duration of the run in the measuring tank was determined with a hand stopwatch. The stopwatch had been tested as to its timing and had 1/10 second divisions. The swivel outlet could then be turned back with equal speed. The duration of the runs was between 100 and 600 seconds. If we assume that a run of 100 sec. is measured accurately to 0.2 sec, and furthermore, that the water height in the gauge glass is read accurately to 0.2 mm., then the error in the flow measurement in the most unfavorable case amounts to 0.3%. This error reduces to 0.05% with a run of 600 sec. The largest error in mass flow results in an error in the average velocity u of 0.13%. The mass flows were determined as the average of several observations (4 to 6) and two different run times.

(b): Temperature Measurements

In general the temperature was measured with a thermometer at the discharge. In order to be certain that the water in the tube had the same temperature as at the discharge, the temperature of the water flowing out through the air vent eh (Figure 5) was also measured. These two temperatures were always found to agree. The thermometer was calibrated, and was divided in tenths of a degree. Thus about 1/20 to 1/30 of a degree could be estimated, which resulted in an error in kinematic viscosity of 0.05% to 0.08%. At the higher temperatures the error in kinematic viscosity is still smaller. The

measurements were undertaken at temperatures of 9° to 38°C. At usual water temperatures constancy of temperature was easily maintained; at higher temperatures, however there was some difficulty. As previously mentioned, the higher temperatures reached were such that the water flowing out of the tank into the reservoir vk (500 to 800 cm^3/sec) was at 80° to 90°C. By preliminary tests the quantity and temperature of this water necessary to obtain a definite temperature of the water in the test section during the duration of the test was found. Corresponding to the inlet, cooled water flowed out through the outlet af (Figure 1) at the lowest point in the reservoir vk.

(c): Determination of the Tube Radius.

If one calculates the pressure gradient $\frac{dp}{dx}$ in the stagnation pressure of the average velocity $\bar{q} = \rho \frac{\bar{u}^2}{2}$,then one obtains the dimensionless coefficient λ ,which is designated as the resistance coefficient.

$$\lambda = \frac{dp}{dx} \frac{2r}{\bar{q}} = \frac{dp}{dx} \frac{4\pi^2}{\rho Q^2} r^5$$

where ρ is the density of the water
Q is the volume of flow per unit time
r is the tube radius.

From this formula it is seen that the resistance coefficient λ which is to be determined from our experiments, is proportional to the fifth power of the radius. Therefore, this radius must necessarily be determined with the greatest possible accuracy. The tube radius was determined from the weight of water which completely filled the test pipe and the length of the section. The weighing was accomplished with an accuracy of $\pm$ 0.01%. The length could be measured accurately to 0.2 mm, which corresponds to an error of $\pm$ 0.007%. If one now calculates the error of the weight and the tube length for the most un-

favorable case, the error in the tube radius r becomes about 0.01%. This error is insignificant for the determination of the resistance coefficient λ.

(d): Static Pressure Measurements

The measurement of static pressure was made under the assumption that the static pressure is equal everywhere in the cross section of measurement. Since the static pressure can be measured quite accurately with well constructed wall taps if the wall is parallel to the direction of flow, the measurements of pressure drop were so undertaken. At each cross section where measurements were to be made four holes were drilled in the test pipe, which were joined by a ring-shaped equalizing chamber ak (Figure 10). The connection to a manometer could be made by means of a tap tü and hose lines. The other leg of the manometer was connected in the same way with the next cross section of measurement. In this way the pressure drop over a length l was measured. Very often a suction or pressure effect entered through the pressure tap holes, which were not perfect. (Raised promontories give a suction effect and cavities give a pressure effect). In order to get a reading of the pressure drop free of error, the most favorable form of the pressure tap hole was sought and the sharp-edged form was established as such. Also in order to determine the influence of the hole size, holes of 0.5 mm diameter were first used and then gradually they were increased to 1.2 mm diameter. In every case it was found that in the region investigated the size of the holes had no effect on the pressure indications.

In producing the sharp-edged hole, an accurately measured brass pin was fitted tightly in the tube at the hole position. In this way severe burr formation and bulging was prevented. By after-polishing

with fine emery paper backed by a wooden cylindrical block, the last burring was easily removed. By way of test, one section of tube containing a hole was cut out and examined with a microscope of 50 fold magnification. No burr could be seen.

Before attaching the equalizing chamber the holes were individually inspected for their quality. Each two holes were connected across a micromanometer. The testing was then undertaken at the greatest obtainable quantity of flow in order to make any errors present as large as possible. In cases where such errors appeared the tube was repolished.

In addition the pressure differences over two measuring sections l_1 and l_2 were measured. The pressure drop data were then only considered correct if equal pressure differences were found with equal lengths of the two measuring sections. In order to neutralize any error in the equality of the pressure differences, the tube was reversed with respect to the direction of flow. Then the same pressure difference had to be indicated at equal Reynolds' Numbers.

In order to obtain greater accuracy of the pressure gradient necessary for analysis, successively longer measuring sections were taken, as can be seen from Table 1. The lengths of the measuring sections were determined accurately to 0.2 mm. The pressure differences up to 50 cm of water or mercury were measured with a micromanometer of the type previously described. Greater pressure differences were obtained with an ordinary mercury U-manometer of 250 cm height.

(e): Velocity Measurements

The measurements of velocity were carried out by comparing the stagnation pressure of the pitot tube with the static pressure of the pressure tap, which was situated in the measuring cross section 2 mm from the edge of the jet, so that the manometer indicated directly

the dynamic pressure. The velocity was calculated with the formula

$$u = 44.3\sqrt{h} \text{ cm./sec.} \qquad (1)$$

where h is the measured dynamic pressure head in cm. of water, and u is the velocity in cm/sec.

This formula is obtained from the Bernoulli equation, which can be derived from the Euler motion equation for frictionless fluids subjected only to gravity by integration along a streamline. The Bernoulli equation then assumes the following form

$$\frac{p}{\rho} + \frac{u^2}{2} + H = \text{Constant} \qquad (2)$$

where H is the elevation of the point considered above a stationary specified horizontal plane.

By multiplying the Bernoulli equation by the density ρ one obtains the pressure equation

$$p + \rho\frac{u^2}{2} + \rho H = p_o \qquad (3)$$

If external forces (gravity) are excluded (since H in our cases has the same value at both probe openings), then the pressure equation becomes

$$p + \rho\frac{u^2}{2} = p_o \qquad (4)$$

p_o is the value of the largest pressure which builds up in the mouth of the pitot tube. It corresponds to the velocity zero and is called the total pressure; p is the static pressure. If one designates $p_o - p = h\gamma$ (with γ = specific weight and h = height of the water column), then one obtains from Eq. (4)

$$\rho \frac{u^2}{2} = h\gamma \qquad (5)$$

or with $\rho = \frac{\gamma}{g}$

$$u = \sqrt{2gh} = 44.3\sqrt{h} \text{ cm./sec.}$$

The velocity distribution was measured with a pitot tube 0.1 to 0.2 mm behind the exit cross section of the test section. The reliability of the measurement at this distance behind the exit cross section was determined from comparison with the velocity distributions which were measured 2 and 5 mm before the exit cross section (Figure 11). A subsequent measurement of the velocities at different Reynolds' Numbers on the tube axis at the exit and at the same time 20 d before the exit gave equal values. The measurements were therefore undertaken behind the exit cross section in order to avoid disturbing the pressure pattern, and also, more important, because only in this way could the velocity be measured up to the immediate vicinity of the wall.

Since the knowledge of the static pressure at the measuring cross section was very important for the measurement of the velocity distribution, this comparison measurement was carried out with a probe which was built into the tip of the pitot tube. In order to eliminate as far as possible the influence of the pitot tube holder on the static pressure, a casing vkl (Figure 4) with a symmetrical profile was so arranged that the probe was situated on the axis of symmetry of the profile. The side ports of the probe were situated in the measuring cross section. The probe was connected across a manometer with a pressure tap in the wall which lay exactly in the

measuring cross section. Since a pressure difference was not established in the manometer, it could be concluded that the static pressure outside the jet was equal to that at the probe. Therefore it was considered legitimate to measure the static pressure for velocity measurements with the pressure tap in the flange. Furthermore a value of $\frac{x}{d}$ (where x is the tube length and d the tube diameter) was sought by velocity measurements in a tube of 5 cm diameter and 500 cm original length, such that the velocity distributions appeared independent of the tube length. For this purpose velocity distributions were undertaken at a Reynolds' Number Re = 900 (10^3) and $\frac{x}{d}$ = 100, 65, and 40, which were obtained by cutting off the tube to these lengths. At all of these values the velocity distribution had already become independent of the tube length. Since in the main portion of the experiments the shortest running length $\frac{x}{d}$ was equal to 50, distance need not be investigated further. This result is reproduced in dimensionless representation in Figure 12.

Pitot tubes of 0.21 mm and 0.30 mm inside diameter and 30 mm length, which were made conical on the basis of flow principles, were used for the measurement of the velocity distribution. In Figure 13 is shown the situation with the pitot tubes at the edge of the test pipe. In this position the indications from the pitot tube do not correspond to the prevailing dynamic pressure at that point. This is explained by the fact that only a portion of the pitot tube opening is in the water stream, and the other portion lies outside the stream, so that the water entering the opening flows out again sideways. However, since the accurate knowledge of the dynamic pressure is also of importance near the wall, a method was developed by which a correction could be made to the velocity measurements in this region. For this

purpose the velocity distribution was measured with three pitot tubes of different inner diameters, namely 0.3, 0.582, and 1.045 mm, at one and the same Reynolds' Number. By extrapolation these measurements served to define the velocity distribution which one would have measured with a pitot tube of zero diameter. In Figure 13 the distance from the wall is plotted as the abscissa and the velocity as the ordinate. If one draws a straight line through points of equal velocit (parallel to the abscissa axis) and plots the corresponding inner diameter of the pitot tubes as a vertical distance at each individual point, then a curve may be drawn through the end points of these distances, which by extrapolation gives an intersection with the straight lines. These intersections are points of a new curve which expresses the velocity distribution which one would obtain with a pitot tube of zero inner diameter. When the pitot tube opening lies completely in the water stream, then, as Figure 13 shows, no correction is required.

For this case the measured velocity curves meet with the theoretical curve at point A_i ($i = 1,2,3$). The distance of point A_i from the wall is also equal to the inner diameter r_i ($i = 1,2,3$) of the opening of the pitot tube used for measurement. In order to determine the correction for any arbitrary pitot tube opening, one draws a vertical line through the point A_i (corresponding to the given r_i) to the abscissa axis (dashed in Figure 13) and determines the distances y' and y'' of this line from two points on the theoretical and the measured curves (respectively) which correspond to equal velocities.

In this way pairs of values are obtained for different Reynolds' Numbers, which pairs are reproduced in dimensionless form in Figure 14. If one has measured a velocity distribution and wants to adjust it in

the vicinity of the wall to the velocity distribution one would have obtained with a pitot tube opening of zero inner diameter, then one uses this figure (Figure 14), displacing the velocities which are measured at the distance y'' to the corresponding distances y'.

In order to establish the percent error in the quantity of flow, which was obtained by integration of the uncorrected velocity distributions, the measured velocities, which were obtained by measurement with different pitot tube openings, were plotted in Figure 15 in relation to the square of the distance from the tube axis, and the quantity of flow was calculated by graphical integration. The corrected velocity distribution is represented by Curve 1 in this figure. Curves 2, 3, and 4 correspond to the velocity distributions which were obtained by measurement with pitot tube openings d = 0.3 mm, 0.582 mm, and 1.054 mm. The table of numbers in Figure 15 shows that the quantity of flow for the corrected velocity distribution amounts to Q_o = 1256 cm^3/sec. One also sees that with decreasing pitot tube opening the graphically determined volume rate of flow decreases toward the measured volume rate of flow (which agrees with that determined graphically from the corrected curve). The velocity distributions represented in Figure 15 were measured in a tube with a diameter d = 2c Similar experiments were made in tubes with diameters d = 3cm, d = 5cm, and d = 10 cm, and the results are shown in Figure 16. Here the dimensionless pitot tube opening d_i/d, which is formed by dividing the diameter of the pitot tube tip by the pipe diameter, is plotted as the abscissa, and the percent error in the volume rate of flow $100\ \frac{(Q-Q_o)}{Q}$ is plotted as the ordinate. This diagram permits the error occurring at a definite ratio $\frac{d_i}{d}$ to be specified.

Part 4. Carrying Out the Experiments

Carrying out the tests with the overflow setup was very simple since the constancy of volume rate of flow was automatically taken care of. When one wanted to undertake the measurements of the velocity distribution, he placed the throttling cone dk (Figure 4) of the velocity measuring apparatus at a definite position which corresponded to the desired volume rate of flow (the relation between the volume rate of flow and the position of the throttle in the velocity measuring apparatus was known from preliminary tests). Then one passed through the water supply line into the water tank just enough water to give a very small overflow. With the micromanometer I, which served to measure the pressure drop, and micromanometer II, which served to measure the velocities, tested as to the correctness of their indications, one determined the tube axis by velocity measurements, the axis then being considered as the reference point for the actual measurements. Then the measurements were begun, consisting of, besides the velocity measurements, the measurements of pressure drop, temperature, and the volume rate of flow.

The experiments with circulating water were more difficult inasmuch as current fluctuations in the electrical circuit caused variation in the speed of the driving motor and thus variation in the rate of flow in the test pipe. Therefore it was necessary to hold the pressure drop constant with the fine regulation of the throttling cone dk.

Carrying out the measurements with the forced flow setup was accomplished by first breaking the connection between the water tank wk (Figure 1) and the compressed air tank dk, and then letting the compressed air, which was in the water tank from the preceding

experiment, escape through the safety valve ksv of the water tank. While the compressed air in the compressed air tank dk was brought up to pressure (about 10 atm. in all measurements) by means of a compressor, the connection between the centrifugal pump kp and the water tank wk was made, and the tank filled with water to a definite height. In the meantime the exit cross section of the test pipe was sealed off with oil paper, which was placed between the flange of the test pipe and a ring flange adjusted to the tube cross section, and now with the aid of a by-pass on the tripping valve sh, the feed tube zr and the test pipe vr were filled with water. The air existing in the feed pipe (zr) could escape through the opened check valve sv. Now the connection between the compressed air tank dk and the water tank wk was remade through the Arca-Regulator, which was previously adjusted to a definite pressure. In this way the preparation was completed, and the actual experiment could begin. The tripping valve was opened at a sign from the manometer observer; the oil paper was torn by the water pressure. After the flow became stabilized at constant conditions, the observer determined the limit of the manometer heights by means of the sliders which were made easily movable on the legs of the manometers (Figure 3). The tripping valve remained open until the water level in the water tank had fallen to about 40 to 50 cm. above the exit cross section. Then the manometers were read, and the preparations for the next test could be started.

II. Evaluation of the Experiments

Part 1 - Velocity Distribution

The velocity distributions have been measured in tubes of 1, 2, 3, 5, and 10 cm diameter from small Reynolds' Nos. (Re = $4 \cdot 10^3$) to the largest Reynolds' No. studied by us 3240(10^3). As is obvious from the further evaluation of velocity distribution, a more accurate knowledge of the velocity distribution is important not only in the vicinity of the wall, where a steep velocity gradient exists, but also near the center of the tube, where only a small velocity gradient is produced.

Therefore, the points of measurement near the wall and near the tube center are chosen especially close together (the velocity distribution across the tube radius contains altogether 18 measured points). The velocity distribution was symmetric and showed either none or only a small difference for points equally distant from the tube axis on each side of the center. About 150 velocity profiles have been measured, from which, however, only 16 profiles have been used for the complete analysis. On account of the complete symmetry of the profiles only one half of the profile has been used in the analysis. The numerical values of these 16 velocity profiles across the tube radius are tabulated in Table 2. In order to obtain the velocity distributions at the smallest possible Reynolds' Nos. the entrance to the tube of 10 mm diameter is covered centrally with a plate which has an opening of 6 mm diameter. The plate produced a violent eddying at the entrance, so that at a Reynolds' No. of Re = $4 \cdot 10^3$, the turbulent flow was already fully developed. Only the three smallest Reynolds' No. were measured with this arrangement.

In order to follow the variation in the form of the velocity dis-

tributions in relation to Reynolds' No., the velocity distributions are made dimensionless in such a way that the local velocities are referred to the maximum velocities and the corresponding distances from the wall are referred to the tube radius. Thus, we obtain the relation

$$\frac{u}{U} = f\left(\frac{y}{r}\right) \qquad (6)$$

which is represented in Figure 17 for six profiles from Re = $4(10^3)$ to $324(10^3)$. This representation shows very clearly that the velocity distribution becomes fuller with increasing Reynolds' Nos. This fact leads us to the conclusion that with very large Reynolds' Nos. the region influenced by viscosity becomes vanishingly small. In Figure 18 the velocity distributions are plotted with $\frac{u}{U}$ as the ordinate, $\log \frac{\bar{u}d}{\nu}$ as the abscissa, and the dimensionless distance from the wall $\frac{y}{r}$ as the parameter. The velocities $\frac{u}{U}$ corresponding to a particular distance from the wall $\frac{y}{r}$ are joined with a curve which is designated by the $\frac{y}{r}$ value belonging to it. This diagram shows that a marked scattering appears for the velocities near the wall. If one wishes to obtain a dimensionless velocity distribution within the measured region, he needs only to select the curve of $\frac{u}{U}$ vs. $\frac{y}{r}$ for the given Reynolds' No. In order to prove how far the velocity distributions as measured by us agree with those obtained by other investigators, let us make the following comparisons:

The most reliable measurement of velocity distribution up until this time is that of T. E. Stanton [16]; first, because he has undertaken the measurements with a very fine pitot tube of 0.33 mm diameter, and second, because he had a sufficiently long, straight test section, $x = 72\,d$ (x = tube length, d = tube diameter = 7.4 cm),

so that his measurements were taken in a region in which velocity distribution no longer changes. A comparison of our measured results with those of Stanton appeared all the more necessary, since Stanton has measured the velocity distribution shortly before (2 to 3) the exit end of the test section, while our measured cross section was 0.1 to 0.2 mm. after the exit end. For this reason the velocity distributions, which belong to approximately equal Reynolds' Nos., are plotted in such a way that the ratio of the local velocities u to the maximum velocity U are taken as a function of the dimensionless distance from the wall $\frac{y}{r}$. The measurements of Stanton are undertaken at Reynolds' Nos. of Re = $37.6 \cdot 10^3$, $56 \cdot 10^3$, and $89.3 \cdot 10^3$. Our measurements give good agreement with those of Stanton at about the same Reynolds' Nos. Figure 19 shows a comparison of the velocity distribution of Stanton at Re = $56 \cdot 10^3$ with ours at Re = $59 \cdot 10^3$. In this connection the following should be noted: data on the average velocity $\bar{u}$ and the kinematic viscosity ν are absent in Stanton's work. We have determined from Stanton's data the average velocity $\bar{u}$ = 1235 cm/sec from the mass flow, which is obtained by integration of the velocity distribution. Since the measurements by Stanton are carried out with air, in which the variation of kinematic viscosity with temperature is very small, we have taken the kinematic viscosity at an average laboratory temperature of 18°C.

For very large Reynolds' Nos. it seemed useful to us to call upon the velocity distributions measured by Bazin [17] for comparison. The test section in Bazin's apparatus measures about $x = 75d$ (d = 80 cm) in length. Data on the temperature and the average velocity in Bazin's work are also unavailable. For this reason the average velocity $\bar{u}$ = 164.9 cm/sec has been obtained from his data by us,

again by integration of the velocity distribution. Bazin's measurements were carried out in free humid air in which temperature variations of 10° to 20° occurred. Indeed, the kinematic viscosity in this temperature region is very dependent on the temperature; on the other hand, the variation of velocity distribution with Reynolds' No. at such very large Reynolds' Nos. as occur here is very small. On the basis of these considerations we have set the kinematic viscosity at $15^{\circ}C$ ($\nu = 0.0113$ cm^2/sec).

Figure 19 also shows a comparison of Bazin's velocity distribution with ours. Except for the last points measured by Bazin in the vicinity of the wall, good agreement is shown by the velocity distributions at approximately equal Reynolds' Nos.

Part 2 - The Power Rule

Prandtl [18] has concluded from the Blasius resistance law that the velocity u in the vicinity of the wall in a turbulent stream varies with the $1/7$ power of the distance from the wall; that is,

$$u = a y^{1/7} \tag{7}$$

where a is a constant for any one velocity profile. The calculation can be carried out as follows: In the formula for the resistance coefficient

$$\lambda = \frac{dp}{dx} \cdot \frac{2d}{\rho \bar{u}^2} \tag{8}$$

we replace the pressure gradient $\frac{dp}{dx}$ by the shearing stress at the wall. The equilibrium condition for a fluid cylinder with radius r and length dx gives

$$\frac{dp}{dx} = \frac{2\tau_0}{r} \tag{9}$$

and thus

$$\lambda = \frac{2\tau_0}{r} \cdot \frac{2d}{\rho \bar{u}^2} \tag{8a}$$

From this it follows that $\frac{\tau_0}{\rho} = \frac{\lambda \bar{u}^2}{8}$. If we introduce the Blasius value $\lambda_B = 0.316(Re)^{-1/4}$ for the resistance coefficient λ , we obtain

$$\frac{\tau_0}{\rho} = K \bar{u}^2 \left(\frac{\bar{u} 2r}{\nu}\right)^{-1/4} \tag{10}$$

or

$$\frac{\tau_0}{\rho} = K \bar{u}^{7/4} r^{-1/4} \nu^{1/4} \tag{10a}$$

where K is same number. The solution of this equation for $\bar{u}$ gives

$$\bar{u} = K' \left(\frac{\tau_0}{\rho}\right)^{4/7} \left(\frac{r}{\nu}\right)^{1/7} \tag{11}$$

According to the Prandtl hypothesis, neither the tube radius nor the velocity at the center should be directly proportional to the wall friction, but the wall friction should first of all be determined by the velocity distribution in the vicinity of the wall.

If the ratio of the average velocity to the maximum velocity is taken as constant, it follows from Equation (11) that

$$U = K' \left(\frac{\tau_0}{\rho}\right)^{4/7} \left(\frac{r}{\nu}\right)^{1/7} \tag{12}$$

This relation can be rewritten in the desired form if we put y for r and substitute the u corresponding to a certain y for U :

$$u = K'' \left(\frac{\tau_0}{\rho}\right)^{4/7} \left(\frac{y}{\nu}\right)^{1/7} \tag{13}$$

Since the velocity distribution is measured at constant values of

$\frac{\tau_0}{\rho}$ and $\nu = \frac{\mu}{\rho}$, we get from Equation (13)

$$u = \text{constant } y^{1/7}$$

$$\text{or } u = a\, y^{1/7} \qquad (14)$$

As can be easily further proved, Equation (11), that is, the Blasius law, is also fulfilled by the velocity distribution of Eq. (13). This resistance law, $\lambda_g = 0.316 (Re)^{-1/4}$, according to which the resistance coefficient is inversely proportional to the fourth root of the Reynolds' No., is valid up to $Re = 100 \cdot 10^3$. Since this Blasius resistance law was the basis for the derivation of the 1/7 power rule, we cannot expect the power rule to be valid for Re above this limit. In the valid region of the Blasius resistance law the slope of the log λ - curve is equal to 1/4. For high Reynolds' Nos. this slope becomes smaller and decreases in the range investigated by us almost to 1/6. If we take, for example, λ proportional to $(Re)^{-1/6}$, the method of calculation described above gives $u = a\, y^{1/9}$. That means that the exponent $n = 1/7$ decreased to 1/8 , 1/9 , etc., with increasing Reynolds' Nos. At $Re = 3240 \cdot 10^3$ the exponent is about $n = 1/10$. The variation of the exponent with increasing Re thus becomes smaller and smaller. Of course, such a power law with a variable exponent can only be considered as an approximate formula. Also in the Blasius region, the 1/7 power rule appears to be only an approximation, as the findings indicate. If we write the power rule in the form

$$u = a\, y^n \qquad (15)$$

and plot the log of the measured velocity in relation to the log of

the distance from the wall, we obtain the n value from the slope of the curve. In Figure 20 the exponent $1/n$ of the velocity is plotted in relation to the distance from the wall for various Reynolds' Nos. We see that in the region of smallest Reynolds' Nos. the exponent has the value $1/n = 6$ at about $Re = 4 \cdot 10^3$. From about $Re = 10 \cdot 10^3$ to $100 \cdot 10^3$, where the Blasius resistance law is valid, we have $1/n = 7$, and at $Re = 3240 \cdot 10^3$ the exponent increases to $1/n = 10$.

If we proceed from the assumption that a specific relation exists between the shearing stress at the wall τ_0, the distance from the wall y, and the velocity u, we can, as follows from Equation (9), & (10), get the relation

$$\frac{\tau_0}{\rho u^2} = f\left(\frac{uy}{\nu}\right) \qquad (16)$$

The quantity $\frac{uy}{\nu}$ is a kind of Reynolds' No., which is related to the distance from the wall y. If we express the velocity distribution in the form of the Prandtl power rule, we obtain the relation

$$\frac{\tau_0}{\rho u^2} = \zeta\left(\frac{uy}{\nu}\right)^m \qquad (17)$$

where ζ is a dimensionless number which can be obtained from the measured velocity distribution in relation to the wall shearing stress belonging to it. In this relation $m = \frac{2n}{1+n}$. If we take the log of both sides of Equation (17) we get

$$\log\left(\frac{\tau_0}{\rho u^2}\right) = \log \zeta + m \log\left(\frac{uy}{\nu}\right) \qquad (18)$$

If we get $\log\left(\frac{\tau_c}{\rho u^2}\right)$ from the measured velocity distribution and plot it in relation to $\log\left(\frac{uy}{\nu}\right)$, we can read off the dimensionless constant ζ from the ordinate at the point where

$\log\left(\frac{u\,y}{\nu}\right) = 0$, as soon as we have connected the points obtained with a straight line. The constant m, which appears as the exponent of the dimensionless distance from the wall (Equation 15) and corresponds to the exponent 1/4 in the Blasius resistance law, can be obtained from our experiments. By solving Equation (18) for m , we get

$$m = \frac{\log\left(\frac{\tau_o}{\rho u^2}\right) - \log \zeta}{\log\left(\frac{u\,y}{\nu}\right)} \qquad (19)$$

The constants ζ obtained from the experiments and the exponent m are plotted in Figure 21 in relation to $\log\left(\frac{\bar{u}\,d}{\nu}\right)$. In Figure 22 m is plotted in relation to the exponent n .

Part 3 - Universal Velocity Distribution

In a new interpretation of his ideas, Prandtl no longer uses any power formulas as a basis, but proceeds only on the basis that the velocity in the vicinity of the wall depends only on the physical quantities which are valid in the vicinity of the wall (τ_o = shearing stress at the wall, ν = viscosity constant, ρ = density), while it is independent of the distance from the opposite wall and of the average or maximum velocity. Now we form, according to Prandtl (19), from the shearing stress at the wall and the density ρ a quantity characteristic of the friction condition, $v_* = \sqrt{\frac{\tau_o}{\rho}}$, which has the dimension of a velocity. With this quantity a dimensionless velocity may be formed in which we divide the local velocity u by v_* , $\phi = \frac{u}{v_*}$. In the same way we form from the distance from the wall y , the velocity v_* , and the kinematic viscosity $\nu = \frac{\mu}{\rho}$, a term something like a Reynolds' No. -- a "dimensionless distance from

the wall", $\eta = \frac{v_* y}{\nu}$. Thus, we obtain in the vicinity of the wall a universal velocity distribution $\phi = \phi(\eta)$. This relationship is represented in Figure 23 (Table 3). In this Figure the dimensionless velocities are shown for a range of Reynolds' Nos. ($4 \cdot 10^3$ to $3240 \cdot 10^3$). On account of the large range of abscissas, $\eta = \frac{v_* y}{\nu}$, three different scales are used. The indicated points are results of measurement.

The universal velocity distribution becomes still more evident if, instead of η , the quantity $\log \eta$ is used as the abscissa, Figure 24. It is to be noted that within a slight scattering the experimental points lie on a straight line. Upon closer examination it is seen that the experimental points for a given Reynolds' No. do not lie accurately on a straight line, but trace a systematic course above and below it. Here it may be mentioned that the measured points reach to the tube center, while according to the Prandtl hypothesis only points in the vicinity of the wall should lie on a smooth curve. The latter is fairly well fulfilled. For $\log(\eta) < 1.0$ in this case a systematic deviation from the straight line is distinguishable.

If we consider particularly points lying near the tube axis, we can represent the graphical straight line #1 in Figure 24 by the equation

$$\phi = 5.5 + 5.75 \log \eta \qquad (20)$$

With this equation we have calculated the η values belonging to a series of ϕ values, and accordingly in Figure 23 we have drawn the curve passing through the experimental points.

For further approximate calculations, however, it is important to favor the points near the wall. Straight line #2 passing through

these points is represented by the equation

$$\phi = 5.84 + 5.52 \log \eta \qquad (20a)$$

In laminar flow, if the velocity u depends only on y, we have for the shearing stress the expression

$$\tau_0 = \mu \left(\frac{du}{dy}\right)_0$$

where $\left(\frac{du}{dy}\right)_0$ is the value of $\frac{du}{dy}$ at the wall, and μ is the viscosity,

$$\text{or} \quad du = \frac{\tau_0 \, dy}{\mu}$$

By integration of this equation we get

$$u = \frac{\tau_0 y}{\mu}$$

If we now put $\tau_0 = \rho v_*^2$ and $\mu = \rho \nu$, then we can write

$$\frac{u}{v_*} = \frac{v_* y}{\nu}$$

$$\text{or} \quad \phi = \eta$$

It is estimated that this relation is valid only up to $\eta = 10$ as a result of the establishment of the turbulent mixing process. This laminar range is shown in Figure 21 by the lower dotted curve. If we divide Equation (13) by $v_* = \sqrt{\frac{\tau_0}{\rho}}$ and substitute ϕ for $\frac{u}{v_*}$, η for $\frac{v_* y}{\nu}$, and calculate the numerical factor, we get

$$\phi = 8.74 \, \eta^{1/7} \qquad (13a)$$

The curve corresponding to this formula is shown dotted in Figure 24. We see that the validity is limited in the range of $\log \eta$ = 1.6 to 2.6.

With this straight line rule we can calculate, with good approximation, the velocity distribution for any arbitrary Reynolds' No., given the physical quantities τ_0, $\nu = \frac{\mu}{\rho}$, and the tube radius r. From the equation of the straight line obtained, we can calculate the ϕ corresponding to various distances from the wall, and we can determine the local velocity u by multiplying by the velocity v_*; $u = \phi v_*$ From the dimensionless distance η, we can obtain the corresponding distances from the wall, $y = \frac{\nu r}{v_*}$. Thus we obtain the velocity distribution $u = f(y)$ for a definite Reynolds' No. In Figure 25 the velocity distributions obtained by this method are shown in dimensionless representation. These dimensionless velocity distributions are shown for Reynolds' Nos. from $Re = 10^5$ to $Re = 10^9$, and they show the variation in the form of the velocity distribution with Reynolds' No.

Of course, it seems somewhat hazardous to calculate the velocity in the center of the tube from a law which defines the velocity only near the wall; however, the velocity differences in the center part of the tube are generally not large. Moreover, the results shown in Figure 24 do yield to this method. Of course, the values at the center nevertheless become inaccurate; the actual velocity distribution show here a horizontal tangent which, contrary to the formula used, shows a finite, if small, slope. This variation, however, makes little difference for the volume of flow.

Part 4 - Mixing Length and Exchange Quantity

In laminar flow, if the velocity u depends only on y, we have the expression for the shearing stress

$$\tau = \mu \frac{du}{dy} \qquad (21)$$

where μ = the viscosity constant. Likewise, in turbulent flow we get, according to Boussinesq [21], for the apparent shearing stress caused by the turbulent impulse exchange

$$\tau' = A \frac{d\bar{u}}{dy} \qquad (22)$$

where $\bar{u}$ = the average (with respect to time), local value of the velocity and A = the exchange quantity. The exchange quantity is not constant but varies from point to point in the fluid. The essential thing now is to bring A into relation with the velocity distribution. For this purpose we imagine, according to Reynolds, the velocity to be decomposed into an average (with respect to time) local value and the fluctuations about this value. We say, therefore,

$$u = \bar{u} + u' \qquad v = \bar{v} + v'$$

where u and v are instantaneous local velocities in the x and y directions, and u' and v' are local fluctuations of the x or y component of the velocity. The velocity fluctuation causes an apparent stressed condition which is given by the following equations

$$\sigma_x = -\rho \overline{u'^2}, \quad \tau_{xy} = -\rho \overline{u'v'}, \quad \sigma_y = -\rho \overline{v'^2} \qquad (23)$$

It is of importance now to express the velocity fluctuations u' and v' in terms of the "main stream" $\bar{u}$ and $\bar{v}$. This has been successfully done by Prandtl with the following consideration. We assume for simplicity's sake, as in Equations 21 and 22, that the main stream flows parallel to the x-axis, and that velocity gradients are produced transverse to the main stream direction. For the turbulent condition the length l, which Prandtl designates as the mixing length, is characteristic of the flow. The physical meaning of the mixing

length l is that in turbulent flow small masses of fluid possess a characteristic motion, and consequently, move a certain distance l transverse to the direction of flow before they are mixed with the new surroundings. Now if a small fluid mass, which originates at a point with the velocity $\bar{u}$, moves transverse to the main stream a distance l, its velocity differs from the average velocity of the new point in close approximation to the amount $l \frac{d\bar{u}}{dy}$. Therefore, we have for the shearing stress, according to Equation 23, and if we take the proportionality constant in with the still unknown l,

$$\tau = \rho l^2 \left|\frac{d\bar{u}}{dy}\right| \frac{d\bar{u}}{dy} \qquad (26)$$

By putting "absolute value" signs on one factor and not on the other, it is assured that τ changes sign with $\frac{d\bar{u}}{dy}$. By comparison of this Prandtl statement for the shearing stress with Equation (22), we find for A the formula

$$A = \rho l^2 \left|\frac{d\bar{u}}{dy}\right| \qquad (27)$$

This Prandtl statement, which gives a thorough physical analysis of turbulent flow, has led to an accurate calculation of the turbulent flow in many cases. For flow in circular tubes, satisfactory regularities can be found by means of this equation. If we divide Equation 22 by the density, we get

$$\frac{\tau}{\rho} = \frac{A}{\rho} \frac{du}{dy}$$

If we now put $\frac{A}{\rho} = \epsilon$, where ϵ represents a kinematic measure of the turbulent impulse exchange, we get

$$\frac{\tau}{\rho} = \epsilon \frac{du}{dy}$$

or

$$\epsilon = \frac{\tau}{\rho} \div \frac{du}{dy} \qquad (28)$$

Thus, we get the kinematic exchange quantity by dividing the "kinematic shearing stress" $\frac{\tau}{\rho}$ by the differential quotient of the velocity $\frac{du}{dy}$. The magnitude of this differential quotient across the tube radius is obtained graphically from the measured velocity distribution. Since the quantity $\frac{du}{dy}$ and $\frac{\tau}{\rho} = \frac{r-y}{2\rho} \frac{dp}{dx}$ (derivation as in Equation 9), both tend to zero on approaching the tube axis, the determination of the impulse exchange quantity in this region is inaccurate. Therefore, measured points for the determination of the velocity distribution on the tube axis were taken closer together. In order to draw a velocity curve from the measured values of the velocity which gives a smooth course of the $\frac{du}{dy}$ values, the differential quotients are formed from the measured points and these are then connected by a smooth curve. From this curve the curve of the velocity distribution is now determined at small distances from the tube center. By this method it was possible to calculate more accurately the ϵ values in the neighborhood of the tube axis. In this way the values in the measured range of Reynolds' Nos. (from $4 \cdot 10^3$ to $3240 \cdot 10^3$) were obtained for the above mentioned 16 velocity profiles, and they are again given in Table 4. In order to make the distribution of the ϵ values across the tube radius comparable for all ranges of Reynolds' Nos., they were divided by $v_* r$ (since ϵ has the dimension of velocity times length), where $v_* = \sqrt{\frac{\tau_0}{\rho}}$ and thus has the dimensions of a velocity. The corresponding conditions

of the wall are referred to the tube radius. The relationship

$$\frac{\epsilon}{v_* r} = f\left(\frac{y}{r}\right)$$

is represented in Figures 26 and 27. If we consider this relation in Figure 26, we see that the $\frac{\epsilon}{v_* r}$ values decrease with increasing Reynolds' Nos. to a constant value, which in this figure is shown as a dotted curve. In Figure 27 the $\frac{\epsilon}{v_* r}$ values are recorded for Reynolds' Nos. greater than $100 \cdot 10^3$. They give, except for a certain scattering of points, a curve which is independent of Reynolds' Number. This curve corresponds to the dotted curve in Figure 26. The dot-dash curve of Figure 27, which represents the $\frac{\epsilon}{v_* r}$ values in the neighborhood of the tube axis, is found by extrapolation. It is characteristic for the course of these values, that the exchange quantity at the wall is zero, since no exchange can occur here; with increasing distance from the wall $\frac{\epsilon}{v_* r}$ increases quickly and almost linearly and reaches a maximum at $y = \frac{r}{2}$. On approaching the tube axis $\frac{\epsilon}{v_* r}$ falls again to a very small value. At the sharp rise in the neighborhood of the wall, one observes considerable scattering of the $\frac{\epsilon}{v_* r}$ values, just as in the neighborhood of the tube axis. That is explained by a strong influence of viscosity which exists in the neighborhood of the wall.

From $\epsilon = \frac{A}{\rho} = l^2 \frac{du}{dy}$, it is evident that the mixing length

$$l = \sqrt{\frac{\epsilon}{\frac{du}{dy}}} \qquad (30)$$

The variation of the mixing length across the tube radius has been

calculated according to this formula for different Reynolds' Numbers, and it has been tabulated in Table 5. The relation between mixing length l and distance from the wall y appears in the dimensionless representation $\frac{l}{r} = f\left(\frac{y}{r}\right)$ in Figures 28 and 29. We see that the mixing length in the immediate vicinity of the wall (up to about $\frac{y}{r} = .07$) increases from zero almost linearly. Karman expresses this linear increase as $l = xy$, where y is the distance from the wall, and x is a proportionality constant; this constant has the value $x = 0.38$ (Figure 29) for $Re = 100 \cdot 10^3$ (Figure 28). Above the value $\frac{y}{r} = 0.07$ the mixing length climbs less steeply and reaches at the tube axis a fixed value, about $\frac{l}{r} = 0.14$ (Figure 29). In this figure the values of the dimensionless mixing length are recorded for the five Reynolds' Numbers $Re = 105 \cdot 10^3$ to $3240 \cdot 10^3$: they give the same curve, within a very small scattering. From this diagram we recognize that with further increases in Reynolds' Number, the values of the dimensionless mixing length $\frac{l}{r}$ for a definite dimensionless wall distance $\frac{y}{r}$ do not decrease further. It is seen, therefore, that for the Reynolds' Numbers given in Figure 29, the influence of viscosity is no longer present. Below $Re = 100 \cdot 10^3$ we observe, as a result of the influence of viscosity, a change in the dimensionless mixing length $\frac{l}{r}$ with Reynolds' Number, and, in fact, $\frac{l}{r}$ increases with decreasing Reynolds' Number. Thus, we obtain, for different Reynolds' Numbers in Figure 28, different $\frac{l}{r}$ curves. The relation $\frac{l}{r}$ as a function of $\frac{y}{r}$, as it is shown in Figure 29, can be given again by the following interpolation formula from Karman:

$$\frac{l}{r} = 0.14 - 0.08\left(1 - \frac{y}{r}\right)^2 - 0.06\left(1 - \frac{y}{r}\right)^4 \qquad (31a)$$

out of which can be obtained:

$$\varkappa = \left[\frac{dl}{dy}\right]_{0,y} = 0.40$$

Bearing in mind the viscosity, we obtain a dimensionally correct statement for the relation between mixing length and wall distance by the following consideration. The flow relations are, of course, defined by the physical quantities τ_0, ρ, μ, and y alone. From these quantities the already mentioned dimensionless quantities $\frac{\rho y}{\mu}\sqrt{\frac{\tau_0}{\rho}} = \frac{v_* y}{\nu}$ can be formed. So, for the mixing length one obtains the statement:

$$l = y\, f\left(\frac{v_* y}{\nu}\right) = y\, f(\eta) \qquad (32)$$

We can conceive of $\eta = \frac{v_* y}{\nu}$ as a (of course, variable) Reynolds' No. in the neighborhood of the wall. The function f is to be obtained empirically. Since

$$v_* = \sqrt{\frac{\tau_0}{\rho}} = l \left|\frac{d\bar{u}}{dy}\right| \qquad (33)$$

$$\frac{d\bar{u}}{dy} = \frac{v_*}{l} = \frac{v_*}{y\, f(\eta)} \qquad (34)$$

or by integration:

$$\bar{u} = \int_{y_0}^{y} \frac{v_*\, dy}{y\, f(\eta)} \qquad (35)$$

This formula clearly joins the velocity distribution with the resistance law. The lower limit of the integral, which is here designated as y_0, with a sufficiently accurate formula for $f(\eta)$ in the neighborhood of the wall assumed, is to be set equal to zero

in a smooth tube, and equal to a length characteristic of the roughness in a rough tube. The determination of the f - function results from the measured velocity distribution with which one first calculates l and then plots $\frac{l}{r} = f(\eta)$. This relation appears in Figure 30 (Table 6) on a logarithmic scale. Each of the curves running from top to bottom expresses a definite Reynolds' No. which is noted as a parameter. The highest points on the curves are in the immediate vicinity of the wall. The curves running from left to right connect points of equal $\frac{y}{r}$ value. The diagram shows further that for a definite $\frac{y}{r}$ curve above a Reynolds' No. of $100 \cdot 10^3$, the $\log \frac{l}{r}$ values are equally great for all Reynolds' numbers. The equality of these values gives new evidence that in this range of Reynolds' Nos., disregarding the immediate vicinity of the wall, no effect of viscosity is present.

Part 5 - Similarity Considerations

Recently Karman has succeeded in proving the Prandtl mixing length rule from a different viewpoint.

We can make, at present, two different basic assumptions about the character of the relationship between turbulent stresses and the flowing field. We can assume that the turbulent stresses can only be explained by an "integral law" of the whole flowing field with its edge conditions, or that the turbulent stresses at a given point are continually determined by the behavior of the adjacent environment and thus by a "differential law". For the stresses produced by molecular motion, and thus laminar flow, it is a well-known case of a differential law; the laminar stresses can be expressed by the velocity gradients at the point in question and the constant of

internal friction, as follows:

$$\tau = \mu \frac{du}{dy} \tag{36}$$

Karman has proved the assumption of a differential law for turbulent stresses. In order that such an equation can exist, the secondary motion must not have a large spatial dimension, as far as it is coherent, and further, it must flow similarly at individual points in the flow field. Since the consideration is valid only for large Reynolds' Nos., we can generally also neglect the influence of viscosity.

The mathematical formulation is now simple. Karman now makes the requisite assumption which is conditioned for the following derivation, that the secondary motion, in a coordinate system, which takes part in the main motion of the observed point, is stationary. The total motion is two-dimensional, the main motion U in the x direction being dependent only on the transverse coordinate y. We let the origin of the coordinate system introduced above synchronize with the points under consideration so that the main velocity in the vicinity of the observed point

$$U = U_o' y + \left(\frac{U_o''}{2}\right) y^2 + \ldots\ldots \tag{37}$$

The total flow function Ψ becomes, with ψ as the flow function of the secondary motion,

$$\Psi(x,y) = \frac{U_o' y^2}{2} + \frac{U_o'' y^3}{6} + \ldots\ldots + \psi(x,y) \tag{38}$$

Since ψ is now to change similarly upon transition to a different point, it changes here only by a factor A, which is a measure of the intensity of the fluctuation motion, and a measure of length l

for the spatial dimensions of the flow field; that is, therefore, if we set

$$x = l\,\xi, \quad y = l\,\eta, \quad \psi = A\,f(\xi,\eta) \tag{39}$$

$f(\xi,\eta)$ should be independent of the choice of points investigated.

If one eliminates the pressure p from the Euler differential equations for a two-dimensional, stationary, frictionless stream,

$$u\frac{\partial u}{\partial x} + v\frac{\partial u}{\partial y} = -\frac{1}{\rho}\frac{\partial p}{\partial x}, \qquad u\frac{\partial v}{\partial x} + v\frac{\partial v}{\partial y} = -\frac{1}{\rho}\frac{\partial p}{\partial y},$$

in which we differentiate the first equation with respect to y and the second with respect to x, and then introduce the flow function by

$$u = U + u' = \frac{\partial \Psi}{\partial y} \quad \text{and} \quad v = v' = -\frac{\partial \Psi}{\partial x}$$

where u' and v' represent the velocity components of the secondary motion, we obtain:

$$\frac{\partial \Psi}{\partial y}\cdot\frac{\partial \Delta \Psi}{\partial x} - \frac{\partial \Psi}{\partial x}\cdot\frac{\partial \Delta \Psi}{\partial y} = 0 \tag{40}$$

where Δ is the Laplacean operator

$$\Delta = \frac{\partial^2}{\partial x^2} + \frac{\partial^2}{\partial y^2}$$

After introduction of the above statement (38) we obtain in the immediate surroundings of the point under consideration

$$\left(U_o' y + \frac{\partial \psi}{\partial y}\right)\frac{\partial \Delta \psi}{\partial x} - \frac{\partial \psi}{\partial x}\,U_o'' - \frac{\partial \psi}{\partial x}\cdot\frac{\partial \Delta \psi}{\partial y} = 0 \tag{41}$$

and in the dimensionless quantities f, ξ, and η

$$\ldots = U_o' l\,\eta\,\frac{A}{l^3}\frac{\partial \Delta f}{\partial \xi} - \frac{A}{l}\frac{\partial f}{\partial \xi}U_o'' + \frac{A^2}{l^4}\left(\frac{\partial f}{\partial \eta}\cdot\frac{\partial \Delta f}{\partial \xi} - \frac{\partial f}{\partial \xi}\cdot\frac{\partial \Delta f}{\partial \eta}\right) \tag{42}$$

where the differentiation of f is now referred to the new variables ξ and η. The prime on U means simply differentiation with respect to y. In order that f be independent of the point considered, and therefore of A, l, U_o' and U_o'', the coefficient of this differential equation for f must be constant. After division of Equation (42) by $\frac{A^2}{l^4}$ we obtain

$$\frac{U_o'}{A} l^2 \eta \frac{\partial \Delta f}{\partial \xi} - U_o'' \frac{l^3}{A} + \left(\frac{\partial f}{\partial y} \cdot \frac{\partial \Delta f}{\partial \xi} - \frac{\partial f}{\partial \xi} \cdot \frac{\partial \Delta f}{\partial \eta} \right) \qquad (43)$$

Also these must be true:

$$U_o' \frac{l^2}{A} = \text{constant} \qquad U_o'' \frac{l^3}{A} = \text{constant}$$

or

$$U_o' \sim \frac{A}{l^2} \ , \ U_o'' \sim \frac{A}{l^3} \qquad (\sim \text{ means proportional})$$

or

$$l \sim \frac{U_o'}{U_o''} \ , \ A \sim \frac{U_o'^3}{U_o''^2} \sim l^2 U_o' \qquad (44)$$

The following very obvious derivation by Bitz (25) can also be given for this result:

The velocity fluctuations of the u component of a definite region of the main stream with the average velocity U_o occurs in such a way that particles from the neighboring regions penetrate the region U_o with smaller or greater velocity, as a result of the turbulent cross motion, and they retain their original velocity in doing so. These particles originate in regions which are removed from the considered region by the distance l, so their velocity is $U_o + l, U_o'$, and the velocity fluctuation of the u-

component in the region U_0 therefore equals

$$u' = \pm l_1 U_0' \qquad (45)$$

We can continue in this line of thought. Besides their velocity $U_0 + l_1 U_0'$, the particles also carry with them in the transverse motion their average rotation

$$\zeta = \text{rot } U = U' ;$$

$\zeta_0 = \text{rot } U_0 = U_0'$ is the average rotation in the considered region U_0, and $\zeta = \zeta_0 \pm l_1 \zeta_0' = \zeta_0 \pm l_1 U_0''$ is the average rotation in the region $\pm l_1$ removed. The rotation of the particles arriving in the region U_0 by the transverse motion thus differs from the average rotation existing there by the amount $\zeta - \zeta_0 = l_1 U_0''$. These particles therefore form a system of right- and left-turning eddies, and we can conceive of the turbulent scattering of velocities as a field of these eddies. If l_2 is the average distance of the right- and left-turning particles, then their diameter is proportional to l_2. For the flow velocity $v = v'$ between two eddies one then obtains

$$v' \sim l_2 (\zeta - \zeta_0) \sim l_2 l_1 U_0'' \qquad (46)$$

On account of the prescribed similarity of the turbulent fluctuating motion, u' must be proportional to v' and $l_1 \sim l_2$, so that instead of l_1 and l_2, we can introduce a common measure of length l. Consequently, we have from (45) and (46)

$$l U_0' \sim l^2 U_0''$$

$$\text{or} \quad l \sim \frac{U_0'}{U_0''} \tag{47}$$

in agreement with Karman's result.

We had previously for the turbulent shearing stress τ the relation $\tau = -\rho \overline{u'v'}$

where u' and v' are the components of the velocity fluctuation. Therefore:

$$\tau = \rho \frac{\partial \psi}{\partial x} \cdot \frac{\partial \psi}{\partial y} = \rho \frac{A^2}{l^2} \cdot \frac{\partial f}{\partial \xi} \cdot \frac{\partial f}{\partial \eta}$$

$$\text{or} \quad \tau = \rho l^2 U_0' \cdot \frac{\partial f}{\partial \xi} \cdot \frac{\partial f}{\partial \eta} \tag{48}$$

since f is independent of x and y, we have confirmed the Prandtl relation for mixing length:

$$\tau = \rho l^2 \left| \frac{dU}{dy} \right|^2 \tag{49}$$

In addition, we obtain an explicit formula for

$$l = \varkappa \frac{\frac{dU}{dy}}{\frac{d^2U}{dy^2}} \tag{50}$$

with a universal dimensionless constant $\varkappa$.

About the validity of the above consideration we can say at the outset that it ends when either U' or U'' disappears, since then Ψ in the region surrounding the considered point can no longer be approached as in the above noted disturbance equation (41). Neither can we clearly and quickly perceive that any other points are distinguished from the point at which the differential quotient of the main motion changes sign (at the center of the channel) so that

fluid at lower velocity exists on each side. Naturally, the entire deliberation remains incomplete, so long as we have not produced really a solution of the above disturbance equation of the desired kind.

Derivation of the Velocity Distribution in Tubes and Channels

We can now calculate easily the velocity distribution in a channel or tube with formulas (49) and (50) for the shearing stress and the mixing length; for the shearing stress in these cases is distributed linearly, so that we have, with τ_0 as the shearing stress at the wall, y as the distance from the center of the tube, and r as the tube radius,

$$\tau = \tau_0 \frac{y}{r}$$

On the other hand, according to Equations (49) and (50)

$$\tau \frac{y}{r} = \rho l^2 \left(\frac{dU}{dy}\right)^2 = \rho \varkappa^2 \frac{\left(\frac{dU}{dy}\right)^4}{\left(\frac{d^2U}{dy^2}\right)^2}$$

or

$$\frac{U''}{U'^2} = \varkappa \frac{\sqrt{r}}{v_*} \cdot \frac{1}{\sqrt{y}}$$

with $$v_* = \sqrt{\frac{\tau_0}{\rho}}$$

These equations can be immediately integrated:

$$-\frac{1}{U'} = 2\varkappa \frac{\sqrt{r}}{v_*} (\sqrt{y} - a)$$

where a is an integration constant,

$$\text{or} \quad U' = \frac{1}{2x} \frac{v_*}{\sqrt{r}} \frac{1}{(a-\sqrt{y})}$$

The integration constant a is defined from the limiting conditions on U'. For very large Reynolds' Nos. $\frac{dU}{dy}$ near the wall is very large and approaches the laminar value $\frac{dU}{dy} = \frac{\tau_0}{\mu}$, which, on account of the small value of μ, is very large. Without committing a great error, we can let the point where $\frac{dU}{dy}$ becomes infinite coincide with the wall $(y=r)$. In this way we obtain the integration constant $a=\sqrt{r}$, and

$$\frac{dU}{dy} = -\frac{1}{2x} \frac{v_*}{\sqrt{r}} \left(\frac{1}{\sqrt{r}-\sqrt{y}}\right)$$

and by integration over the limits O to y,

$$\frac{U_{max}-U}{v_*} = -\frac{1}{x}\left[\ln\left(1-\sqrt{\frac{y}{r}}\right) + \sqrt{\frac{y}{r}}\right] \qquad (51)$$

According to this solution, the mixing length increases linearly from the wall, a fact which may also be confirmed in the following simple way. In this region the shearing stress is approaching τ_0, so that here the equation

$$\tau_0 = \rho x^2 \frac{U'^4}{U''^2}$$

is valid. It follows that with y_1 as the distance from the wall

$$-\int_r^{r-y} \frac{U''}{U'^2} dy = \left[\frac{1}{U'}\right]_{r-y} = \int_r^{r-y} v_* \, dy = \frac{x y_1}{v_*},$$

where the integration constant can be set equal to zero, subject to later refinement (see section on the resistance law), since U' at the wall becomes very large in this case. Accordingly:

$$U'' = - \varkappa v_* \frac{1}{y_1^2}$$

and

$$l = \varkappa \left(\frac{U'}{U''} \right) = \varkappa y_1 \qquad (52)$$

as was asserted. In which region this relation is confirmed by our experiments, follows from Figures 30 and 31.

Resistance Law

Independent of this theory, Karman has given a satisfactory explanation of the resistance law in smooth and rough tubes.

For this consideration he assumes about the mixing path only that it first increases from the wall out($l = \varkappa y$, where y once more means the distance from the wall) and, moreover, it has a similar course in all tubes, independent of the wall conditions and the viscosity.

$$\frac{l}{r} = \varkappa \frac{y}{r} f\left(\frac{y}{r}\right) \quad \text{with } f = 1 \quad \text{for small } \frac{y}{r}$$

or

$$l = \varkappa y \, f\left(\frac{y}{r}\right)$$

A zone immediately next to the wall, where laminar flow is produced, must naturally be excluded from this relation. The equilibrium condition requires that

$$\tau_0 = \rho l^2 \left(\frac{dU}{dy}\right)^2 = \tau_0 \left(1 - \frac{y}{r}\right)$$

or on account of Equation (53)

$$x y f\left(\frac{y}{r}\right) \left(\frac{dU}{dy}\right) = v_* \sqrt{1 - \frac{y}{r}}$$

and if we integrate between the limits and , we obtain

$$U_{max} - U = v_* \int \frac{\sqrt{1 - y/r}}{x y f(y/r)} \, dy$$

$$U_{max} - U = v_* g\left(\frac{y}{r}\right), \qquad (54)$$

where g for all smooth tubes is the same function. The equation $\frac{U_{max} - U}{v_*} = f\left(\frac{y}{r}\right)$ is computed according to our experiments and is reproduced in Table 7. This relation is represented in Figure 31. The solid line in this figure is the velocity curve according to Equation(51)with $x = 0.36$. The dotted curve is drawn through the experimental points. We see that in the vicinity of the wall the calculated curve shows a deviation from the measured curve. This arises from the fact that the similarity considerations in the vicinity of the wall, where an influence of viscosity is present, are not fulfilled.

The friction or roughness on the inner surface has, according to this, only an influence in the form of an edge condition. Karman finds this for smooth tubes in the following way. In a narrow region of thickness δ at the wall, the velocity is determined only by the viscosity, a fact which should immediately agree with the velocity distribution calculated by the above formula with the help of mixing length. This is naturally only a greatly simplified representation of the viscosity influence. l should, therefore, only be taken up

to a value of $x\delta$. On the other hand δ can depend only on the physical quantities in the vicinity of the wall, τ_0 , ρ , μ , according to the recognized train of thought, which according to Prandtl and Karman leads to the velocity laws in the vicinity of the wall (1/7 power rule, etc.). Therefore, we place $\delta = \frac{a}{x} \cdot \frac{\nu}{v_*}$ where a again is a dimensionless constant independent of Reynolds' No. In the laminar region $\tau_0 = \mu \frac{du}{dy}$; at the edge of the laminar region we have, according to this, the velocity

$$U_1 = \frac{a}{x} v_*$$

The velocity outside of the laminar region becomes

$$U = \int_{\delta}^{y} v_* \sqrt{1 - \frac{y}{r}} \; \frac{1}{x y f\left(\frac{y}{r}\right)} \, dy + U_1$$

Since the principal velocity increase occurs very near the wall, it is sufficient to carry out the integration with $f\left(\frac{y}{r}\right) = 1$. With that it becomes with new constants c and β , approximately

$$U_{max} = \frac{1}{x} v_* \left[c - \ln \frac{\delta}{x} + a \right] = \frac{1}{x} v_* \left[\ln \frac{r v_*}{\nu} + \beta \right] \qquad (55)$$

If we introduce the resistance numeral corresponding to the maximum velocity

$$\psi = \frac{2}{U_{max}^2} v_*^2$$

and the Reynolds' Number corresponding to it

$$Re_{max} = \frac{U_{max} r}{\nu}$$

then $\frac{1}{\sqrt{\psi}} = a + \frac{1}{\varkappa\sqrt{2}} \ln (Re_{max}\sqrt{\psi})$ (56)

The values obtained by experiment for this equation are reproduced in Table 8, and represented in Figure 32. $\frac{1}{\sqrt{\psi}}$ is plotted as the ordinate and the common logarithm of $Re_{max}\sqrt{\psi}$ as the abscissa. Since the similarity considerations are valid, strictly speaking, only for frictionless fluids, and thus only such flows are in question for comparison with the experiments in which the influence of viscosity inside the tubes is very small, we have drawn a straight line (1) through those points at which practically no more influence of viscosity is present. Figure 32 shows that below $\log (Re_{max}\sqrt{\psi}) = 3.6$ a deviation from the plotted straight line is present. This deviation increases with decreasing $\log (Re_{max}\sqrt{\psi})$. This means that the influence of viscosity becomes stronger with decreasing Reynolds' Nos. This straight line is reproduced by the equation:

$$\frac{1}{\sqrt{\psi}} = A + B \log (Re_{max}\sqrt{\psi}) \qquad (56a)$$

The constants A and B obtained from this figure are $A = 4.75$, $B = 3.77$. As the discussion above indicates, the equation of this straight line is valid for all flows which are uninfluenced by viscosity. Thus, we are justified in extrapolating the relation $\frac{1}{\sqrt{\psi}}$ vs. $\log (Re_{max}\sqrt{\psi})$ to any large Re_{max}.

We have drawn for the following approximate calculations a second straight line which particularly considers the points in the center region;

$$\frac{1}{\sqrt{\psi}} = 4.16 + 3.90 \log (Re_{max}\sqrt{\psi}) \qquad (56b)$$

Similarity Consideration by Prandtl

The basic principle of the Karman similarity consideration represented completely above is the assumption of the geometrical and mechanical similarity of the turbulent exchange mechanism. By use of the hypothesis that the turbulent fluctuating motion at different places in the main stream distinguished itself only by a length and a time measure, Karman arrived at his universal velocity distribution law for tube and channel flow. By this, only the first and second derivatives of the mainstream $u=u(y)$, $\frac{du}{dy}$ and $\frac{d^2u}{dy^2}$, were brought into consideration. Prandtl[26] maintains that one can expect such a similarity of the secondary motion strictly speaking only if the main motion also satisfies the same similarity. If (1) and (2) are two points on the profile of the main flow, then one has to vary upon transition from (1) to (2), y as the measure of length and $\frac{y}{u}$ as the measure of time (y = distance from the axis of symmetry). The general velocity distribution $u(y)$, which fulfills the similarity considerations, that is, whose curve retraces itself with variation in the y and u measures, is represented by the equation

$$u = ay^n + b \tag{57}$$

where a and b are constants. We have already introduced the quantity characteristic of turbulent flow $v_* = \sqrt{\frac{\tau_0}{\rho}}$ $(\tau_0 = \rho v_*^2)$ The quantity v_* defined in this way by the turbulent shearing stress τ_0, which v_* has the dimension of a velocity, can be regarded as a measure of the turbulent disturbance motion. On account of the equality of two coordinate systems which move toward each other with constant velocity, the turbulent fluctuation velocity at any point in the flow cannot depend on the velocity u of the main

flow, but only on the value of the derivatives $\frac{du}{dy}$, $\frac{d^2u}{dy^2}$, ... at the point in question, and on the distance y of the point from the axis of symmetry. On this account Prandtl makes the simple statement, with the, for the moment undefined, exponents p and q

$$v_* \approx y^p \left(\frac{d\bar{u}}{dy}\right)^q \tag{58}$$

The only possible values for which this formula is dimensionally correct are $p = 1$ and $q = 1$, so that we have

$$v_* = \chi y \frac{du}{dy}$$

where χ is a universal constant. As the simplest case Prandtl now assumes τ = constant, and, therefore, v_* = constant. Then we can integrate the last equation and get

$$u = \frac{v_*}{\chi} \ln y + \text{const.} = \frac{v_*}{\chi} \ln\left(\frac{y}{y_0}\right) \tag{59}$$

It may be said about the constant y_0 , that it has the dimension of a length. It is a measure of the thickness of the laminar region present in the immediate vicinity of the wall. The only possible length which we can form from the characteristic constants of the turbulent flow is $\frac{\nu}{v_*}$. We write, therefore:

$$y_0 = \text{some number } \frac{\nu}{v_*} = m\frac{\nu}{v_*} \tag{60}$$

Therefore, from (59)

$$u = \frac{v_*}{\chi}\left\{\ln \frac{y v_*}{\nu} - \ln m\right\} \tag{61}$$

or

$$\frac{u}{v_*} = \frac{1}{\chi}\left\{\ln \frac{y v_*}{\nu} - \ln m\right\}$$

and with

$$\frac{u}{v_*} = \psi \quad \text{and} \quad \frac{y v_*}{\nu} = \eta$$

we have (62)

$$\psi = A + B \ln \eta$$

The measurements give

$$A = -\frac{1}{x} \ln m = 5.5, \qquad B = \frac{1}{x} = 2.5$$

Therefore,

$$x = 0.40 \quad \text{and} \quad m = \frac{1}{9}$$

The thickness of the laminar region δ is of the order of

$$y_0 = \frac{1}{9} \frac{\nu}{v_*}$$

where nothing has yet been said about the numerical factor still to be added to y_0. Equation (62) is as close to the equal expression of the velocity distribution, arrived at by Karman from his similarity consideration, as can be expected.

Part 6 - Resistance Law

The resistance number $\lambda = \frac{dp}{dx} \cdot \frac{d}{q}$, already defined, has been obtained as a function of Reynolds' No. over a large range, and is plotted on a logarithmic scale in Figure 34. The recorded points (Table 9) represent the values of log (1000 λ) from very small Re of about $3 \cdot 10^3$ to the upper limit. The measured values up to Re = $100 \cdot 10^3$ (log Re = 5) agree very well with the Blasius formula $\lambda_0 = \frac{0.316}{(Re)^{1/4}}$, which is represented in this Figure by the curve 1. Above this limit the measured λ values deviate upward more and more from the Blasius curve with increasing Re. Lees[27]

has obtained a formula of the type

$$\lambda = a + \frac{b}{Re^n}$$

from the measurements of Stanton and Pannell, which reaches to a Reynolds' No. of $460 \cdot 10^3$ ($\log Re = 5.67$); namely, $\lambda = 0.0072 + \frac{0.6104}{Re^{0.35}}$. Since our measured results agree with those of Stanton and Pannell, they are also produced in this range by Lees' formula. Outside of this range, our values of λ deviate from the Lees' curve, which is designated with a 2 in Figure 34. As is evident from this figure, this deviation increases with increasing Re. Recently Schiller and Hermann[28] on the basis of their and our measurements, have submitted, according to the Lees statement $\lambda = a + \frac{b}{Re^n}$, the approximate formula

$$\psi = 0.00270 + \frac{0.161}{Re^{0.3}}$$

where $\psi = \frac{\lambda}{2}$ and $Re = \frac{\bar{u} r}{\nu}$. Since it is generally customary to refer the Reynolds' No. and the resistance number to the tube diameter, we have recalculated the Schiller formula on this basis. This gives the formula

$$\lambda = 0.0054 + \frac{0.396}{Re^{0.3}} \qquad (63)$$

which is represented in Figure 34 by the dot-dash curve 3. One sees that Schiller's curve and that of Stanton and Pannell coincide up to $Re = 4.6 \cdot 10^5$ ($\log Re = 5.67$). From there on Schiller's curve agrees with the values measured by us to about $Re = \frac{\bar{u} d}{\nu} = 2.5 \cdot 10^6$, or $\log Re = 6.4$. From $\log Re = 6.4$ up, Schiller's curve

deviates from our curve. This deviation becomes greater with increasing Re . The deviation of the formulas of Lees and Schiller-Hermann from the measured curve arises from the fact that the formulas were calculated directly from measurements, and therefore agree only so far as the experiments extended at that time. We succeeded in obtaining an approximate formula in another way, described below, which joins the Blasius law at its upper limit, and the validity of which appears certain up to a Reynolds' No. of $Re = 1 \cdot 10^8$ ($\log Re = 8.0$). This formula is reproduced as curve 4. It is seen that this curve at the upper limit ($\log Re = 6.4$) of the Schiller-Hermann curve branches off downward, and at $Re = 1 \cdot 10^8$ it deviates more from Schiller's curve than from Lees'.

The methods known up until now yield only formulas for the regions investigated experimentally. The representation of Karman on page 56 nevertheless makes clear that a formula constructed equal to the Karman formula is to be connected, namely:

$$\frac{1}{\sqrt{\lambda}} = A + B \log \left(Re\sqrt{\lambda} \right) \qquad (64)$$

The difference consists of the fact that Karman referred the resistance and Reynolds' Numbers to the maximum velocity and the tube radius, while we used the average velocity and the tube diameter. If we place $\frac{1}{\sqrt{\lambda}} = y$ and $\log(Re\sqrt{\lambda}) = x$, then this formula takes the form

$$y = A + Bx$$

In Figure 35 $y = \frac{1}{\sqrt{\lambda}}$ as a function of $x = \log(Re\sqrt{\lambda})$ is plotted according to measurements (Table 9). It gives the straight line (1) and for A and B , the values $A = -0.8$, $B = 2.0$.

The experimental results of other investigators are also plotted in Figure 35, and in drawing the line through these points, little weight was given the values of Ombeck, because these experiments carried out with air are somewhat less certain on account of the variation in volume of the air. From $x = \log Re\sqrt{\lambda}$ we calculated the values of $Re\sqrt{\lambda}$, divided by $\frac{1}{y} = \sqrt{\lambda}$, and got the Reynolds No. Re. So we have obtained from the above equation a relation for the resistance number in terms of Re

$$\lambda = f(Re).$$

One can expect with a certain probability that we may also extrapolate this formula to a somewhat greater range, if not to $Re = \infty$, as we can the Karman formula.

The relation $\lambda = f(Re)$ is shown in Figure 36, as it results when we extrapolate it to large Re (to $Re = 1 \cdot 10^8$) from the constants A and B defined from measurements.

We can now use this representation in a similar way to obtain a convenient approximate formula for λ, as Lees, Schiller, and Hermann have done on the basis of their experiments. The range of Reynolds' Nos. covered by this new formula will begin where the Blasius formula leaves off. We will set the end of the region constant at $Re = 1 \cdot 10^8$.

From curve 4 of Figure 34 we find for the constants of the approximate formula

$$\lambda = a + \frac{b}{Re^n}$$

the values

$$a = 0.0032 \qquad b = 0.221 \qquad n = 0.237;$$

the equation therefore becomes

$$\lambda = 0.0032 + \frac{0.221}{Re^{0.237}} \qquad (65)$$

In order to prove the validity of the formulas given above by Blasius, Lees, Schiller, Hermann, and us, the relation $\frac{1}{\sqrt{\lambda}} = (\log Re\sqrt{\lambda})$ is calculated and plotted according to the corresponding formula in Figure 37. The recorded points are calculated from values measured by us. Below $\log (Re\sqrt{\lambda}) = 3.7$ the values of $\frac{1}{\sqrt{\lambda}}$ lie below these straight lines. This is explained by the fact that the influence of viscosity at these Reynolds' Nos. becomes considerable. Above this set limit the influence of viscosity is negligible, and the experimental points lie on the straight line. Curve 1, calculated from Blasius' formula below $\log (Re\sqrt{\lambda}) = 4.0$ (which means Reynolds' No. is about $40 \cdot 10^3$) deviates from curve 4; above this Reynolds' No. to about $\log (Re\sqrt{\lambda}) = 5$ (Re = about $100 \cdot 10^3$) curve 3 coincides with curve 4. Continuing to higher Reynolds' No., curve 1 deviates considerably upward from curve 4. In addition, curve 1, in agreement with earlier work, shows that the Blasius law is only valid to $(Re\sqrt{\lambda}) = 5.1$ (Re = $100 \cdot 10^3$). Curves 2 and 3 are calculated according to the formula of Lees and Schiller and they deviate from the straight lines at $\log (Re\sqrt{\lambda}) = 4.7$ (Re = about $4.5 \cdot 10^5$) and $\log (Re\sqrt{\lambda}) = 5.25$ (Re = about $1.9 \cdot 10^6$) respectively. If we record the resistance value in curve 4 for Reynolds' Nos. greater than $1 \cdot 10^8$, then a corresponding deviation also occurs here.

For the following approximate calculations a second straight

line (2, Figure 35) is drawn with the equation

$$\frac{1}{\sqrt{\lambda}} = -0.55 + 1.95 \log\left(Re\sqrt{\lambda}\right) \qquad (63a)$$

Part 7 - Relation Between the Average and the Maximum Velocity

(a) Prof. Prandtl has suggested that the Karman resistance law (Equation 56b) can be joined with our Equation (64b) with the help of Equation (54):

According to the Karman representation Equation (54) is

$$\frac{U-u}{v^*} = f\left(\frac{y}{r}\right)$$

From this relation the average velocity $\bar{u}$ can be obtained by plotting $\frac{U-u}{v^*}$ as a function of $\left(\frac{y}{r}\right)^2$ and using graphical integration, so that one obtains

$$\frac{U-\bar{u}}{v^*} = \text{a number} = \beta$$

By carrying out the integration β is given as 4.03. With the help of this relation we get the connection between the Karman resistance law and ours, as follows: From the Karman Equation (56b) it follows, if we place

$$Re_{max} = \frac{Ur}{\nu} \quad \text{and} \quad \sqrt{\psi} = 1.414\,\frac{v^*}{U}$$

that

$$\frac{U}{v^*} = A + B \log\left[1.414\left(\frac{v^* r}{\nu}\right)\right]$$

or

$$\frac{U}{v^*} = A' + B \log\left(\frac{v^* r}{\nu}\right) \qquad (67)$$

In an analogous way we obtain from our resistance law, Equation (64b), if we place

$$Re = \frac{\bar{u} 2r}{\nu} \quad \text{and} \quad \sqrt{\lambda} = 2.828 \frac{v*}{\bar{u}}$$

$$\frac{\bar{u}}{v*} = a + b \log \left[2.828 \left(\frac{v* r}{\nu} \right) \right]$$

or

$$\frac{\bar{u}}{v*} = a' + b \log \left(\frac{v* r}{\nu} \right) \qquad (68)$$

Relation (66) now requires that the constants B and b in Equations (67) and (68) agree. We can employ this relation in order to get the best value of B = b by equalization between the different diagrams. The curve #2 already mentioned in the figures is based on this equalization. The best value of B = b is thus given as 5.52. Therefore, we find further

$$A = 5.87 \qquad a = -1.555$$

and from these

$$A' = 6.68 \qquad a' = 2.63$$

Upon introduction of these values and subtraction of Equation (68) from (67) it follows then that

$$\frac{U - \bar{u}}{v*} = 4.08 \qquad (69)$$

in good agreement with the earlier result. In Figure 38 the experimental vlaues of $\frac{U}{v*}$ and $\frac{\bar{u}}{v*}$ are plotted in relation to $\frac{v* r}{\nu}$. The two straight lines through these points are parallel, and the difference between the two functions amounts to, on the average, 4.03, as was predicted above.

The equation for the universal velocity distribution $\psi = c_1 + c_2 \log \eta$ should from theoretical principles be in harmony with

Equations (67) and (68), if we put the straight line $\psi = \psi(\eta)$ only through points near the wall, since C_2 should = b . Actually

$$\psi = 5.84 + 5.52 \log \eta$$

is in good agreement with the experimental points near the wall. To the value 5.52 there corresponds a value of the Karman universal constant

$$x = \frac{2.3025}{5.52} = 0.417$$

(b) By division of Equation (67) and (68), $\frac{\bar{u}}{U}$ results as a function of $\frac{v_* r}{\nu}$, and also as a function of Reynolds' Number, which can be expressed by $\frac{v_* r}{\nu}$, for it is

$$Re = \frac{2\bar{u}r}{\nu} = \frac{2\bar{u}}{v_*} \cdot \frac{v_* r}{\nu} = 2(2.828)\left(\frac{v_* r}{\nu}\right)\frac{1}{\sqrt{\lambda}}$$

$\frac{1}{\sqrt{\lambda}}$, however, can be expressed by means of Equation (64a) also by $\frac{v_* r}{\nu}$. In Figure 39 the relation so obtained:

$$\frac{\bar{u}}{U} = f\left(\frac{\bar{u} d}{\nu}\right)$$

is represented for $Re = 3 \cdot 10^3$ to $1 \cdot 10^8$ by the solid curve. In addition the experimental points by Stanton and Pannell and us are plotted here (Table 9). In the range in which laminar flow is developing $\frac{\bar{u}}{U} = 0.5$. The upper limit of laminar flow occurs at log Re = 3.1, corresponding to a $Re = 12.6 \cdot 10^3$. We see that the measured points deviate from the calculated curve up to $Re = 200 \cdot 10^3$ (log Re = 5.4); they are connected by the dashed curve. This deviation is explained by the influence of viscosity, which the formula does not reproduce. On continuing above $Re = 200 \cdot 10^3$, the agreement is fairly good. The results of measurements by

Stanton and Pannell agree very well with ours up to log Re = 4.2. Above this limit an almost constant deviation occurs. This deviation is assuredly caused by the method of measurement. We have undertaken further measurements at different Reynolds' Numbers 20 d before the entrance cross section; the same values as our earlier measurements have resulted.

Summary

The objective of this work was to investigate the regularities of the turbulent flow in smooth tubes over the largest possible range of Reynolds' Numbers. For this purpose an experimental set up was constructed which made it possible for us to obtain turbulent flow of water in circular tubes up to a Reynolds' Number of $3240 \cdot 10^3$. By evaluation of the measured velocity distributions and the pressure gradients, the following were established:

1. The form of the velocity distribution varies with Reynolds' Number, and, in fact, the velocity distribution becomes fuller and fuller with increasing Reynolds' Numbers. The comparison of the velocity distributions of Bazin and of Stanton with ours gives good agreement.

2. The exponent n in the Prandtl Power Law ($u = a y^n$, where y = distance from wall) has the constant value $n = 1/7$ in the Blasius range of resistance up to $Re = 100 \cdot 10^3$. At very small Reynolds' Numbers, the exponent is greater than 1/7. Above a Reynolds' Number of $100 \cdot 10^3$ we observe a decrease in the exponent n with increasing Re. At the largest $Re = 3240 \cdot 10^3$, the exponent reaches the value $n = 1/10$. By forming suitable dimensionless ratios from the quantities characteristic of the turbulent

flow in the vicinity of the wall, τ_0 = shearing stress at the wall, ν = kinematic viscosity, ρ = density, a velocity distribution law valid in the vicinity of the wall for all Reynolds' Numbers is obtained

$$\psi = \psi(\eta)$$

in which

$$\frac{u}{v_*} = \psi \quad , \quad \frac{v_* y}{\nu} = \eta \quad , \quad v_* = \sqrt{\frac{\tau_0}{\rho}}$$

For sufficiently large values of η (above $\eta = 10$) it is sufficiently accurate to state

$$\psi = A + B \log \eta$$

(A and B are universal constants),

3. The turbulent exchange quantity was determined in relation to the distance from the wall. The dimensionless ratio $\frac{\epsilon}{v_* r}$ in relation to $\frac{y}{r}$ shows that above a Reynolds' Number, Re = $100 \cdot 10^3$, the distribution of the exchange quantity across the cross section is independent of the Reynolds' Number. Below this Reynolds' Number this distribution is closely dependent on the Reynolds' Number. For the Prandtl mixing length, which is related to the turbulent impulse exchange, we have learned that the ratio $\frac{l}{r}$ for each point in the cross section decreases with increasing Reynolds' Number. When Re exceeds the value $100 \cdot 10^3$, the dimensionless mixing length distribution $\frac{l}{r} = f(\frac{y}{r})$ becomes independent of Reynolds' Number. This independence indicates that above this Reynolds' Number an influence of viscosity is no longer present.

4. The measured velocity distributions and the resistance law are compared with the distribution calculated by Karman on the basis of his similarity consideration, and in the region of large Reynolds'

Numbers where the influence of viscosity is not present, they are found to be in good agreement.

In connection with the Prandtl similarity consideration, new deliberations by Prandtl and Betz are given.

5. If $\lambda = \frac{dp}{dx} \cdot \frac{2d}{\rho \bar{u}^2}$, the tube resistance number, then the Blasius resistance formula $\lambda_B = \frac{0.316}{Re^{1/4}}$ is confirmed up to $Re = 100 \times 10^3$ For larger Reynolds' Numbers the following formula results

$$\lambda = 0.0032 + \frac{0.221}{Re^{0.237}}$$

In connection with the resistance formulas of Prandtl and ourselves, relations between the average velocity $\bar{u}$ and the maximum velocity U are determined, which demonstrate new correlations among the different formulas.

NOTES

(1) Blasius, H., "Das Ähnlichkeitsgesetz bei Reibungsvorgängen in Flüssigkeiten", Forsch.-Arb. Ing.-Wes. 131 (1913), Berlin.

(2) Saph, V. and Schoder, E. H., "An Experimental Study of the Resistance to the Flow of Water in Pipes", Trans. Amer. Soc. Civil Engr. 51 (1903), Paper 944.

(3) Nusselt, W., "Wärmeübergang in Rohrleitungen", Forsch.-Arb. Ing.-Wes. 89 (1910), Berlin.

(4) Ombeck, H., "Druckverlust strömender Luft in geraden zylindrischen Rohrleitungen", Forsch.-Arb. Ing.-Wes. 158 and 159 (1914), Berlin.

(5) Stanton, T. E. and Pannell, J. R., "Similarity of Motion in Relation to the Surface Friction of Fluids", Proc. Roy. Soc. 214 (1914), 199, Berlin.

(6) Lees, C. H., "On the Flow of Viscous Fluids through Smooth Circular Pipes", Proc. Roy. Soc. 91 (1915), 46, London (A).

(7) Jacob, M. and Erk, S., "Der Druckabfall in glatten Rohren und die Durchflussziffer von Normaldüsen", Forsch.-Arb. Ing.-Wes. 267 (1924), Berlin.

(8) Hermann, R., Experimentelle Untersuchung zum Widerstandsgesetz des Kreisrohres bei hohen Reynoldsschen Zahlen und grossen Anlauflängen, Leipzig Dissertation. Leipzig, Akadem. Verlagsgesellschaf m.b.H., 1930.

(9) Schiller, L., "Rohrwiderstand bei hohen Reynoldsschen Zahlen", in Vorträge aus dem Gebiete der Aerodynamik und

verwandte Gebiete, Aachen, 1929, edited by A. Gilles, L. Hopf, and Th. v. Karman, p. 69. Berlin, J. Springer, 1930.

(10) Prandtl, L., "Diskussionsbemerkungen zum Vortrag von L. Schiller" (see reference 9), in Vorträge aus dem Gebiete der Aerodynamik und verwandte Gebiete, Aachen, 1929, edited by A. Gilles, L. Hopf, and Th. v. Karman, p. 78. Berlin, J. Springer, 1930.

(11) Stanton, T. E., "The Mechanical Viscosity of Fluids", Proc. Roy. Soc. 85 (1938), 366-376, London (A).

(12) Nikuradse, J., "Untersuchung über die Geschwindigkeitsverteilung in turbulenten Strömungen", Forsch.-Arb. Ing.-Wes. 281 (1926), Berlin.

(13) Karman, Th. v., "Mechanische Ahnlichkeit und Turbulenz", Nachr. Ges. Wiss. Göttingen Math. Phys. Klasse (1930), p. 58.

(14) The author has given a short report on these investigations at the Congress of Aerodynamic and Allied Fields in Aachen. Nikuradse, J., "Über turbulente Wasserströmungen in geraden Rohren bei sehr grossen Reynoldsschen Zahlen", in Vorträge aus dem Gebiete der Aerodynamik und verwandte Gebiete, Aachen, 1929, edited by A. Gilles, L. Hopf, and Th. v. Karman, p.63. Berlin, 1930.

In the same volume on page 69 is to be found a report by L. Schiller on investigations made at the same time as ours, which will be taken up in the following numerous references.

(15) The tripping valve of 150 mm diameter, which was generally used in all experiments with supersonic velocities, was constructed by Prof. J. Ackeret.

(16) Stanton, T. E. See reference 11.

(17) Bazin, M., "Expériences nouvelles sur la distribution des vitesses dans les tuyaux", Mémoires présentés par divers savants à l'Académie des Sciences de l'Institut de France, Vol. 32, No. 16. 1902.

(18) Prandtl, L., "Über den Reibungswiderstand strömender Luft", in Ergebnisse der Aerodynamischen Versuchsanstalt zu Göttingen, III issue, 1927, p. 1.

Karman, Th. v., "Über laminare und turbulente Reibung", Z. Angew. Math Mech. 1 (1921), 233.

(19) Prandtl, L., loc. cit.

----- "Zur turbulenten Strömung in Rohren und längs Platten", in Ergebnisse der Aerodynamischen Versuchsanstalt zu Göttingen, IV issue, 1932, p. 18.

(20) The author has already reported on this relation in the summer of 1929 at the Colloquium for Applied Mechanics in Göttingen.

(21) Boussinesq, J., "Essai sur la théorie des eaux courantes", in Mémoires présentés par divers savants à l'Académie des Sciences de l'Institut de France. 1877.

(22) Prandtl, L., "Bericht über Untersuchungen zur ausgebildeten Turbulenz", Z. Angew Math. Mech. 5 (1925), 136.

----- "Bericht über neuere Turbulenzforschungen", in Hydraulische Probleme, p. 1, Berlin, VDI-Verlag, 1926.

Tollmien, W., "Berechnung turbulenter Ausbreitungsvorgänge", Z. Angew. Math. Mech. 6 (1926), 468.

Prandtl, L. "Über ausgebildete Turbulenz", in Verh. d. 2. intern. Kongr. für techn. Mech. Zürick, 1927.

Nikuradse, J., "Untersuchungen über die Strömungen des Wassers in konvergenten und divergenten Kanälen", Forsch.-Arb. 289 (1929).

----- "Über turbulente Wasserströmungen in geraden Rohren bei sehr grossen Reynoldsschen Zahlen", in Vorträge aus dem Gebiete der Aerodynamik und verwandte Gebiete, Aachen, 1929, edited by A. Gilles, L. Hopf, and Th. v. Karman, p. 63.

Fritsch, W., "Der Einfluss der Wandrauhigkeit auf die turbulente Geschwindigkeitsverteilung in Rinnen", Z. Angew. Math. Mech. 8 (1928), 215.

Swain, L. M., "On the Turbulent Wake Behind a Body of Revolution", Proc. Roy. Soc. 125 (1929), 647, London.

Betz, A., "Über turbulente Reibungsschichten an gekrümmten Wanden", in Vorträge aus dem Gebiete der Aerodynamik und verwandte Gebiete, Aachen, 1929. edited by A. Gilles, L. Hopf, and Th. V. Karman, p. 10. 1929.

Nikuradse, J., "Widerstandsgesetz und Geschwindigkeitsverteilung von turbulenten Wasserströmungen in glatten und rauhen Rohren", Verh. d. 3. intern. Kongr. für techn. Mechanik, p. 239. Stockholm, 1930.

Schlichting, H., "Über das ebene Windschaltenproblem", Göttinger Dissertation. Ing.-Arch. 1 (1930), 533.

(23) Prandtl, L., "Turbulenz und ihre Entstehung", Tokiovortrag, 1929. Report of the Aeronautical Research Institute, Tokyo, No. 65, 1930.

(24) See reference 13.

(25) Betz, A., "Die v. Karmansche Ähnlichkeitsüberlegung für turbulente Vorgänge in physikalischer Auffassung", Z.

Angew. Math. Mech. 11 (1931), 397.

(26) This viewpoint was presented by Prandtl in a supplementary lecture to Hydrodynamik, summer semester, 1931.

(27) Lees, C. H. See reference 6.

(28) Schiller, L. and Hermann, R., "Widerstand von Platte und Rohr bei hohen Reynoldsschen Zahlen", Ing.-Arch. 1 (1930), 392.

(29) Schiller, L., "Rohrwiderstand bei hohen Reynoldsschen Zahlen", in Vorträge aus dem Gebiete der Aerodynamik und verwandte Gebiete, Aachen, 1929, edited by A. Gilles, L. Hopf, and Th. v. Karman, p. 78. Berlin, 1930.

(30) See reference 13.

APPENDIX

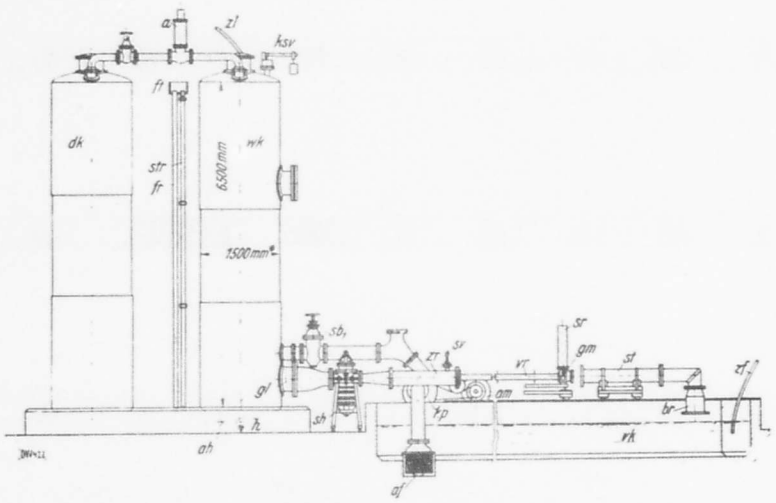

Fig. 1. Experimental Setup

zl	feed pipe
wk	water tank
dk	compressed air tank
sb_1	gate valve between wk and kp
sb_2	gate valve between wk and zr
sh	tripping valve
str	standpipe
fr	downpipe
ft	collector basin
ah	flow-off valve
h	drain valve
gl	flow straightener
zr	entrance pipe
skv	safety valve for water tank
br	quieting chamber
sv	check valve
vr	test pipe
gm	velocity measuring apparatus
sr	standpipe
st	jet collector
a	Arca regulator
kp	centrifugal pump
am	driving motor
vk	reservoir
an	motor starter
zf	hose
af	flow off
qws	mercury manometer

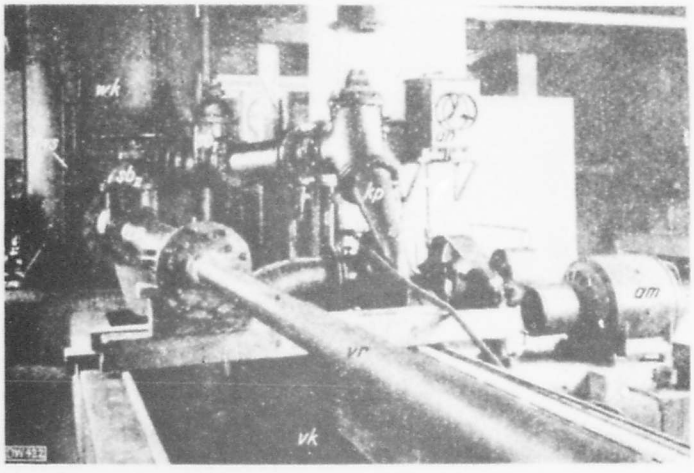

Fig. 2. View of the Experimental Setup
with Circulation of the Water

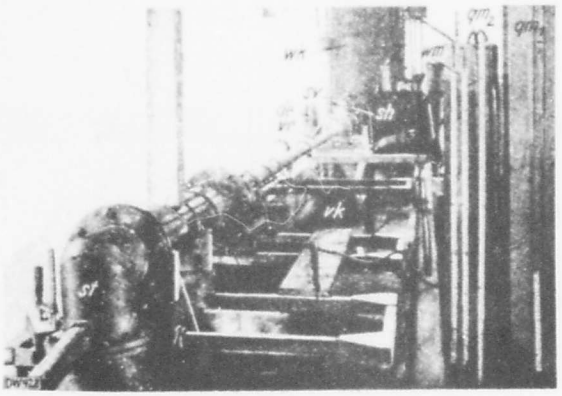

Fig. 3. View of the Setup for
Forced Flow Experiments

de pressure inlet qm_1, qm_2 mercury manometers
wm water manometer

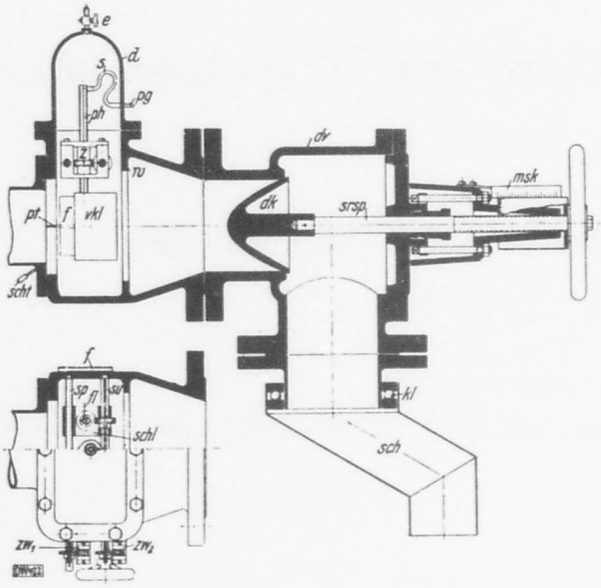

Fig. 4. The Large Velocity Measuring
Apparatus with Throttle and Swivel Outlet

m	housing	srsp	screw
d	cover	dk	throttling cone
sp, su	spindles	msk	measuring scale
schl	sliding carriage	kl	ball bearings
pt	pitot tube	dv	throttle valve
ph	pitot tube holder	w	wall
f	window	e	venting valve
pg	line connection for total pressure	vkl	casing for the pitot tube holder
z	screw wheel	sch	swivel outlet
fl	guides	zw_1, zw_2	scales
s	hose	scht	hose connection

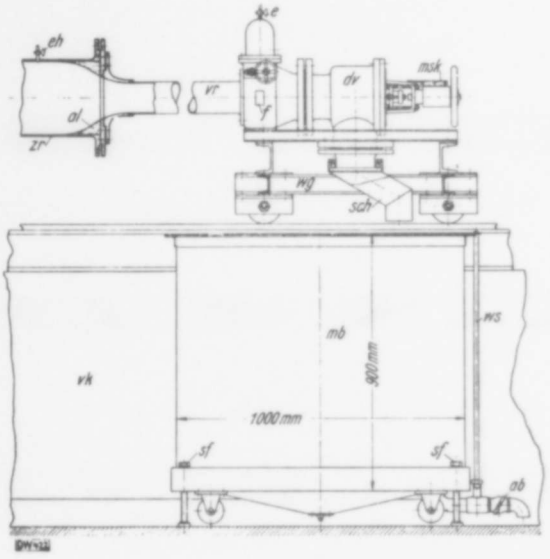

Fig. 5. A Portion of the Experimental Set-up

zr	entrance pipe	dv	throttle valve
eh	air venting valve	msk	measuring scale on throttle valve
al	tapered section	sch	swivel outlet
vr	test pipe	wg	truck
e	air vent on measuring apparatus	mb	measuring tank
f	window of the velocity measuring apparatus	ms	gauge glass
		ab	outlet valve
wk	reservoir	sf	screw feet

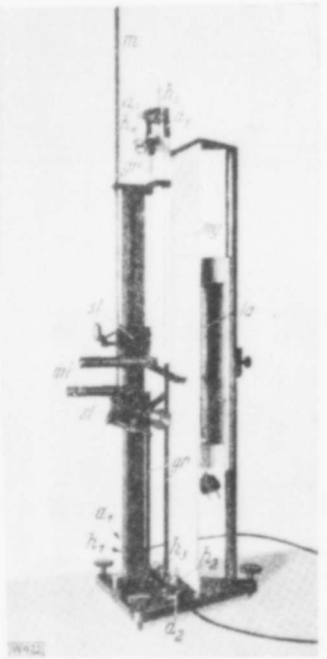

Fig. 6

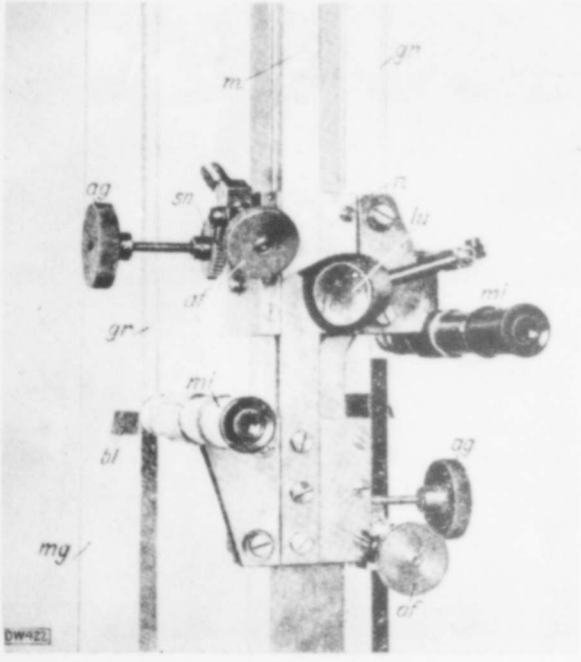

Fig. 7.

Figs. 6 and 7. View and Closeup of the Micromanometer

h_1, h_2, h_3, h_4, h_5 valves

a_1, a_2, a_3, a_4 pressure lead connections

mi	reading microscope
bl	adjustable screen
gr	glass tubes
mg	milk glass plate
la	lamp
sl	slides
m	measuring scale
sn	worm drive
n	vernier scale
lu	swiveled magnifying glass
ag	driving wheel for coarse adjustment
af	driving wheel for fine adjustment

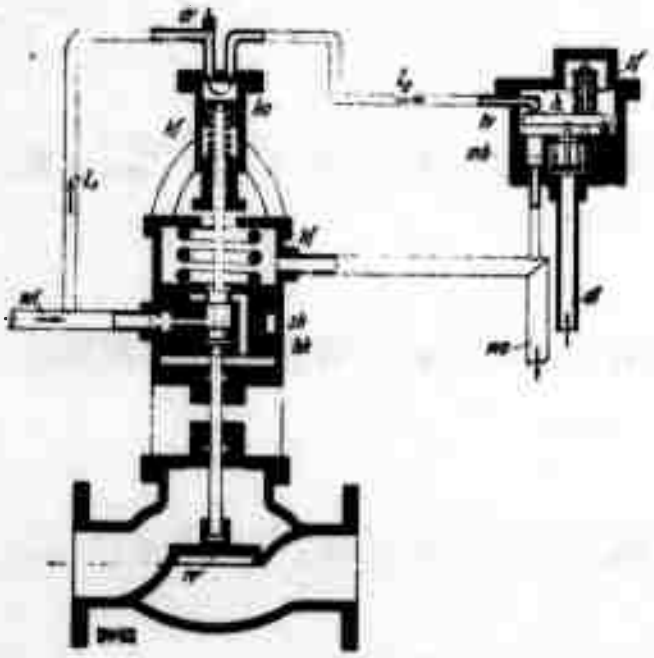

Fig. 8. Area Regulator

wl	supply line
l_1	water line
l_2	water line
dr	throttle
ko	piston
kf	piston spring
hf	spring
sk	control piston
hk	piston
sf	spring
h	lever
tv	disk valve
mb	diaphragm bellows
dl	pressure line
wa	flow off
rv	regulating valve

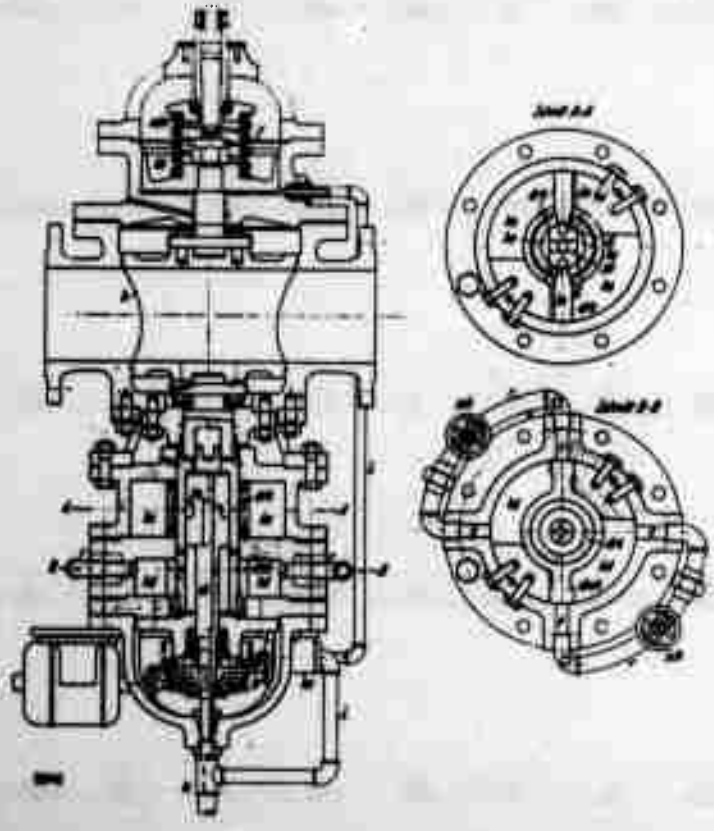

Fig. 9. The Tripping Valve

sr	control wheel
ha	valve
k	cone
schr	cone stop
drk	rotating piston
sk	control piston
ka	control piston chamber
c,d	slots
ku,ko	compressed air chamber
l	compressed air leads
hk	piston
dmk	damping piston
kd	oil chambers
le	supply lines
sch	gate valves
e	inlet ports
Schnitt	section

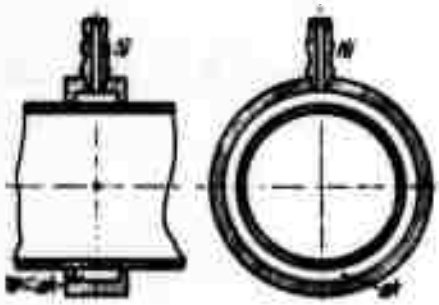

Fig. 10. Measuring Section for the Measurement of the Static Pressure

ak equalizing chamber
tu pressure taps

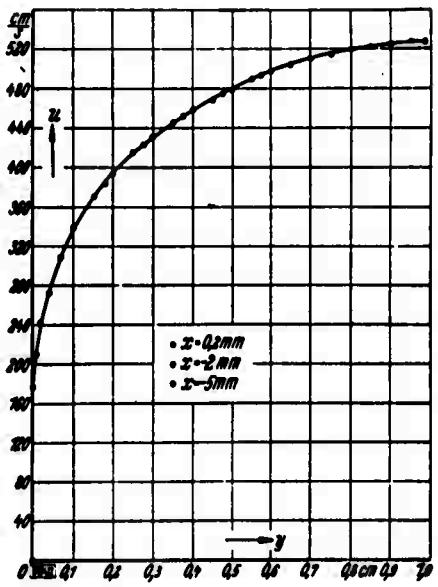

Fig. 11. The Velocity Distributions at x = 0 mm, x = -2 mm, and x = -5 mm.

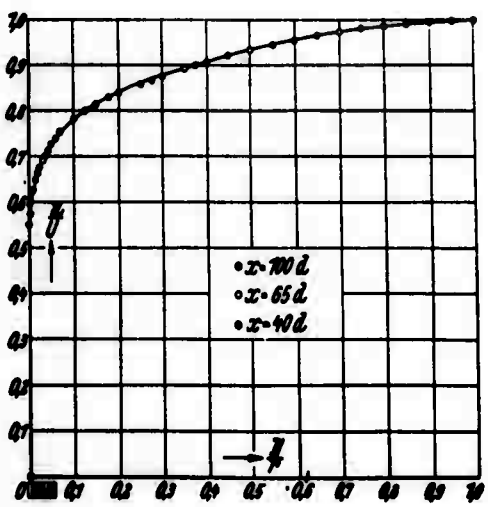

Fig. 12. The Velocity Distributions at x = 100 d, x = 65 d, and x = 40 d.

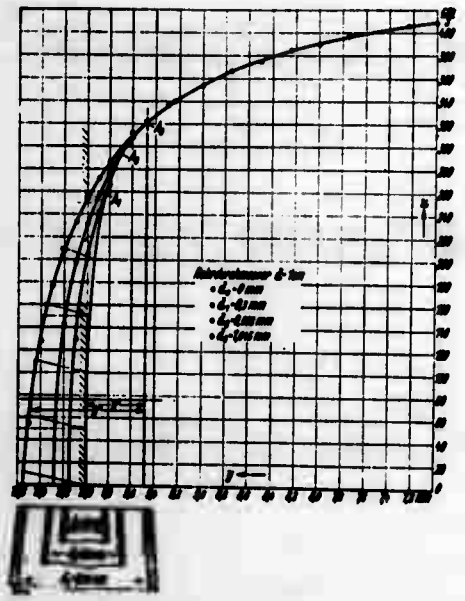

Fig. 13. Reduction of the Pitot Tube Opening to Zero

Rohrdurchmesser = tube diameter

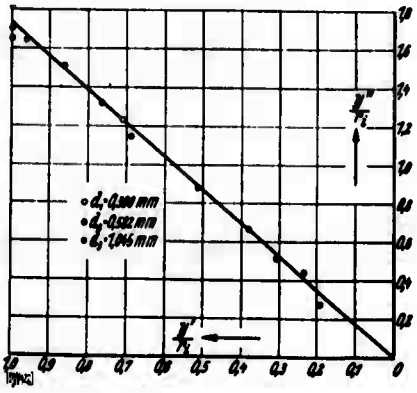

Fig. 14. y'/r_i in Relation to y''/r_i

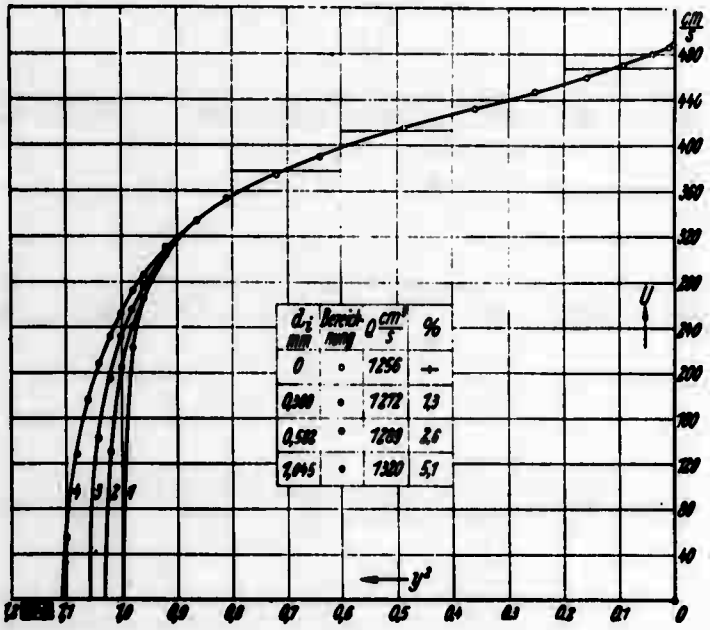

Fig. 15. $100\left(\frac{Q-Q_0}{Q}\right) = f(d_i)$

Bezeichnung = designation

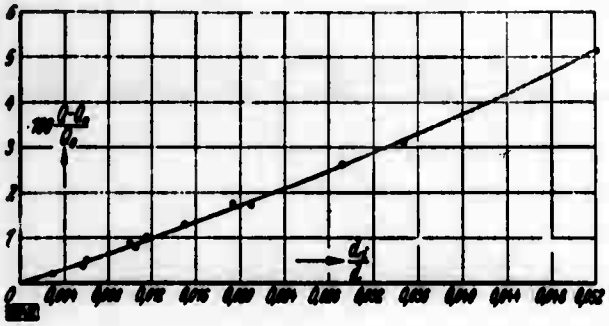

Fig. 16. $100\left(\frac{q-q_0}{q}\right) = f\left(\frac{d_1}{d}\right)$

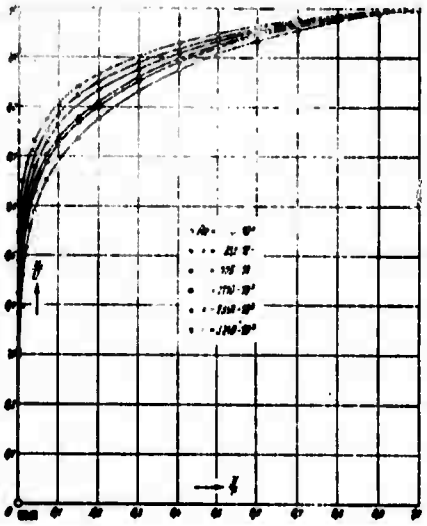

Fig. 17. u/U in Relation to y/r

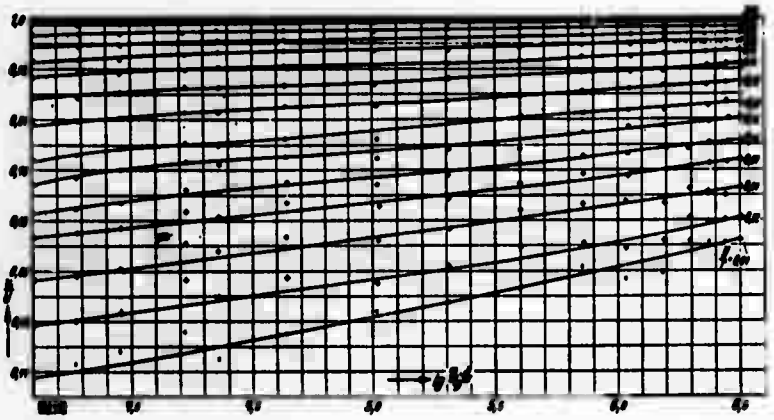

Fig. 18. u/U in Relation to log $\left(\frac{\overline{u}d}{\nu}\right)$

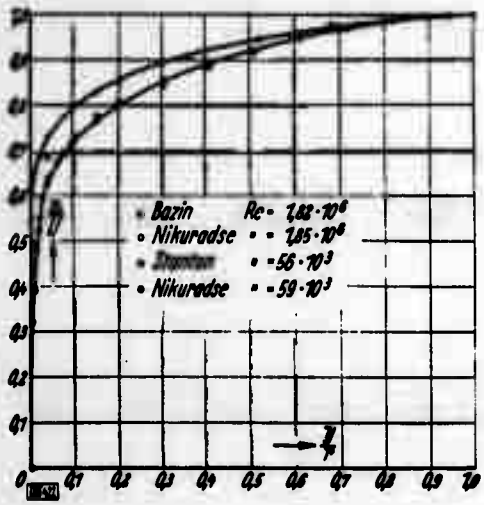

Fig. 19. Comparison of the Velocity Distribution of Stanton, Bazin, and Nikuradse

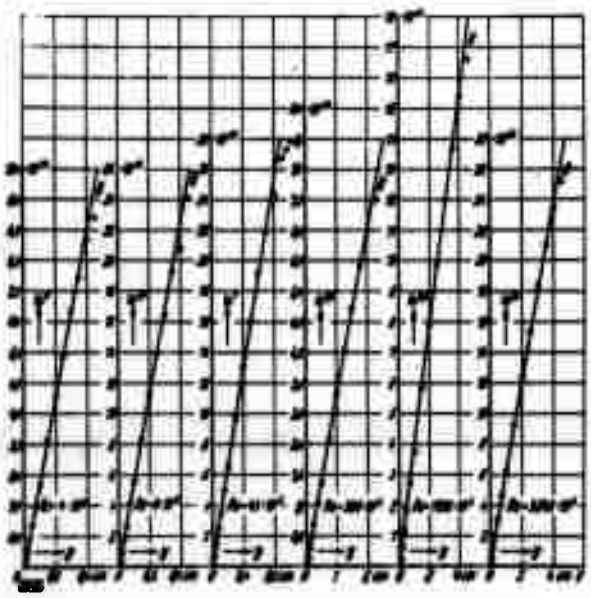

Fig. 20. 1/n Power of the Velocity in Relation to the Distance from the Wall

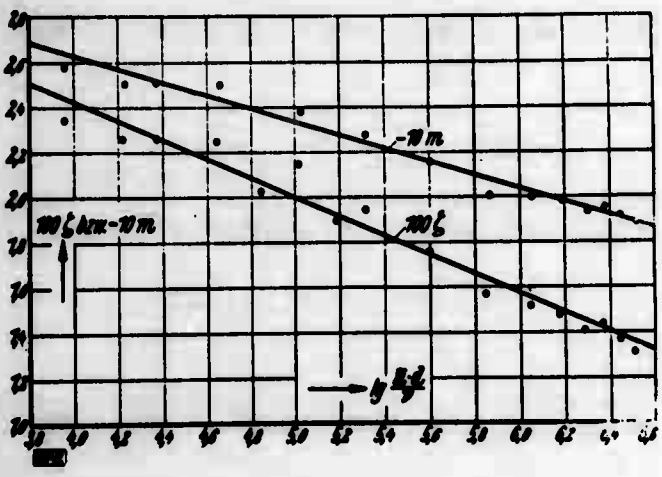

Fig. 21. 100ζ, or 10 m, in Relation to $\log\left(\frac{Wd}{\nu}\right)$

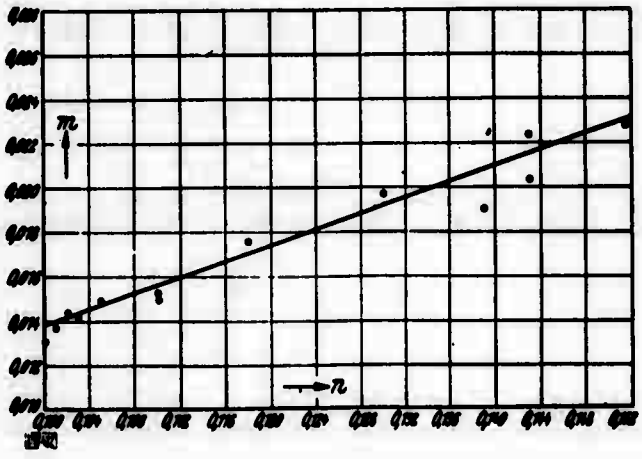

Fig. 22 m in Relation to n

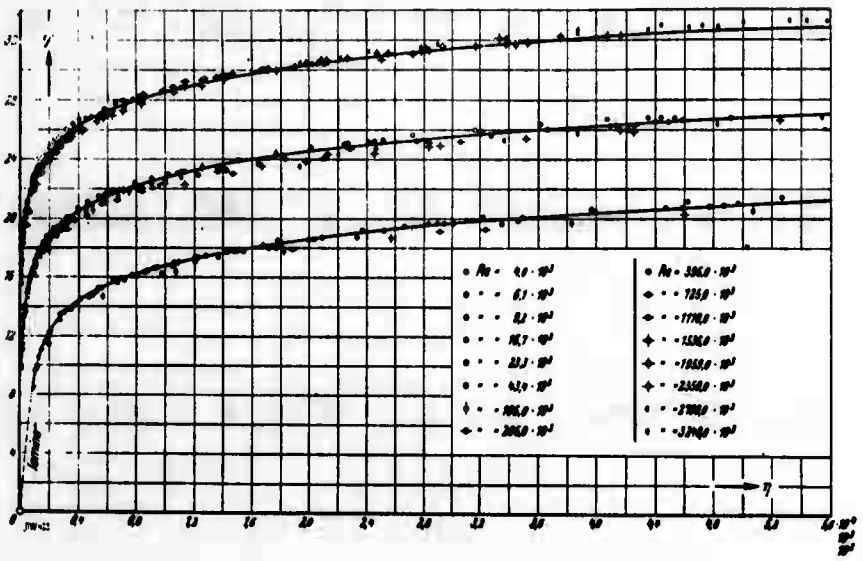

Fig. 23. Universal Velocity Distribution ($\phi = \phi[\eta]$)

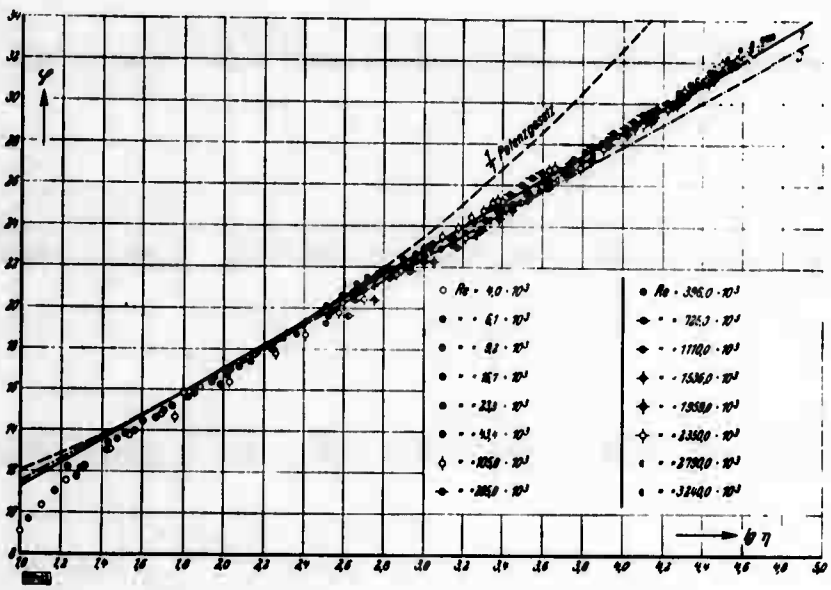

Fig. 24. ϕ in Relation to log η

Potenzgesetz = power law

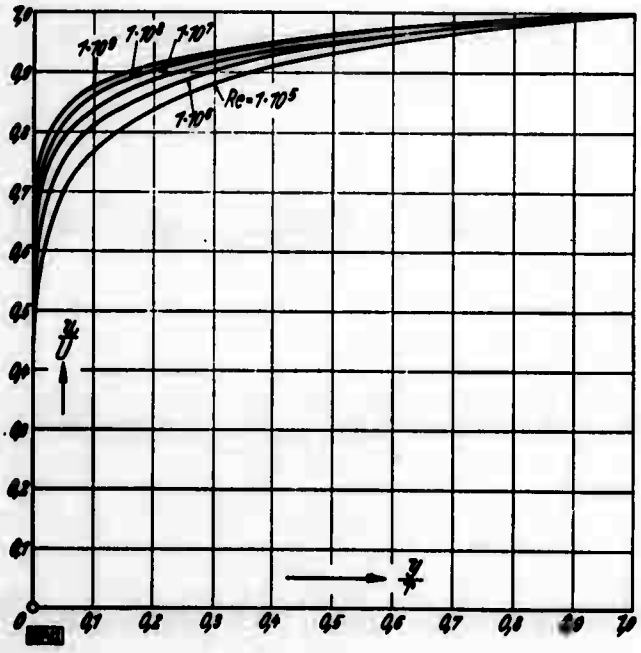

Fig. 25. Calculated Velocity Distributions for very large Reynolds' Numbers

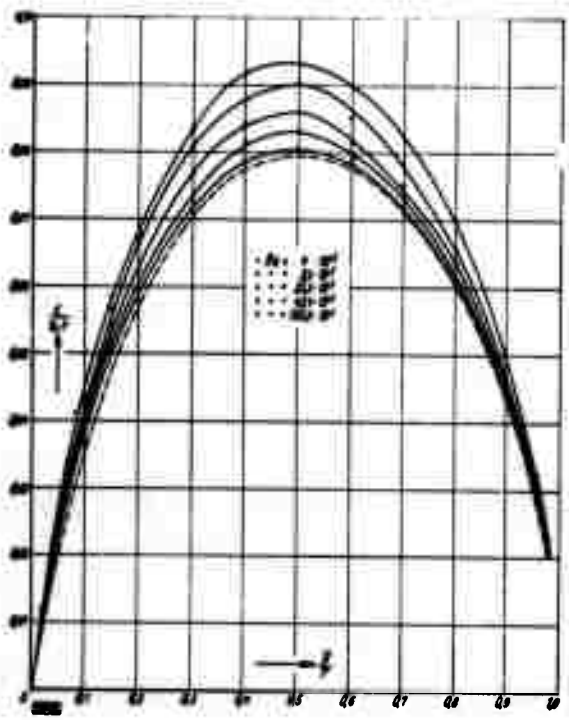

Fig. 26. $\frac{\varepsilon}{v_0 r}$ in Relation to y/r for small Reynolds' Numbers

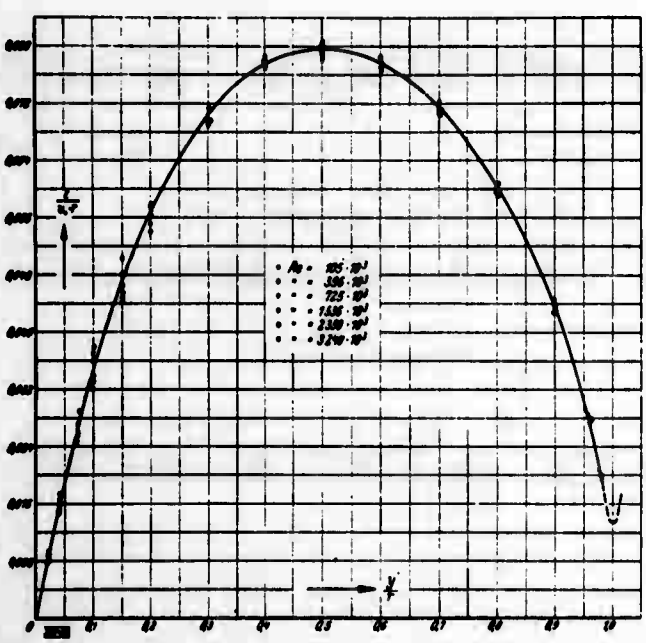

Fig. 27. $\frac{\varepsilon}{v_0 r}$ in Relation to y/r for large Reynolds' Numbers

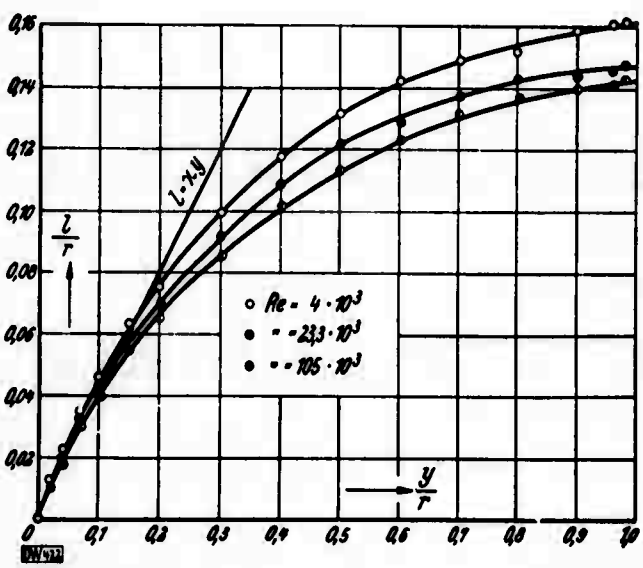

Fig. 28. l/r in Relation to y/r for small Reynolds' Numbers

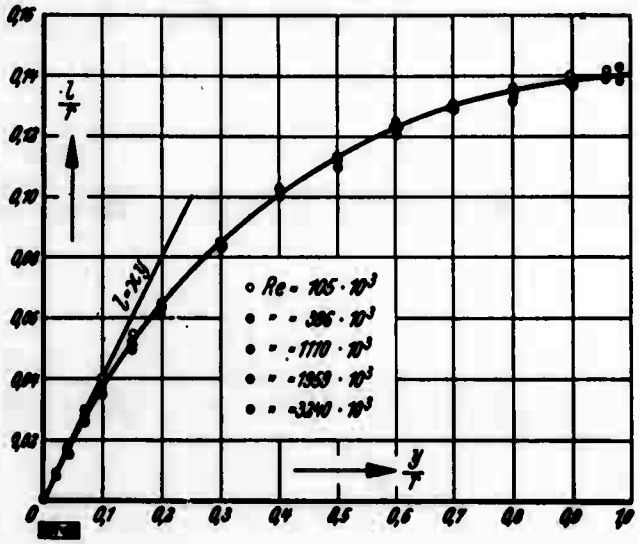

Fig. 29. l/r in Relation to y/r for Large Reynolds' Numbers

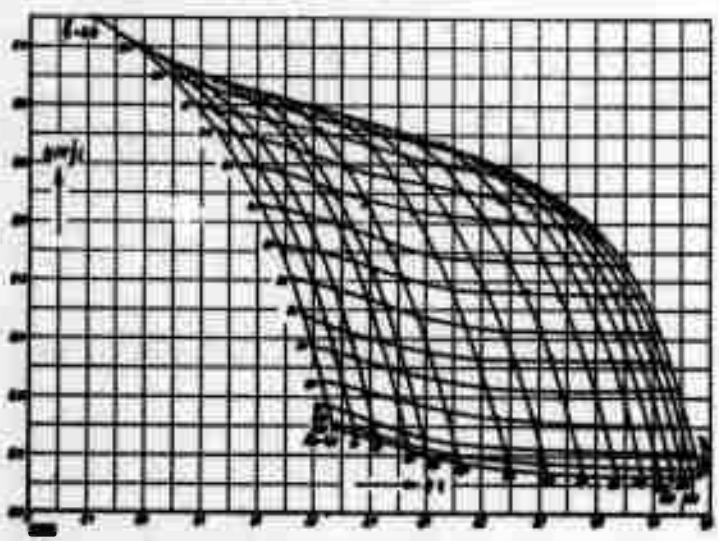

Fig. 30. Log $10\frac{l}{y}$ in Relation to log η .

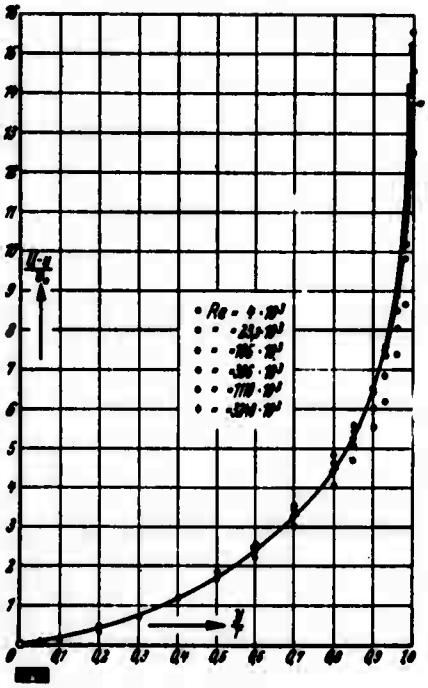

Fig. 31. $\frac{U_{max} - u}{v_*}$ in Relation to y/r

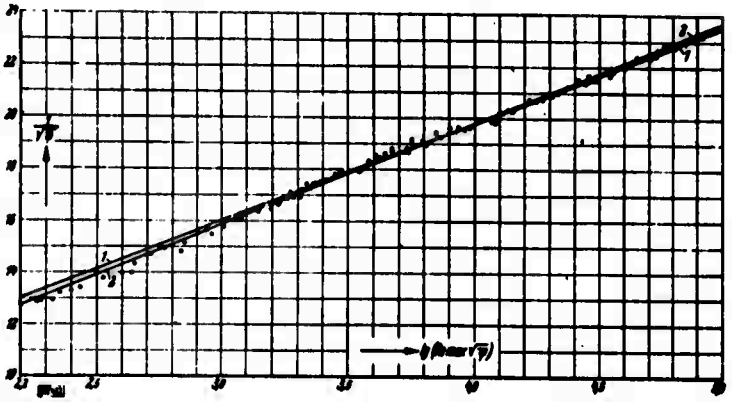

Fig. 32. $\frac{\lambda}{\sqrt{\psi}}$ in Relation to log $(Re_{max}\sqrt{\psi})$

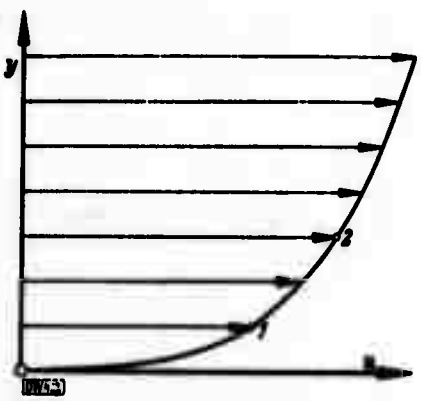

Fig. 33. Defining Diagram

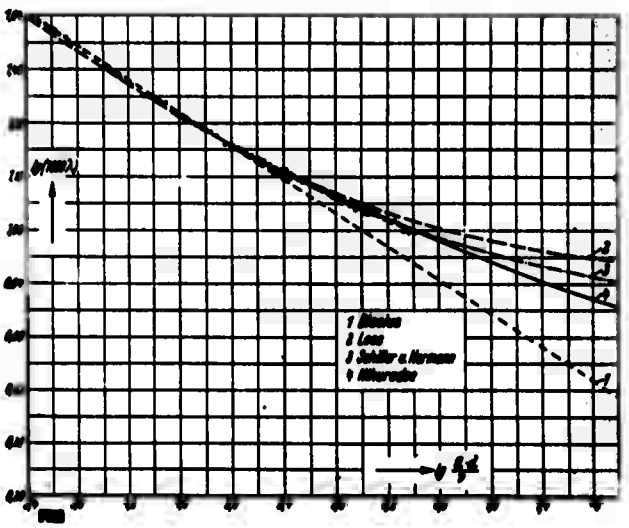

Fig. 34. log $(1000\,\lambda)$ in Relation to log $\frac{\bar{u}d}{\nu}$

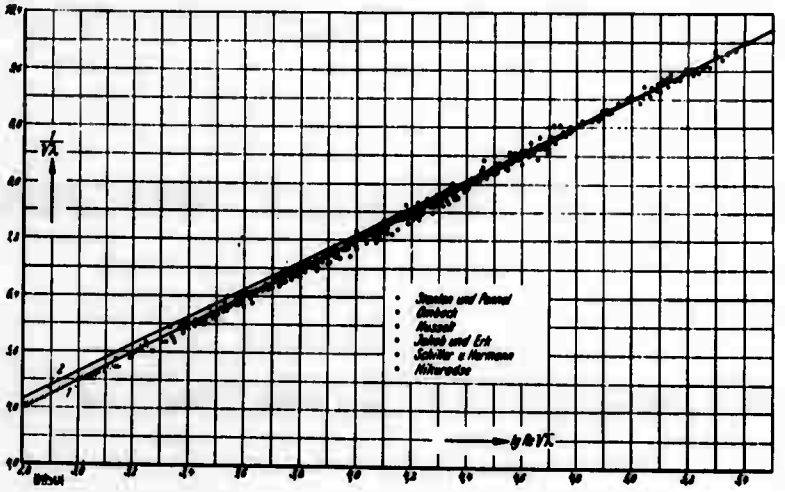

Fig. 35. $\frac{1}{\sqrt{\lambda}}$ in Relation to log ($Re\sqrt{\lambda}$)

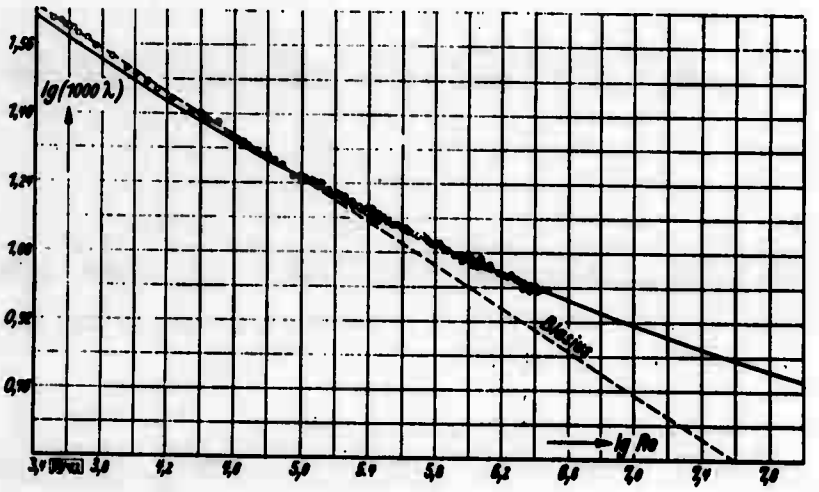

Fig. 36. log (1000 λ) in Relation to log (Re)

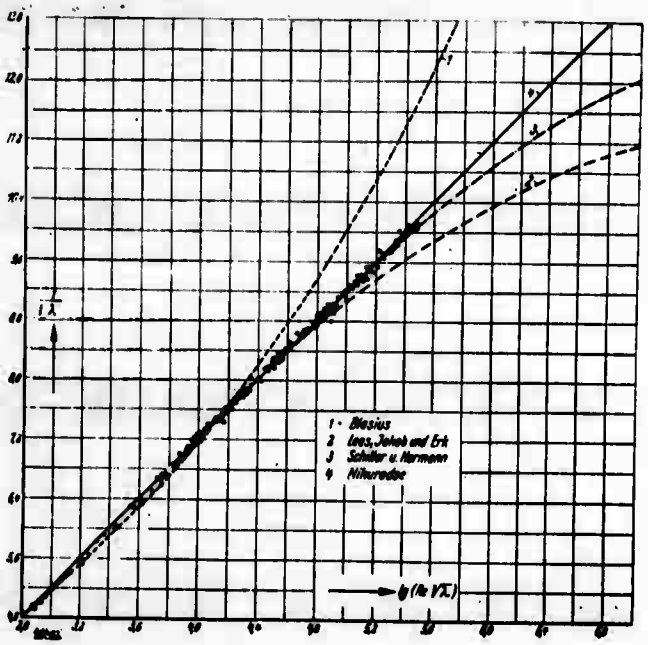

Fig. 37. $\frac{1}{\sqrt{\lambda}}$ in Relation to log $(Re\sqrt{\lambda})$

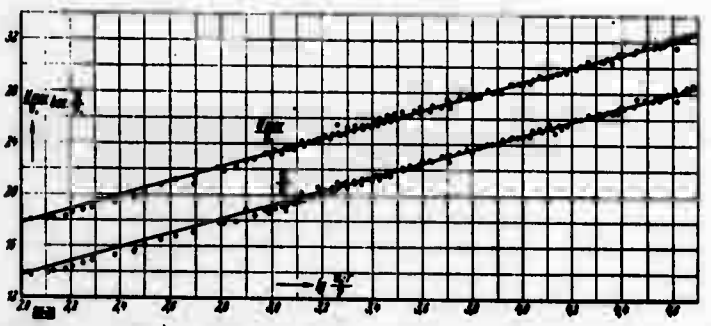

Fig. 38. $\frac{U_{max}}{v_*}$ or $\frac{\bar{u}}{v_*}$ in Relation to $\left(\frac{v_* r}{\nu}\right)$

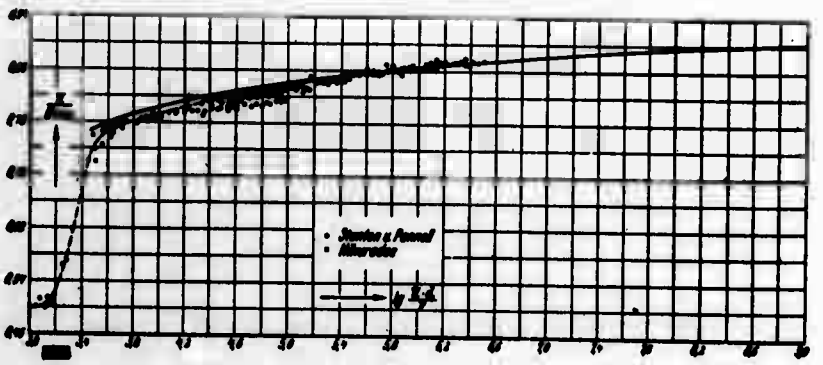

Fig. 39. $\frac{\bar{u}}{U_{max}}$ in Relation to $\log\left(\frac{\bar{u}\, d}{\nu}\right)$

Table 2

u in Comparison with y

$\frac{dp}{dx}$ $\frac{dyn}{cm^3}$	0.0595	0.1210	0.245	0.723	1.255	—	0.365	—	0.495	—	0.247
$\bar{u}$ cm/s	54.5	81.8	123.5	225.5	315	—	258.2	—	400	—	394
ν cm^2/s	0.0135	0.0135	0.0135	0.0135	0.0135	—	0.0119	—	0.0114	—	0.0096
$10^{-3}Re$	4.0	6.1	9.2	16.7	23.3	—	43.4	—	105	—	205
y cm	u cm/s	u cm/s	u cm/s	u cm/s	u cm/s	y cm	u cm/s	y cm	u cm/s	y cm	u cm/s
0.000	20.2	35.0	47.0	112.0	117.0	0.00	102.0	0.00	204.0	0.00	178.0
0.005	28.0	46.0	72.0	140.0	174.0	0.01	155.0	0.015	258.0	0.025	258.0
0.010	35.0	53.0	81.5	163.0	214.0	0.02	183.0	0.030	280.0	0.050	284.0
0.020	39.8	60.2	92.0	179.0	242.0	0.04	203.0	0.060	113.0	0.100	312.0
0.035	44.4	67.2	102.0	193.0	263.0	0.07	220.0	0.105	339.0	0.175	335.0
0.050	47.0	71.2	108.0	202.5	277.0	0.10	230.0	0.150	356.0	0.250	352.0
0.075	50.2	76.1	116.0	214.5	294.0	0.15	242.5	0.225	375.0	0.375	371.0
0.10	52.7	79.7	121.0	223.0	306.0	0.20	252.0	0.30	390.0	0.500	387.0
0.15	56.6	85.2	128.5	236.5	326.0	0.30	267.0	0.45	415.0	0.750	407.0
0.20	59.5	89.2	134.5	247.0	341.0	0.40	278.5	0.60	433.0	1.00	422.0
0.25	61.7	92.5	139.0	255.0	353.0	0.50	287.0	0.75	446.0	1.25	434.0
0.30	63.5	95.0	142.5	261.5	362.0	0.60	294.5	0.90	458.0	1.50	444.0
0.35	65.0	97.3	146.0	267.0	370.0	0.70	300.0	1.05	466.0	1.75	453.0
0.40	66.4	99.2	148.5	271.6	376.0	0.80	304.5	1.20	473.0	2.00	459.0
0.45	67.4	100.7	151.0	275.5	381.0	0.90	308.7	1.35	479.0	2.25	464.5
0.48	67.9	101.4	152.0	277.2	382.7	0.96	309.6	1.44	481.0	2.40	467.0
0.49	68.0	101.7	152.3	277.5	383.1	0.98	310.0	1.47	481.5	2.45	467.5
0.50	68.1	101.8	152.5	278.0	383.5	1.00	310.5	1.50	482.0	2.50	468.0

Table 2 continued — u in Comparison with y

$\frac{dP}{dx}$ $\frac{dyn}{cm^3}$	0.755	—	0.48	0.91	1.59	2.45	1.90	2.262	2.82
$\bar{u}$ cm/s	732	—	875	1245	1690	2150	1928	2145	2430
ν cm^2/s	0.00925	—	0.0121	0.01125	0.011	0.011	0.0082	0.0077	0.0075
10^{-3} Re	396	—	725	1110	1536	1959	2350	2790	3240
y cm	u cm/s	y cm	u cm/s	u cm/s	u cm/s	u cm/s	u cm/s	u cm/s	u cm/s
0.00	360	0.000	505	705	950	1310	1310	1423	1510
0.025	490	0.05	617	847	1160	1598	1426	1578	1794
0.05	546	0.10	654	918	1260	1685	1496	1666	1890
0.10	597	0.20	717	1026	1380	1805	1604	1758	2026
0.175	632	0.35	765	1084	1480	1896	1700	1890	2142
0.250	660	0.50	794	1133	1549	1966	1772	1967	2230
0.375	690	0.75	833	1190	1613	2050	1845	2060	2326
0.500	714	1.00	859	1229	1668	2110	1900	2122	2396
0.75	751	1.5	899	1284	1744	2204	1980	2212	2492
1.00	778	2.0	929	1325	1799	2270	2040	2272	2566
1.25	799	2.5	954	1359	1840	2325	2088	2322	2622
1.50	816	3.0	973	1386	1876	2370	2128	2362	2670
1.75	831	3.5	988	1407	1902	2410	2156	2392	2706
2.00	842	4.00	1000	1424	1925	2437	2181	2418	2736
2.25	851	4.5	1010	1436	1940	2456	2198	2436	2755
2.40	854	4.8	1014	1441	1946	2463	2202	2445	2762
2.45	855	4.9	1015	1442	1948	2465	2203	2448	2764
2.50	856	5.0	1015.5	1443	1944	2466	2204	2449	2766

u = particular velocity

y = distance from the wall

Re = Reynolds' number

$\bar{u}$ = mean velocity

d = tube diameter

ν = kinematic viscosity

Table 3

ϕ in Comparison with η

$\phi = \frac{u}{v_*}$ = dimensionless velocity; u = particular velocity; $v_* = \sqrt{\frac{\tau_o}{\rho}}$ = shearing stress velocity; $\eta = \frac{v_* y}{\nu}$ = dimensionless distance from wall; ν = kinematic viscosity; τ_o = shearing stress at the wall; ρ = density; Re = Reynolds's Number

η	ϕ	η	ϕ	η	ϕ	η	ϕ	η	ϕ	η	ϕ	η	ϕ	η	ϕ
Re = $4 \cdot 10^3$		Re = $6.1 \cdot 10^3$		Re = $9.2 \cdot 10^3$		Re = $16.7 \cdot 10^3$		Re = $23.3 \cdot 10^3$		Re = $43.4 \cdot 10^3$		Re = $105 \cdot 10^3$		Re = $205 \cdot 10^3$	
10	9.16	11	9.75	13	10.50	17	12.28	20	12.20	30	13.6	57	14.70	98	16.31
13	10.41	15	11.08	19	11.85	27	13.45	33	13.86	52	15.1	107	16.42	188	17.90
17	11.60	21	12.35	27	13.15	41	14.50	52	15.00	86	16.35	182	17.80	324	19.25
21	12.30	27	13.08	36	13.92	56	15.20	72	15.79	120	17.10	257	18.70	460	20.21
28	13.13	37	14.00	50	14.95	80	16.11	105	16.75	176	18.00	383	19.70	687	21.30
35	13.80	47	14.65	65	15.60	105	16.79	137	17.40	233	18.70	507	20.50	913	22.22
50	14.58	68	15.65	93	16.65	154	17.80	202	18.60	346	19.83	759	21.80	1367	23.40
64	15.58	87	16.40	122	17.32	203	18.56	267	19.41	459	20.72	1007	22.75	1817	24.23
78	16.15	108	17.00	151	17.90	252	19.18	332	20.10	572	21.32	1258	23.40	2267	24.96
92	16.61	128	17.47	180	18.35	301	19.68	397	20.60	685	21.90	1511	24.05	2727	25.50
106	17.00	148	17.88	208	18.70	349	20.09	462	21.10	798	22.30	1761	24.50	3177	26.00
120	17.38	168	18.21	237	19.12	399	20.40	527	21.40	911	22.62	2007	24.80	3627	26.40
134	17.62	188	18.49	266	19.45	447	20.70	592	21.70	1024	22.95	2267	25.15	4082	26.61
143	17.77	201	18.56	283	19.60	477	20.82	631	21.80	1092	23.00	2412	25.30	4357	26.80
146	17.79	205	18.66	289	19.63	487	20.85	643	21.81	1116	23.03	2467	25.33	4447	26.85
149	17.80	209	18.70	294	19.65	497	21.00	657	21.83	1137	23.10	2511	25.36	4537	26.90

Table 3 continued

ψ in Comparison with η

η	ψ	η	ψ	η	ψ	η	ψ	η	ψ	η	ψ	η	ψ	η	ψ
Re = $396 \cdot 10^3$		Re = $725 \cdot 10^3$		Re = $1110 \cdot 10^3$		Re = $1536 \cdot 10^3$		Re = $1959 \cdot 10^3$		Re = $2350 \cdot 10^3$		Re = $2790 \cdot 10^3$		Re = $3240 \cdot 10^3$	
171	17.98	299	19.08	427	17.91	580	20.20	700	21.72	830	21.92	967	22.40	1110	22.75
335	19.65	573	20.92	847	19.45	1140	22.10	1410	23.27	1670	23.50	1934	23.60	2220	24.40
581	20.80	997	22.32	1477	21.70	1980	23.70	2460	24.45	2920	24.90	3380	25.40	3880	25.80
827	21.70	1426	23.16	2107	24.00	2830	24.80	3520	25.35	4160	26.00	4835	26.38	5550	26.82
1237	22.70	2129	24.30	3160	25.20	4250	25.85	5270	26.45	6250	27.00	7250	27.70	8330	28.00
1647	23.45	2842	25.06	4210	26.00	5660	26.70	7040	27.22	8340	27.80	9670	28.50	11100	28.82
2467	24.76	4257	26.23	6310	27.20	8500	27.95	10540	28.42	12510	29.00	14500	29.65	16650	30.00
3287	25.60	5667	27.10	8410	28.05	11300	28.80	14080	29.28	16680	29.90	19340	30.50	22200	30.90
4107	26.22	7087	27.92	10510	28.75	14150	29.50	17580	30.00	20850	30.60	24200	31.20	27740	31.60
4927	26.82	8507	28.35	12600	29.35	17000	30.07	21120	30.60	25020	31.20	29000	31.74	33300	32.17
5752	27.40	9907	28.53	14700	29.80	19800	30.50	24620	31.10	29190	31.60	33800	32.10	38800	32.58
6567	27.70	11327	29.17	16800	30.20	20600	30.84	28160	31.40	33360	32.00	38680	32.40	44400	32.90
7727	28.00	12757	29.46	18910	30.40	25500	31.10	31620	31.60	37530	32.20	43500	32.70	50000	33.10
7877	28.05	13610	29.58	20210	30.53	27200	31.18	33750	31.79	40000	32.28	46420	32.80	53300	33.21
8057	28.15	13910	29.59	20610	30.57	27800	31.20	34450	31.80	40900	32.30	47400	32.86	54400	33.24
8217	28.20	14200	29.60	21000	30.60	28300	31.21	35200	31.82	41700	32.31	48400	32.90	55500	33.30

Table 4 $\frac{\epsilon}{v_* r}$ in Comparison with $\frac{y}{r}$

$\frac{y}{r}$	$\frac{\tau}{\rho}$	$\frac{du}{dy}$	$\frac{\epsilon}{v_* r}$	$\frac{\tau}{\rho}$	$\frac{du}{dy}$	$\frac{\epsilon}{v_* r}$	$\frac{\tau}{\rho}$	$\frac{du}{dy}$	$\frac{\epsilon}{v_* r}$	$\frac{\tau}{\rho}$	$\frac{du}{dy}$	$\frac{\epsilon}{v_* r}$
	$Re = 4 \cdot 10^3$; $v_* = 3.82$ cm/s			$Re = 6.1 \cdot 10^3$; $v_* = 5.44$ cm/s			$Re = 9.2 \cdot 10^3$; $v_* = 7.76$ cm/s			$Re = 16.7 \cdot 10^3$; $v_* = 13.3$ cm/s		
	r = 0.5 cm			r = 0.5 cm			r = 0.5 cm			r = 0.5 cm		
0.02	14.30	631.0	0.0119	29.0	945.0	0.01135	59.0	1392	0.0108	173.7	2540	0.01025
0.04	14.00	340.0	0.0216	28.4	501.0	0.01042	57.8	738	0.0202	170.0	1322	0.01935
0.07	13.55	210.0	0.0338	27.5	318.0	0.0320	56.0	454	0.0318	164.6	782	0.03170
0.10	13.12	157.0	0.0437	26.0	231.0	0.0427	54.1	331	0.0422	159.2	583	0.0410
0.15	12.40	111.0	0.0585	25.2	163.0	0.0572	51.1	233	0.0565	150.4	405	0.0560
0.20	11.68	90.0	0.0680	23.6	129.0	0.0678	48.1	187	0.0662	141.5	330	0.0645
0.30	10.21	64.0	0.0835	20.7	93.0	0.0825	42.1	134	0.0812	124.0	232	0.0804
0.40	8.75	50.0	0.0916	17.75	73.0	0.0905	36.1	106	0.0878	106.2	184	0.0869
0.50	7.30	41.0	0.0933	14.80	59.0	0.0930	30.1	86	0.0904	88.5	152	0.0876
0.60	5.84	34.0	0.0900	11.82	50.0	0.0875	24.1	73	0.0852	70.8	129	0.0825
0.70	4.38	29.0	0.0820	8.88	41.0	0.0804	18.1	59	0.0788	53.1	104	0.0767
0.80	2.95	22.0	0.0700	5.92	32.0	0.0685	12.0	47.0	0.0659	35.4	83	0.0641
0.90	1.46	15.2	0.0502	2.96	22.0	0.0500	6.0	33	0.0469	17.7	58	0.0459
0.96	0.584	9.5	0.0322	1.183	13.8	0.0317	2.4	20	0.0310	7.08	35.5	0.0301
0.98	0.292	6.7	0.0228	0.592	9.8	0.0224	1.2	14	0.0221	3.54	25	0.0212
	$Re = 23.3 \cdot 10^3$; $v_* = 17.55$ cm/s			$Re = 43.4 \cdot 10^3$; $v_* = 13.44$ cm/s			$Re = 105 \cdot 10^3$; $v_* = 19.05$ cm/s			$Re = 205 \cdot 10^3$; $v_* = 17.4$ cm/s		
	r = 0.5 cm			r = 0.5 cm			r = 1.5 cm			r = 2.5 cm		
0.02	302.0	3410	0.0101	177.0	1348	0.0098	356	1338	0.0093	297.0	755	0.0091
0.04	296.0	1760	0.0192	173.5	693	0.0186	350	698	0.0175	291.0	390	0.0172
0.07	286.0	1040	0.0313	168.0	411	0.0304	338	407	0.0290	282.0	232	0.0280
0.10	277.0	778	0.0406	162.6	302	0.0401	328	302	0.0380	273.0	170	0.0369
0.15	262.0	550	0.0542	153.6	220	0.0520	310	215	0.0504	258.0	121	0.0490
0.20	246.0	448	0.0625	144.6	181	0.0594	290.5	175	0.0580	242.0	96	0.0580
0.30	215.0	318	0.0770	126.5	129	0.0730	255	125	0.0714	212.0	69	0.0707
0.40	185.0	250	0.0844	108.5	99	0.0816	218	97	0.0787	182.0	53	0.0790
0.50	154.0	204	0.0860	90.4	81	0.0832	182	79	0.0805	151.5	44	0.0791
0.60	123.0	172	0.0815	72.4	68	0.0795	145.6	65	0.0784	121.0	36.3	0.0768
0.70	92.5	140	0.0753	54.2	55	0.0735	109.2	53.3	0.0718	90.9	29.2	0.0715
0.80	61.5	110	0.0638	36.2	44	0.0612	72.8	41.6	0.0610	60.6	22.9	0.0610
0.90	30.8	77	0.0455	18.1	30	0.0450	36.4	28.8	0.0443	30.3	15.8	0.0441
0.96	12.3	478	0.0293	7.24	18.5	0.0292	14.5	17.9	0.0284	12.1	9.9	0.0280
0.98	6.15	335	0.0210	3.62	13.0	0.0208	7.3	12.6	0.0210	6.05	7.0	0.0199

Table 4 continued $\frac{\epsilon}{v_* r}$ in Comparison with $\frac{y}{r}$

$\frac{y}{r}$	$\frac{\tau}{\rho}$	$\frac{du}{dy}$	$\frac{\epsilon}{v_* r}$	$\frac{\tau}{\rho}$	$\frac{du}{dy}$	$\frac{\epsilon}{v_* r}$	$\frac{\tau}{\rho}$	$\frac{du}{dy}$	$\frac{\epsilon}{v_* r}$	$\frac{\tau}{\rho}$	$\frac{du}{dy}$	$\frac{\epsilon}{v_* r}$
	$Re = 396 \cdot 10^3$; $v_* = 30.4$ cm/s, $r = 2.5$ cm			$Re = 725 \cdot 10^3$; $v_* = 34.28$ cm/s, $r = 5.0$ cm			$Re = 1110 \cdot 10^3$; $v_* = 47.2$ cm/s, $r = 5.0$ cm			$Re = 1536 \cdot 10^3$; $v_* = 62.4$ cm/s, $r = 5.0$ cm		
0.02	906	1370	0.0087	1151	795	0.0085	2185	1117	0.0083	3830	1506	0.0082
0.04	887	704	0.0166	1129	410	0.0160	2140	576	0.0157	3750	770	0.0156
0.07	860	416	0.0272	1092	237	0.0269	2075	337	0.0261	3630	460	0.0254
0.10	832	304	0.0360	1058	174	0.0354	2007	243	0.0350	3510	333	0.0339
0.15	785	215	0.0480	998	124	0.0470	1898	173	0.0465	3320	230	0.0465
0.20	740	169	0.0577	940	97	0.0565	1785	134.5	0.0562	3122	179	0.0561
0.30	647	123	0.0692	823	68	0.0705	1560	94.0	0.0705	2730	127	0.0691
0.40	555	92.5	0.0790	705	53.5	0.0770	1340	72.3	0.0785	2340	97.5	0.0771
0.50	462	76	0.0802	587	43.7	0.0782	1115	59.2	0.0796	1950	80.0	0.0785
0.60	370	62	0.0785	470	35.7	0.0766	893	48.4	0.0781	1560	64.8	0.0775
0.70	277	51.7	0.0705	352	29.0	0.0710	670	39.2	0.0725	1170	53.1	0.0709
0.80	185	41.0	0.0595	235	23.0	0.0596	446	31.2	0.0606	780	41.9	0.0600
0.90	92.5	27.8	0.0438	117.5	16.0	0.0428	223	21.5	0.0439	390	28.8	0.0435
0.96	37.0	17.5	0.0278	47.0	9.9	0.0277	89.3	13.5	0.0280	156	18.0	0.0279
0.98	18.5	12.3	0.0189	23.5	7.0	0.0196	44.6	9.6	0.0197	78	12.8	0.0196

Table 4 continued — $\frac{\epsilon}{v_* r}$ in Comparison with $\frac{y}{r}$

$\frac{y}{r}$	$\frac{\tau}{\rho}$	$\frac{du}{dy}$	$\frac{\epsilon}{v_* r}$	$\frac{\tau}{\rho}$	$\frac{du}{dy}$	$\frac{\epsilon}{v_* r}$	$\frac{\tau}{\rho}$	$\frac{du}{dy}$	$\frac{\epsilon}{v_* r}$	$\frac{\tau}{\rho}$	$\frac{du}{dy}$	$\frac{\epsilon}{v_* r}$
	$Re = 1959 \cdot 10^3$; $v_* = 77.5$ cm/s, $r = 5.0$ cm			$Re = 2350 \cdot 10^3$; $v_* = 68.3$ cm/s, $r = 5.0$ cm			$Re = 2790 \cdot 10^3$; $v_* = 74.5$ cm/s, $r = 5.0$ cm			$Re = 3240 \cdot 10^3$; $v_* = 83.1$ cm/s, $r = 5.0$ cm		
0.02	5900	1890	0.0081	4567	1670	0.0080	5460	1860	0.0079	6760	2080	0.0078
0.04	5770	977	0.0154	4474	872	0.0151	5345	968	0.0148	6620	1085	0.0147
0.07	5595	575	0.0251	4330	514	0.0248	5172	573	0.0242	6412	645	0.0243
0.10	5410	414	0.0338	4194	370	0.0332	5000	414	0.0324	6210	466	0.0321
0.15	5110	288	0.0459	3870	254	0.0447	4730	280	0.0454	5860	319	0.0442
0.20	4810	223	0.0558	3730	198.5	0.0551	4450	221	0.0540	5515	246	0.0540
0.30	4210	157	0.0692	3265	138	0.0693	3900	151	0.0692	4882	168	0.0697
0.40	3604	118	0.0790	2800	106	0.0775	3360	114.7	0.0787	4140	128	0.0775
0.50	3005	98	0.0792	2330	86.2	0.0791	2780	95.0	0.0786	3450	104	0.0797
0.60	2404	81	0.0767	1865	70.2	0.0780	2224	76.7	0.0780	2760	86.7	0.0765
0.70	1803	65.6	0.0710	1400	57.0	0.0721	1669	63.2	0.0708	2068	69.5	0.0714
0.80	1202	52.0	0.0596	932	45.5	0.0600	1112	50.5	0.0591	1380	55.7	0.0595
0.90	601	35.6	0.0435	466	31.7	0.0431	556	34.5	0.0433	690	38.8	0.0427
0.96	240	22.3	0.0278	186.4	19.8	0.0276	222	21.4	0.0278	276	23.7	0.0280
0.98	120	15.9	0.0195	93.2	13.9	0.0196	111	15.1	0.0197	138	16.8	0.0197

ϵ = amount of turbulent exchange; $v_* = \sqrt{\frac{\tau}{\rho}}$ = shearing stress velocity; r = tube radius; y = distance from the wall; τ = shearing stress at the wall; ρ = density; $\frac{du}{dy}$ = differential quotient of velocity; Re = Reynolds's Number; $\bar{u}$ = mean velocity; ν = kinematic viscosity.

Table 5 $\frac{l}{r}$ in Comparison with $\frac{y}{r}$

l = mixing length; r = tube radius; y = distance from the wall; Re = Reynolds' Number; $\bar{u}$ = mean velocity; ν = kinematic viscosity.

$\frac{y}{r}$	$\frac{l}{r}$ Re = $4.0 \cdot 10^3$ r = 0.5 cm	$\frac{l}{r}$ Re = $6.1 \cdot 10^3$ r = 0.5 cm	$\frac{l}{r}$ Re = $9.2 \cdot 10^3$ r = 0.5 cm	$\frac{l}{r}$ Re = $16.7 \cdot 10^3$ r = 0.5 cm	$\frac{l}{r}$ Re = $23.3 \cdot 10^3$ r = 0.5 cm	$\frac{l}{r}$ Re = $43.4 \cdot 10^3$ r = 1.0 cm	$\frac{l}{r}$ Re = $105 \cdot 10^3$ r = 1.5 cm	$\frac{l}{r}$ Re = $205 \cdot 10^3$ r = 2.5 cm
0.02	0.0120	0.0114	0.0110	0.0104	0.0102	0.0099	0.0094	0.0092
0.04	0.0220	0.0212	0.0206	0.0197	0.0195	0.0190	0.0179	0.0175
0.07	0.0351	0.0340	0.0330	0.0328	0.0325	0.0315	0.0300	0.0290
0.10	0.0460	0.0446	0.0444	0.0432	0.0428	0.0423	0.0400	0.0389
0.15	0.0634	0.0616	0.0614	0.0606	0.0588	0.0564	0.0546	0.0532
0.20	0.0758	0.0752	0.0742	0.0720	0.0700	0.0665	0.0652	0.0649
0.30	0.0996	0.0978	0.0968	0.0960	0.0922	0.0872	0.0850	0.0845
0.40	0.1180	0.1156	0.1132	0.1120	0.1088	0.1049	0.1015	0.1016
0.50	0.1320	0.1304	0.1276	0.1218	0.1216	0.1173	0.1136	0.1120
0.60	0.1422	0.1372	0.1344	0.1304	0.1288	0.1250	0.1236	0.1210
0.70	0.1492	0.1454	0.1440	0.1400	0.1374	0.1346	0.1310	0.1305
0.80	0.1520	0.1520	0.1472	0.1432	0.1428	0.1383	0.1367	0.1360
0.90	0.1590	0.1564	0.1486	0.1450	0.1440	0.1417	0.1398	0.1395
0.96	0.1608	0.1574	0.1548	0.1500	0.1466	0.1454	0.1418	0.1411
0.98	0.1614	0.1572	0.1564	0.1540	0.1480	0.1464	0.1430	0.1400

Table 5 continued $\frac{l}{r}$ in Comparison with $\frac{y}{r}$

$\frac{y}{r}$	Re = $396 \cdot 10^3$ r = 2.5 cm $\frac{l}{r}$	Re = $725 \cdot 10^3$ r = 2.5 cm $\frac{l}{r}$	Re = $1110 \cdot 10^3$ r = 5.0 cm $\frac{l}{r}$	Re = $1536 \cdot 10^3$ r = 5.0 cm $\frac{l}{r}$	Re = $1959 \cdot 10^3$ r = 5.0 cm $\frac{l}{r}$	Re = $2350 \cdot 10^3$ r = 5.0 cm $\frac{l}{r}$	Re = $2790 \cdot 10^3$ r = 5.0 cm $\frac{l}{r}$	Re = $3240 \cdot 10^3$ r = 5.0 cm $\frac{l}{r}$
0.02	0.0088	0.0086	0.0084	0.0082	0.0081	0.0081	0.0080	0.0079
0.04	0.0169	0.0164	0.0161	0.0158	0.0156	0.0154	0.0151	0.0150
0.07	0.0282	0.0279	0.0270	0.0262	0.0260	0.0256	0.0251	0.0248
0.10	0.0370	0.0374	0.0368	0.0356	0.0355	0.0350	0.0342	0.0338
0.15	0.0520	0.0509	0.0505	0.0500	0.0496	0.0490	0.0492	0.0481
0.20	0.0645	0.0631	0.0628	0.0624	0.0622	0.0615	0.0607	0.0604
0.30	0.0830	0.0845	0.0840	0.0820	0.0827	0.0829	0.0826	0.0833
0.40	0.1020	0.0994	0.1011	0.0990	0.1017	0.1000	0.1010	0.1000
0.50	0.1130	0.1110	0.1130	0.1101	0.1120	0.1120	0.1110	0.1130
0.60	0.1240	0.1218	0.1238	0.1220	0.1211	0.1230	0.1230	0.1211
0.70	0.1290	0.1294	0.1319	0.1290	0.1294	0.1312	0.1291	0.1310
0.80	0.1329	0.1330	0.1353	0.1337	0.1330	0.1340	0.1320	0.1332
0.90	0.1382	0.1359	0.1389	0.1340	0.1377	0.1360	0.1368	0.1359
0.96	0.1390	0.1389	0.1400	0.1390	0.1391	0.1380	0.1390	0.1400
0.98	0.1400	0.1381	0.1390	0.1380	0.1380	0.1390	0.1390	0.1400

Table 6

l/y in Comparison with y/r and Log $(100\, l/y)$ in Comparison with Log η

l = mixing length; y = distance from the wall; $\eta = \frac{v_* y}{\nu}$ = dimensionless wall distance;

$v_* = \sqrt{\frac{\tau_o}{\rho}}$ = shearing stress velocity; ν = kinematic viscosity; r = tube radius; Re = Reynolds' Number

$\bar{u}$ = mean velocity

$\frac{y}{r}$	η	l/y	η	l/y	η	l/y	η	l/y	η	l/y	η	l/y	η	l/y	η	l/y
	Re $=4\cdot10^3$ r =0.5 cm		Re $=6.1\cdot10^3$ r =0.5 cm		Re $=9.2\cdot10^3$ r = 0.5 cm		Re $=16.6\cdot10^3$ r = 0.5 cm		Re $=23.3\cdot10^3$ r =0.5 cm		Re $=43.4\cdot10^3$ r =1.0 cm		Re $=105\cdot10^3$ r =1.5 cm		Re $=205\cdot10^3$ r =2.5 cm	
0.02	2.83	0.600	4.03	0.569	5.75	0.552	9.8	0.518	13	0.510	22.6	0.495	50	0.470	90.5	0.457
0.04	5.66	0.550	8.10	0.531	11.5	0.515	19.6	0.493	26	0.488	45.2	0.475	100	0.447	181	0.437
0.07	9.90	0.501	14.1	0.485	20.1	0.470	34.2	0.468	46	0.464	79.1	0.450	175	0.430	317	0.415
0.10	14.14	0.460	20.2	0.446	28.7	0.443	49.0	0.433	65	0.429	113.0	0.423	250	0.400	453	0.389
0.15	21.20	0.422	30.2	0.410	43.1	0.409	73.4	0.404	98	0.392	169.4	0.376	376	0.364	680	0.355
0.20	28.30	0.379	40.3	0.376	57.5	0.371	98.0	0.360	130	0.350	226.0	0.333	500	0.326	906	0.324
0.30	42.50	0.333	60.5	0.326	86.3	0.323	147	0.320	195	0.307	339	0.291	752	0.284	1360	0.2822
0.40	56.60	0.295	80.5	0.289	115.0	0.288	196	0.280	260	0.272	452	0.262	1000	0.254	1810	0.254
0.50	70.70	0.264	101.0	0.261	143.8	0.256	245	0.248	325	0.243	565	0.2346	1251	0.227	2260	0.224
0.60	85.00	0.237	121.0	0.229	172.5	0.224	294	0.217	390	0.215	678	0.2083	1504	0.206	2720	0.202
0.70	99.00	0.213	141.0	0.208	201.0	0.206	342	0.200	455	0.1965	791	0.1920	1754	0.187	3170	0.186
0.80	113.00	0.190	161.0	0.190	230.0	0.184	392	0.179	520	0.1785	904	0.1716	2000	0.171	3620	0.170
0.90	127.30	0.1765	181.2	0.175	258.5	0.165	440	0.161	585	0.160	1017	0.1574	2260	0.1555	4075	0.155
0.96	136.0	0.1675	193.5	0.164	276.0	0.1615	470	0.1563	624	0.153	1085	0.1515	2405	0.1478	4350	0.147
0.98	138.8	0.1645	197.5	0.163	282.0	0.1595	480	0.1535	636	0.1512	1109	0.1480	2460	0.146	4440	0.143

Table 6 continued $\frac{l}{y}$ in Comparison with $\frac{y}{r}$ and Log $(100\ \frac{l}{y})$ in Comparison with Log η

	η	$\frac{l}{y}$	η	$\frac{l}{y}$	η	$\frac{l}{y}$	η	$\frac{l}{y}$	η	$\frac{l}{y}$	η	$\frac{l}{y}$	η	$\frac{l}{y}$	η	$\frac{l}{y}$
$\frac{y}{r}$	Re = 396·10³ r = 2.5 cm		Re = 725·10³ r = 2.5 cm		Re = 1110·10³ r = 5.0 cm		Re = 1536·10³ r = 5.0 cm		Re = 1959·10³ r = 5.0 cm		Re = 2350·10³ r = 5.0 cm		Re = 2790·10³ r = 5.0 cm		Re = 3240·10³ r = 5.0 cm	
0.02	0.164	0.439	0.284	0.427	0.42	0.418	0.566	0.411	0.704	0.406	0.834	0.404	0.967	0.398	1.11	0.395
0.04	0.328	0.423	0.566	0.410	0.84	0.401	1.13	0.394	1.41	0.389	1.668	0.384	1.934	0.378	2.22	0.375
0.07	0.574	0.404	0.990	0.399	1.47	0.386	1.98	0.375	2.46	0.372	2.92	0.366	3.380	0.358	3.88	0.355
0.10	0.820	0.380	1.419	0.375	2.10	0.367	2.83	0.356	3.52	0.355	4.16	0.350	4.835	0.332	5.55	0.338
0.15	1.230	0.347	2.122	0.339	3.15	0.336	4.25	0.334	5.27	0.331	6.25	0.327	7.25	0.328	8.33	0.321
0.20	1.64	0.322	2.835	0.316	4.20	0.314	5.66	0.312	7.04	0.311	8.34	0.308	9.67	0.304	11.10	0.302
0.30	2.46	0.277	4.250	0.282	6.30	0.281	8.50	0.274	10.54	0.276	12.51	0.276	14.50	0.276	16.65	0.278
0.40	3.28	0.255	5.66	0.249	8.40	0.253	11.30	0.248	14.08	0.254	16.68	0.250	19.34	0.253	22.20	0.250
0.50	4.10	0.227	7.08	0.222	10.50	0.226	14.15	0.221	17.58	0.224	20.85	0.224	24.20	0.222	27.74	0.226
0.60	4.92	0.207	8.50	0.203	12.60	0.206	17.00	0.203	21.12	0.202	25.02	0.205	29.00	0.205	33.30	0.202
0.70	5.745	0.184	9.90	0.185	14.70	0.188	19.80	0.184	24.62	0.185	29.19	0.188	33.80	0.185	38.80	0.187
0.80	6.56	0.166	11.32	0.166	16.80	0.169	22.60	0.167	28.16	0.166	33.36	0.138	38.68	0.165	44.40	0.167
0.90	7.72	0.154	12.75	0.151	18.90	0.154	25.50	0.152	31.62	0.153	37.53	0.151	43.50	0.152	50.0	0.151
0.96	7.87	0.145	13.60	0.145	20.20	0.146	27.20	0.145	33.75	0.145	40.00	0.144	46.42	0.145	53.3	0.146
0.98	8.05	0.143	13.90	0.141	20.60	0.142	27.80	0.141	34.45	0.141	40.90	0.142	47.40	0.1422	54.40	0.143

Table 7

$\frac{U-u}{v_*}$ in Comparison with $\frac{y}{r}$

10^{-3}Re	4	6.1	9.2	16.7	23.3	43.4	105	205	396	725	1110	1596	1959	2350	2790	3240
$\frac{y}{r}$	$\frac{U-u}{v_*}$	$\frac{U-u}{v_*}$	$\frac{U-u}{v_*}$	$\frac{U-u}{v_*}$	$\frac{U-u}{v_*}$	$\frac{U-u}{v_*}$	$\frac{U-u}{v_*}$	$\frac{U-u}{v_*}$	$\frac{U-u}{v_*}$	$\frac{U-u}{v_*}$	$\frac{U-u}{v_*}$	$\frac{U-u}{v_*}$	$\frac{U-u}{v_*}$	$\frac{U-u}{v_*}$	$\frac{U-u}{v_*}$	$\frac{U-u}{v_*}$
1.00	12.52	12.92	13.48	12.50	15.20	15.50	14.60	16.65	16.30	14.90	15.60	16.00	14.90	13.09	13.80	15.10
0.98	8.66	8.98	9.15	8.65	9.65	9.48	10.60	10.59	10.20	10.54	11.06	11.05	10.09	10.36	10.50	10.54
0.96	7.40	7.65	7.80	7.45	8.06	8.00	8.88	8.95	8.50	8.71	8.83	9.11	8.54	8.79	9.30	8.90
0.93	6.20	6.36	6.76	6.39	6.86	6.74	7.51	7.64	7.35	7.31	7.59	7.51	7.35	7.39	7.51	7.50
0.90	5.53	5.63	5.74	5.67	6.06	5.99	6.62	6.66	6.45	6.45	6.55	6.41	6.45	6.33	6.47	6.45
0.85	4.69	4.73	4.70	4.77	5.10	5.05	5.61	5.56	5.45	5.33	5.35	5.49	5.37	5.25	5.23	5.29
0.80	4.04	4.06	4.07	4.14	4.42	4.35	4.84	4.65	4.66	4.56	4.52	4.50	4.60	4.45	4.40	4.45
0.70	3.02	3.05	3.10	3.20	3.28	3.24	3.52	3.50	3.45	3.40	3.36	3.28	3.38	3.28	3.18	3.30
0.60	2.26	2.32	2.32	2.33	2.42	2.38	2.58	2.64	2.58	2.52	2.50	2.40	2.53	2.40	2.38	2.40
0.50	1.68	1.71	1.74	1.73	1.74	1.75	1.89	1.95	1.87	1.80	1.77	1.75	1.82	1.70	1.71	1.73
0.40	1.21	1.23	1.29	1.24	1.23	1.19	1.26	1.38	1.31	1.24	1.20	1.17	1.24	1.11	1.17	1.56
0.30	0.81	0.83	0.84	0.83	0.77	0.78	0.84	0.86	0.82	0.80	0.76	0.75	0.72	0.70	0.77	0.72
0.20	0.39	0.48	0.52	0.48	0.43	0.45	0.47	0.57	0.46	0.45	0.40	0.39	0.37	0.34	0.42	0.36
0.10	0.13	0.20	0.19	0.19	0.143	0.134	0.158	0.20	0.16	0.16	0.15	0.14	0.13	0.09	0.17	0.13
0.04	0.05	0.07	0.065	0.06	0.046	0.067	0.052	0.03	0.07	0.04	0.04	0.05	0.04	0.03	0.05	0.05
0.02	0.03	0.02	0.026	0.04	0.023	0.037	0.026	0.02	0.03	0.02	0.02	0.02	0.01	0.02	0.01	0.02
0.00	0.00	0.00	0.000	0.00	0.000	0.000	0.000	0.00	0.00	0.00	0.00	0.00	0.00	0.00	0.00	0.00

U = maximum velocity; u = particular velocity; v_* = shearing stress velocity; τ_0 = shearing stress at the wall; $q = \rho \frac{U^2}{2}$ = pressure rise of maximum velocity; ρ = density; y = distance from center of tube; r = tube radius.

Table 8

$\frac{1}{\sqrt{\psi}}$ in Comparison with Log ($Re_{MAX}\sqrt{\psi}$)

Nr.	U_{MAX} cm/s	$Re_{MAX} \cdot 10^{-3}$	$\tau_o \frac{Dyn}{cm^2}$	$Re_{MAX}\sqrt{\psi}\,10^{-3}$	$\frac{1}{\sqrt{\psi}}$
			d = 1 cm		
1	56.2	2.01	0.00995	0.159	12.72
2	63.4	2.35	0.01240	0.183	12.88
3	66.6	2.46	0.01375	0.192	12.82
4	74.6	2.76	0.0169	0.213	12.95
5	80.4	2.97	0.0190	0.225	13.18
6	90.0	3.33	0.0234	0.250	13.30
7	98.5	3.65	0.0275	0.272	13.42
8	125.7	4.65	0.0425	0.337	13.77
9	150.8	6.14	0.0595	0.440	13.97
10	152.5	5.65	0.0612	0.405	13.95
11	174	6.44	0.0753	0.450	14.34
12	206	7.63	0.1000	0.518	14.71
13	237.8	8.80	0.1300	0.590	14.93
14	226	10.20	0.1806	0.690	14.79
15	311	14.22	0.3140	0.920	15.48
			d = 2 cm		
16	143.5	10.62	0.0460	0.705	15.12
17	184.0	13.62	0.0710	0.870	15.62
18	218.0	16.14	0.0983	1.030	15.74
19	263.0	19.48	0.1370	1.210	16.10
20	294.0	21.78	0.1645	1.325	16.40
21	265.0	22.2	0.134	1.355	16.40
22	290.0	24.3	0.1552	1.463	16.60
23	317.0	26.6	0.184	1.595	16.69
24	317.3	26.6	0.186	1.598	16.65
25	337	28.27	0.207	1.690	16.70
26	384	32.2	0.257	1.870	17.10
27	424	35.6	0.311	2.070	17.18
28	450	37.7	0.340	2.160	17.42
29	475	39.9	0.379	2.29	17.41
30	512	43.0	0.437	2.460	17.50
31	547	46.0	0.495	2.6160	17.58
32	596	50.0	0.580	2.825	17.65
33	644	54.0	0.662	3.015	17.91
34	768	64.4	0.925	3.575	18.00
35	827	69.4	1.032	3.775	18.35
36	901	75.5	1.2025	4.060	18.55
37	975	82.6	1.3915	4.430	18.60
38	1040	88.1	1.5800	4.710	18.69
39	1155	99.5	1.9400	5.310	18.71
40	1254	108.2	2.2200	5.700	18.95
			d = 3 cm		
41	483	63.5	0.371	3.54	17.94
42	530	69.8	0.428	3.81	18.31
43	592	78.0	0.525	4.22	18.48
44	657	88.8	0.652	4.70	18.80
45	754	99.4	0.820	5.38	18.80
46	819	108.0	0.935	5.64	19.15
47	901	118.6	1.140	6.20	19.08
48	1045	137.0	1.480	7.06	19.42
49	1198	156.0	1.910	7.96	19.60
50	1304	169.0	2.245	8.60	19.62
			d = 5 cm		
51	112.5	22.8	0.0245	1.400	16.25
52	151.5	30.7	0.0414	1.825	16.84
53	210.0	42.6	0.0736	2.340	17.48
54	247.0	50.2	0.0985	2.820	17.80
55	286.0	58.1	0.1300	3.240	17.92

Table 8 continued

$\frac{1}{\sqrt{\psi}}$ in Comparison with Log ($Re_{MAX}\sqrt{\psi}$)

Nr.	U_{MAX} cm/s	$Re_{MAX} 10^{-3}$	$\tau_o \frac{Dyn}{cm^2}$	$Re_{MAX}\sqrt{\psi} \cdot 10^{-3}$	$\frac{1}{\sqrt{\psi}}$
		d = 5 cm (continued)			
56	87.5	18.0	0.01520	1.125	16 04
57	111.8	23.0	0.0238	1.405	16.36
58	125.4	25.7	0.0296	1.562	16.45
59	142.3	28.0	0.0373	1.680	16.65
60	171.0	35.2	0.0511	2.06	17.10
61	187.0	38.5	0.0600	2.23	17.25
62	218.0	44.8	0.0788	2.55	17.55
63	260.0	53.5	0.1075	2.99	17.94
64	126.0	23.5	0.0300	1.43	16.48
65	172.0	32.4	0.0529	1.92	16.88
66	236.0	46.1	0.0876	2.56	18.02
67	503.0	101.7	0.370	5.44	18.70
68	468.0	121.5	0.360	6.43	18.95
69	671.0	130.0	0.610	7.00	19.42
70	770.0	155.8	0.800	8.00	19.50
71	856.0	232.0	0.946	11.70	19.84
72	858.0	232.0	0.940	11.60	20.00
73	1068.0	285.0	1.425	14.10	20.25
74	1256.0	388.0	1.850	18.70	20.82
		d = 10 cm			
75	405	187.0	0.217	9.52	19.60
76	442	204.5	0.250	10.25	19.95
77	458	211.5	0.273	10.70	19.80
78	545	552.0	0.373	12.50	20.21
79	562	261.0	0.396	12.92	20.21
80	596	276.0	0.440	13.60	20.32
81	622	288.0	0.480	14.20	20.29
82	666	309.0	0.544	15.15	20.42
83	693	324.0	0.585	15.80	20.50
84	770	346.0	0.710	16.75	20.65
85	813	366.5	0.790	17.70	20.65
86	896	404.0	0.943	19.36	20.85
87	1015	420.0	1.200	20.04	20.22
88	948	430.5	1.055	20.60	20.88
89	976	450.0	1.110	21.48	20.96
90	1085	500.0	1.340	23.60	21.19
91	915	594.0	0.930	27.80	21.36
92	1443	640.0	2.270	29.80	21.50
93	1015	660.0	1.138	30.70	21.50
94	1084	613.0	1.305	28.60	21.45
95	1155	760.0	1.440	34.80	21.80
96	1120	780.0	1.350	35.70	21.82
97	1170	825.0	1.240	37.50	21.98
98	1045	746.0	1.176	34.20	21.82
99	793	555.0	0.695	25.80	21.50
100	882	617.0	0.850	28.50	21.65
101	958	671.0	1.000	31.00	21.65
102	1108	775.0	1.305	35.40	21.92
103	306	141.0	0.1284	7.33	19.26
104	336	155.0	0.1530	7.98	19.42
105	364	168.0	0.177	8.59	19.57
106	384	177.0	0.197	9.05	19.55
107	846	347.0	0.850	16.75	20.71
108	937	387.5	1.040	18.70	20.76
109	1168	519.0	1.557	24.55	21.25
110	1528	670.0	2.540	31.00	21.65
111	1949	885.0	4.000	40.3	22.00
112	2020	920.0	4.170	41.6	22.13
113	1620	978.0	2.675	44.75	22.38
114	2212	1005.0	5.000	45.2	22.25
115	1869	1169.0	3.550	52.0	22.42
116	1870	1183.0	3.540	52.9	22.44

Table 8 continued $\frac{1}{\sqrt{\psi}}$ in Comparison with Log $(Re_{MAX}\sqrt{\psi})$

Nr.	U_{MAX} cm/s	$Re_{MAX} 10^{-3}$ d = 10 cm	$\tau_o \frac{Dyn}{cm^2}$ (continued)	$Re_{MAX}\sqrt{\psi}\,10^{-3}$	$\frac{1}{\sqrt{\psi}}$
117	2010	1220.0	4.030	54.0	22.65
118	2207	1318.0	4.780	57.6	22.82
119	2208	1345.0	4.850	59.2	22.68
120	2465	1135.0	6.250	51.0	22.31
121	2300	1470.0	5.200	64.2	22.80
122	2446	1650.0	5.800	71.5	23.0
123	2463	1610.0	5.86	70.0	23.0
124	2525	1701.0	6.04	73.5	23.1
125	2756	1930.0	7.20	83.2	23.2

$\psi = \frac{\tau_o}{q}$ = Resistance number related to maximum velocity; τ_o = shearing stress at the wall; $q = \rho \frac{U^2}{2}$ = pressure rise of maximum velocity; ρ = density; $Re = \frac{Ur}{\nu}$ = Reynolds' Number of Maximum Velocity; r = tube radius; ν = kinematic viscosity.

Table 9

Log λ in Comparison with Log Re and $\frac{1}{\sqrt{\lambda}}$ in Comparison with Log $Re\sqrt{\lambda}$

Nr.	$\bar{u}$ cm/s	ν cm^2/s	Re $\cdot 10^{-3}$	$\frac{dp}{dx}$ Dyn/cm^3	λ	$Re\sqrt{\lambda} \cdot 10^{-3}$	$\frac{1}{\sqrt{\lambda}}$	$\frac{\bar{u}}{U_{MAX}}$
				d = 1 cm				
1	42.8	0.0140	3.07	0.0398	0.0426	0.634	4.85	0.760
2	48.5	0.0135	3.59	0.0496	0.0414	0.780	4.92	0.765
3	51.4	0.0135	3.81	0.0550	0.0408	0.770	4.95	0.770
4	57.6	0.0135	4.27	0.0676	0.0399	0.854	5.00	0.771
5	62.0	0.0135	4.60	0.0760	0.0388	0.906	5.08	0.771
6	70.2	0.0135	5.20	0.0936	0.0372	1.004	5.18	0.780
7	76.9	0.0135	5.70	0.1100	0.0363	1.086	5.25	0.780
8	98.5	0.0135	7.30	0.1700	0.0343	1.352	5.40	0.784
9	118.8	0.0135	8.80	0.238	0.0326	1.590	5.54	0.788
10	121.0	0.0135	8.97	0.245	0.0329	1.626	5.52	0.794
11	137.5	0.0135	10.9	0.3012	0.0311	1.800	5.67	0.791
12	163.3	0.0135	12.1	0.400	0.0294	2.075	5.83	0.793
13	189.0	0.0135	14.0	0.520	0.0285	2.362	5.92	0.795
14	226.0	0.0135	16.7	0.723	0.0278	2.785	6.00	0.811
15	311.0	0.0136	23.0	1.255	0.0254	3.665	6.28	0.815
				d = 2 cm				
16	114.6	0.0135	17.0	0.092	0.0274	2.81	6.04	0.800
17	148.4	0.0135	22.0	0.142	0.0253	3.50	6.29	0.807
18	175.5	0.0135	26.0	0.1966	0.0250	4.11	6.33	0.805
19	212.5	0.0135	31.5	0.274	0.0237	4.85	6.50	0.808
20	240.0	0.0135	35.6	0.329	0.0224	5.33	6.68	0.816
21	214.4	0.0119	36.0	0.264	0.02243	5.40	6.68	0.809
22	233.6	0.0119	39.2	0.3104	0.0223	5.85	6.70	0.806
23	258.0	0.0119	43.2	0.368	0.02274	6.51	6.64	0.814
24	259.6	0.0117	44.4	0.372	0.0216	6.53	6.80	0.818
25	275.8	0.0119	46.4	0.414	0.0212	6.76	6.86	0.818
26	315	0.0119	53.0	0.514	0.0196	7.42	7.14	0.820
27	349	0.0119	58.7	0.622	0.0201	8.33	7.06	0.823
28	370	0.0119	62.2	0.680	0.0188	8.52	7.30	0.822

Table 9 continued

Log λ in Comparison with Log Re and $\frac{1}{\sqrt{\lambda}}$ in Comparison with Log $Re\sqrt{\lambda}$	Nr.	$\bar{u}$ cm/s	ν cm^2s	$Re \cdot 10^{-3}$	$\frac{dp}{dx}$ Dyn/cm^3	λ	$Re\sqrt{\lambda} \cdot 10^{-3}$	$\frac{1}{\sqrt{\lambda}}$	$\frac{\bar{u}}{U_{MAX}}$
				d = 2 cm (continued)					
	29	392	0.0119	66.0	0.758	0.0194	9.19	7.18	0.825
	30	425	0.0119	71.4	0.874	0.0190	9.84	7.26	0.830
	31	454	0.0119	76.2	0.990	0.01885	10.45	7.28	0.830
	32	495	0.0119	83.3	1.160	0.0188	11.41	7.29	0.831
	33	533.6	0.0119	89.6	1.324	0.0183	12.11	7.40	0.829
	34	638	0.0119	107.3	1.850	0.0178	14.33	7.50	0.831
	35	687	0.0119	115.2	2.064	0.0172	15.12	7.62	0.831
	36	752	0.0119	126.5	2.405	0.0167	16.35	7.74	0.835
	37	811	0.0118	137.5	2.783	0.01665	17.74	7.76	0.832
	38	863	0.0118	146.0	3.16	0.0166	18.80	7.77	0.830
	39	972	0.0116	168.0	3.88	0.01614	21.32	7.88	0.842
	40	1053	0.0116	182.0	4.44	0.0157	22.93	7.94	0.840
					d = 3 cm				
	41	402	0.0114	106.0	0.495	0.0180	14.22	7.46	0.832
	42	439	0.0114	115.5	0.570	0.0174	15.25	7.58	0.828
	43	488	0.0114	128.5	0.700	0.0173	16.90	7.60	0.824
	44	559	0.0114	147.0	0.870	0.01638	18.81	7.82	0.850
	45	627	0.0114	165.0	1.092	0.01638	21.11	7.82	0.831
	46	688	0.0114	181.0	1.246	0.01549	22.54	8.04	0.840
	47	756	0.0114	199.0	1.520	0.01560	24.86	8.01	0.839
	48	879	0.0114	231.0	1.970	0.01500	28.30	8.16	0.841
	49	1010	0.0115	266.0	2.545	0.01470	32.30	8.24	0.843
	50	1106	0.0115	288.0	2.990	0.01435	34.50	8.35	0.848
					d = 5 cm				
	51	91.4	0.01233	37.0	0.0196	0.0230	5.61	6.59	0.812
	52	124.4	0.01233	50.3	0.0331	0.02104	7.30	6.90	0.818
	53	172.0	0.01230	70.0	0.0588	0.0195	9.78	7.16	0.819
	54	203.5	0.01230	82.6	0.0787	0.0186	11.26	7.34	0.819
	55	237.0	0.01230	96.4	0.1040	0.01811	12.96	7.44	0.829

Table 9 continued

Log λ in Comparison with Log Re and $\frac{1}{\sqrt{\lambda}}$ in Comparison with Log $Re\sqrt{\lambda}$

Nr.	$\bar{u}$ cm/s	ν cm^2/s	Re $\cdot 10^{-3}$	$\frac{dp}{dx}$ Dyn/cm^3	λ	$Re\sqrt{\lambda}\cdot 10^{-3}$	$\frac{1}{\sqrt{\lambda}}$	$\frac{\bar{u}}{U_{MAX}}$
			d = 5 cm (continued)					
56	71.2	0.01214	29.3	0.01215	0.0226	4.40	6.66	0.814
57	90.8	0.01214	37.4	0.0190	0.0226	5.62	6.66	0.812
58	102.5	0.0122	42.0	0.0237	0.0220	6.23	6.75	0.817
59	116.5	0.0122	47.7	0.0298	0.02146	6.98	6.83	0.819
60	140.0	0.01215	57.6	0.0409	0.02042	8.23	7.00	0.819
61	153.5	0.01215	63.2	0.0480	0.01990	8.92	7.09	0.821
62	179.5	0.01215	73.8	0.0630	0.01915	10.21	7.23	0.823
63	214.4	0.01214	88.3	0.0860	0.01830	11.95	7.40	0.825
64	103.0	0.0134	38.4	0.0240	0.0222	5.72	6.71	0.817
65	141.0	0.0133	53.0	0.0423	0.02085	7.65	6.93	0.820
66	194.5	0.0128	76.0	0.0701	0.0182	10.25	7.42	0.824
67	423.5	0.01235	171.5	0.296	0.01617	21.8	7.86	0.842
68	395.0	0.00925	213.4	0.250	0.01567	26.71	7.99	0.844
69	570.0	0.0097	294	0.488	0.01470	35.63	8.26	0.849
70	652.0	0.01235	264	0.640	0.01475	32.18	8.24	0.847
71	733	0.00925	396	0.757	0.0138	41.52	8.51	0.856
72	740.0	0.00925	400	0.752	0.01344	46.40	8.63	0.862
73	912.8	0.00925	493.4	1.140	0.01325	56.8	8.69	0.855
74	1082.0	0.0081	670	1.470	0.01229	74.3	9.02	0.861
			d = 10 cm					
75	345.9	0.01083	318.9	0.0868	0.01421	38.0	8.39	0.854
76	377.1	0.01080	348.6	0.1008	0.01388	41.06	8.49	0.853
77	392.7	0.01083	363.0	0.1092	0.01390	42.80	8.48	0.857
78	466.3	0.01080	431.5	0.1492	0.01342	50.00	8.62	0.856
79	482.8	0.01079	446.8	0.1582	0.01334	51.6	8.66	0.859
80	510.0	0.01079	472.0	0.1760	0.01328	54.40	8.67	0.855
81	533.2	0.01080	493.7	0.1920	0.01324	56.82	8.69	0.857
82	569.1	0.01079	562.6	0.2175	0.01320	60.50	8.71	0.855
83	602.0	0.01072	597.0	0.2340	0.01277	63.30	8.87	0.869
84	660.3	0.0110	600.0	0.2840	0.01277	67.80	8.86	0.858

Table 9 continued

Log λ in Comparison with Log Re and $\frac{1}{\sqrt{\lambda}}$ in Comparison with Log $Re\sqrt{\lambda}$

Nr.	$\bar{u}$ cm/s	ν cm^2/s	$Re \cdot 10^{-3}$	$\frac{dp}{dx}$ Dyn/cm^3	λ	$Re\sqrt{\lambda} \cdot 10^{-3}$	$\frac{1}{\sqrt{\lambda}}$	$\frac{\bar{u}}{U_{MAX}}$
				d = 10 cm (continued)				
85	704.0	0.0111	634	0.316	0.0125	70.90	8.95	0.866
86	769.8	0.0110	700	0.387	0.0129	79.50	8.80	0.859
87	876	0.0121	725	0.480	0.01228	80.40	9.02	0.863
88	810	0.0111	737	0.422	0.0126	82.80	8.91	0.854
89	843.4	0.01094	771	0.444	0.01227	85.42	9.02	0.864
90	940.0	0.01086	865	0.536	0.01188	94.24	9.18	0.866
91	790	0.0077	1025	0.372	0.01170	110.9	9.25	0.863
92	1248	0.01125	1108	0.92	0.01159	119.3	9.29	0.864
93	882	0.0077	1148	0.455	0.01146	123.0	9.34	0.869
94	944	0.0077	1225	0.522	0.01150	131.25	9.33	0.871
95	1005	0.0076	1320	0.576	0.01118	139.60	9.46	0.870
96	982	0.0072	1364	0.540	0.0110	143.20	9.53	0.877
97	1020	0.0071	1438	0.596	0.01122	152.3	9.45	0.872
98	900	0.0070	1285	0.471	0.01144	137.5	9.35	0.861
99	685	0.0070	979	0.278	0.01161	105.0	9.28	0.864
100	761	0.0070	1088	0.340	0.0115	116.7	9.33	0.862
101	830	0.0070	1185	0.400	0.0114	126.6	9.37	0.866
102	958	0.0070	1368	0.522	0.01115	144.4	9.47	0.865
103	259	0.01087	238.8	0.514	0.0150	29.25	8.17	0.846
104	286.8	0.01083	264.4	0.612	0.01459	31.92	8.29	0.854
105	309.5	0.01083	285.4	0.708	0.01446	34.30	8.32	0.850
106	325.4	0.01083	300.0	0.788	0.01457	36.24	8.28	0.847
107	726.0	0.0122	595	0.340	0.01265	66.90	8.90	0.858
108	806	0.0121	666	0.416	0.01255	74.60	8 93	0.860
109	1013	0.01125	900	0.623	0.0119	98.10	9.17	0.867
110	1325	0.01125	1178	1.015	0.0113	125.2	9.41	0.867
111	1691	0.0110	1539	1.600	0.01098	161.4	9.54	0.868
112	1765	0.0110	1600	1.670	0.0105	164.0	9.76	0.874
113	1410	0.0083	1700	1.070	0.01060	175.1	9.71	0.870
114	1926	0.0083	1850	2.000	0.01058	190.4	9.72	0.871
115	1630	0.0080	2038	1.420	0.01043	208.0	9.80	0.872

Table 9 continued

Log λ in Comparison with Log Re and $\frac{1}{\sqrt{\lambda}}$ in Comparison with Log $Re\sqrt{\lambda}$

Nr.	$\bar{u}$ cm/s	ν cm^2/s	Re $\cdot 10^{-3}$	$\frac{dp}{dx}$ Dyn/cm^3	λ	Re $\sqrt{\lambda} \cdot 10^{-3}$	$\frac{1}{\sqrt{\lambda}}$	$\frac{\bar{u}}{U_{MAX}}$
		d = 10 cm (continued)						
116	1630	0.0079	2062	1.415	0.01045	210.5	9.79	0.872
117	1758	0.00825	2130	1.615	0.01029	216.0	9.87	0.875
118	1940	0.0084	2310	1.910	0.00995	230.8	10.02	0.879
119	1930	0.0082	2351	1.94	0.01021	237.5	9.89	0.874
120	2150	0.0110	1964	2.499	0.0106	202.3	9.71	0.872
121	2010	0.0078	2580	2.050	0.00995	257.2	10.02	0.874
122	2150	0.0079	2722	2.317	0.0098	269.5	10.10	0.879
123	2162	0.0077	2810	2.345	0.00985	279.2	10.06	0.878
124	2220	0.0074	3000	2.470	0.00988	298.2	10.06	0.879
125	2425	0.0075	3230	2.88	0.00960	321.0	10.07	0.880

$\bar{u}$ = mean velocity; $\nu = \frac{\mu}{\rho}$ = kinematic viscosity; μ = viscosity constant; ρ = density; Re = Reynolds' Number; d = tube diameter; $\frac{dp}{dx}$ = pressure grad.; $\lambda = \frac{dp}{dx} \cdot \frac{d}{q}$ = resistance number; $q = \rho \frac{\bar{u}^2}{2}$ = pressure rise of mean velocity; U_{MAX} = maximum velocity.

DISTRIBUTION LIST

PUR- 11

1. Courant - Policy Committee
2. Gilliland - Policy Committee
3. Kinzel - Policy Committee
4. Roberts - Policy Committee
5. Taylor - Policy Committee
6. von Karman - Policy Committee
7. Charyk - PRN
8. Clauser - JHU
9. Foa - CAL
10. Harrington - PIB
11. Woody - NYU
12. Zucrow - PUR
13. Wohl - DEL
14. Markstein - CAL
15. Libby - PIB
16. Guerrieri - DEL
17. Lees - PRN
18. Rudinger - CAL
19. Smith - PUR
20. Yuan - PIB
21. Colburn - DEL
22. Meikle - PUR
23. Kahane - PRN
24. Corrsin, S. - JHU

25/35. Chief of Naval Research, Code 429

36. C.O., ONR, N.Y.
37. C.O., ONR, Pasadena

38/39. Chief, BuAer, Power Plants Div., Exp. Engines Branch

40. Chief BuAer, Power Plants, Fuels and Lubricants Branch
41. Dr. D. G. Samaras, O.A.R., Wright Field

42/43. Guided Missiles Div., Bu Ord, Washington, D.C. (Tanczos)

44. Dr. C.F.Yost, U.S.A.F.
45. Univ.ofCalifornia, Berkeley, Calif. Prof. C. Folsom
46. Columbia Univ. Library, N.Y., N.Y. Attn: Engineering Librarian
47. Guggenheim Aero.Lab., C.I.T., Attn: Prof. C. Millikan
48. Dept.of Chemistry, U.of Minnesota, Dr.B.L.Crawford
49. O.in C., N.O.T.S., Pasadena
50. C.O., ONR, San Francisco
51. Purdue U. Library, Lafayette, Ind., Attn: Mr. J. Moriarty
52. Aerojet, Azusa, Cal., Attn: Mr.G. Henning, Librarian
53. Dept.of Engr.,U. of California, Attn. Dean L.N.K.Boelter
54. Grad.School of Aero.Engr., Cornell, Prof. A. R. Kantrowitz
55. Guggenheim Aero. Lab., C.I.T., Attn: Dr. P.A.Lagerstrom
56. M.I.T., Cambridge, Prof. J. H. Keenan
57. Dept.of Aero.Eng., U. Of Minnesota, Attn: Prof. J.D.Akerman
58. Dr.B. Lewis, Bu.of Mines, Pittsburgh
59. Crocco, PRN
60. Parkor, PRN
61. Summerfield, PRN
62. Wakelin, PRN